A STUDY OF SEVERAL ODD-ODD s-d SHELL NUCLEI VIA THE (p, d) REACTION AT 35 MeV

Thesis for the Degree of Ph. D.
MICHIGAN STATE UNIVERSITY

James Allen Rice

1973

LIBRARY
Michigan State
University

This is to certify that the

thesis entitled

A Study of Several Odd-Odd s-d Shell Nuclei

via the (p,d) Reaction at 35 MeV

presented by

James Allen Rice

has been accepted towards fulfillment
of the requirements for

Ph.D. degree in Physics

B. L. Wilkerthal

Major professor

Date June 10, 1973

O-7639

ABSTRACT

A STUDY OF SEVERAL ODD-ODD s-d SHELL NUCLEI
VIA THE (p,d) REACTION AT 35 MeV

By

James Allen Rice

States in ^{22}Na, ^{34}Cl, ^{36}Cl, and ^{38}K have been studied via the (p,d) reaction at an incident proton energy of 35 MeV. Reaction products were analyzed with the Michigan State University split-pole magnetic spectrograph. The deuteron spectra were recorded both with a single-wire, position-sensitive proportional counter, at a total resolution of $\sim$50 keV, FWHM, and on nuclear emulsion plates, with resolutions of 8-18 keV, FWHM. Levels to 6 MeV of excitation in ^{22}Na, ^{34}Cl, and ^{38}K, and to 8 MeV in ^{36}Cl have been observed and excitation energies assigned to an accuracy of $\leq$1 keV per MeV.

Angular distributions were measured from 3^{o} to 60^{o}, with special emphasis on the region from 3^{o} to 35^{o}. This has allowed a precise definition of the forward angle shapes for ℓ=0 and ℓ=2 single neutron pick-up angular distributions in the s-d shell. A careful screening of deuteron optical-model parameters available from the literature was conducted in an effort to reproduce the experimentally observed

shapes via distorted wave Born approximation calculations. The best overall fits to pure ℓ-transfer distributions for the A>30 nuclei were obtained with standard finite-range, non-locality corrected calculations which include a density-dependent damping of the V_{pn} interaction. A good ℓ=0 fit to the $^{23}Na(p,d)^{22}Na$ data could not be obtained for calculations which also yielded good fits for the A>30 nuclei.

Spectroscopic factors, ℓ-values and parity assignments, and excitation energies from the present work are compared with previous experimental studies and recent shell model calculations. The agreement between the present experimental results and theoretical predictions is good for low-lying levels in the residual nuclei, but observed ℓ=3 angular distributions and spectroscopic factors for higher excited states indicate a need for consideration of 2 (or 4 or 6) particle excitations to the f-p shell in the ground state configurations of the A>30 target nuclei.

A STUDY OF SEVERAL ODD-ODD s-d SHELL NUCLEI VIA THE (p,d) REACTION AT 35 MeV

By

James Allen Rice

A THESIS

Submitted to

Michigan State University

in partial fulfillment of the requirements

for the degree of

DOCTOR OF PHILOSOPHY

Department of Physics

1973

G4395

For Linda,
with whom all things are possible.

ACKNOWLEDGEMENTS

I wish to express my appreciation to the entire cyclotron staff for their generous assistance in making these experiments possible. Specifically, I would like to thank:

My Thesis Advisor, Professor Hobson Wildenthal, for his aid and counsel in all aspects of this work—conception of the experiments, data taking and analysis, and the writing of this manuscript;

Dr. Barry Preedom for many useful discussions concerning the DWBA and for suggesting the approach used in the analysis of this data;

Professor Jerry Nolen for his aid in the excitation energy analysis of the data and many discussions of nuclear physics in general;

Richard Au, Larry Learn, and John Collins for their invaluable computer assistance;

David Show for his assistance during many long nights of data taking;

The many plate scanners who extracted accurate data from the nuclear emulsions;

Andy Kaye for his good-will and most efficient efforts in obtaining photographs;

Sandi Bauer for typing this thesis;

and the National Science Foundation for its financial support throughout my graduate career at MSU.

Finally, this thesis most certainly could not have been realized without the continuous encouragement of my parents, and the patience, hard-work, and self-sacrifice of my wife, Linda.

TABLE OF CONTENTS

	Page
ACKNOWLEDGEMENTS.	iii
LIST OF TABLES	vi
LIST OF FIGURES	viii
I. INTRODUCTION	1
II. THE $^{23}Na(p,d)^{22}Na$ AND $^{35}Cl(p,d)^{34}Cl$ REACTIONS .	7
II.1. Introductory Remarks	7
II.2. Experimental Procedures and Results . .	10
II.3. Analysis of the Angular Distributions. .	22
II.4. Discussion of Results	40
II.4.A. Levels of ^{22}Na	40
II.4.B. Results for ^{34}Cl.	42
II.5. Conclusions	48
III. THE $^{37}Cl(p,d)^{36}Cl$ REACTION.	50
III.1. Introductory Remarks	50
III.2. Experimental Procedure.	52
III.3. Excitation Energies.	57
III.4. Angular Distributions	60
III.4.A. General Discussion	60
III.4.B. Analysis of Experimental Angular Distributions	65
III.5. Discussion.	85
III.5.A. Energy Levels.	85
III.5.B. ℓ and π Assignments.	86
III.5.C. Experimental C^2S Values . . .	88
III.5.D. Comparison with Shell-Model Calculations	91
III.6. Summary.	95
IV. THE $^{39}K(p,d)^{38}K$ REACTION	97
IV.1. Introductory Remarks	97
IV.2. Experimental Procedure.	98
IV.3. Excitation Energies.	100

Page

IV.4. Angular Distributions. 108

IV.4.A. Discussion of DWBA Calculations 108
IV.4.B. Analysis of Experimental Angular Distributions 118
IV.4.C. Assignment of ℓ-values . . . 129
IV.4.D. Discussion of Values Extracted for C^2S 130

IV.5. Discussion of Results. 134

IV.5.A. Comparison with Previous Experimental Results 134
IV.5.B. Comparison of Results with Structure Theory 137

IV.6. Conclusions 140

LIST OF REFERENCES. 142

APPENDIX A A-1

MONSTER2 . . . . . A-1

1. Cross-Section Transformation A-1
2. Excitation Energies A-2
3. Particle Group Positions. A-7
4. Contaminant Identification A-7
5. Multi-angle Averaging. A-8

APPENDIX B B-1

ELASTIC SCATTERING DATA B-1

LIST OF TABLES

Table		Page
1.	Excitation energies, ℓ-values, J^{π} and T values and pick-up spectroscopic factors for states of ^{22}Na. All C^2S values extracted from the present data have been normalized to yield 0.59 for the ground state.	19
2.	Excitation eneriges, ℓ-values, J^{π} and T values, and pick-up spectroscopic factors for states of ^{34}Cl. All C^2S values extracted from the present data are normalized such that C^2S=0.35 for the ground state.	20
3.	Optical-model parameters used in the analysis of the $^{23}Na(p,d)^{22}Na$ and $^{35}Cl(p,d)^{34}Cl$ data.	36
4.	States used for the energy calibration of the $^{37}Cl(p,d)^{36}Cl$ reaction data. Some energies in ^{22}Na extracted in the present work and in a previous (p,d) study are shown to illustrate calibration consistency.	58
5.	Energy levels in ^{36}Cl observed in the present study and in other works.	61-62
6.	Optical-model parameters used in the analysis of the $^{37}Cl(p,d)^{36}Cl$ data.	66
7.	Experimental values of ℓ and C^2S_ℓ for the $^{37}Cl(p,d)^{36}Cl$ reaction as observed in the present investigation. All assignments are based on the DFRNL analysis, with the spectroscopic factors normalized to yield C^2S_ℓ=1.10 for the transition to the ^{36}Cl ground state.	84
8.	Experimental values of C^2S_ℓ for transitions from ^{37}Cl to ^{36}Cl. Absolute values for the ground state are presented in parentheses. All other values are normalized such that C^2S_ℓ=1.10 for the ground state.	89
9.	A comparison of $C^2S(\ell)$ values obtained in the present study with those from various shell model calculations.	92

Table Page

10. States used in the energy calibration for the $^{39}K(p,d)^{38}K$ reaction data. 104

11. Energy levels of ^{38}K excited in the present investigation of the (p,d) reaction and in previous studies of other reactions. 106

12. Optical-model parameters used in the analysis of the $^{39}K(p,d)^{38}K$ data. 111

13. Experimental values of ℓ and C^2S_ℓ, obtained from the DFRNL analysis for transitions from ^{39}K to ^{38}K as observed in the present investigation. All values are normalized so that C^2S_ℓ for the ground state is 1.75. The assumed j-values are 3/2 for ℓ=2, 3/2 (n=2) for ℓ=1, and 7/2 for ℓ=3. 128

14. Experimental values of C^2S_ℓ for the transitions from ^{39}K to ^{38}K. The absolute values for the ground state are presented in parentheses. All other values are normalized such that C^2S=1.75 for the ground state. 132

15. Experimental and theoretical values of C^2S for single neutron pick-up from ^{39}K. 138

A1. Extrapolations from the MONSTER2 momentum matching fits to known energy levels. Nominal energies and calibration parameters were obtained from a complete calibration run on the test spectrum. All other energies (MeV) are obtained from a fit to the first three (0.000, 0.130, 0.459 MeV) levels after the indicated shift the given parameter had been assumed. . . A-6

LIST OF FIGURES

Figure — Page

1. Complementary spectra from the (p,d) reaction on the ^{23}Na, ^{23}Na-^{35}Cl and Li-^{35}Cl targets, measured at 35 MeV and 14°, as recorded on nuclear emulsion plates. The resolution of the deuteron groups is 15-20 keV, FWHM. Selected peaks are labeled with excitation energy assignments from the present work, the "boxed" values indicating levels in ^{34}Cl. 14

2. A spectrum from the (p,d) reaction on the ^{23}Na-^{35}Cl target, measured at 35 MeV and 8°, as recorded on nuclear emulsion plates. The resolution of the deuteron groups is 8 keV, FWHM. All excitation energy values are from the present work, with those "boxed" indicating levels in ^{34}Cl. 16

3. Experimental angular distributions for states in ^{22}Na as observed in the $^{23}Na(p,d)^{22}Na$ reaction at 35 MeV. The solid curves are fits of the DFRNL calculations to the data in the angular range from 3° to 35°. The dotted curves show the contribution of the first indicated ℓ-value for mixed-ℓ distributions. . 24

4. Experimental angular distributions for states in ^{22}Na as observed in the $^{23}Na(p,d)^{22}Na$ reaction at 35 MeV. The solid curves are fits of the DFRNL calculations to the data in the angular range from 3° to 35°. The dotted curves show the contribution of the first indicated ℓ-value for mixed-ℓ distributions. . . 26

5. Experimental angular distributions for states in ^{22}Na as observed in the $^{23}Na(p,d)^{22}Na$ reaction at 35 MeV. The solid curves are fits of the DFRNL calculations to the data in the angular range from 3° to 35°. The dotted curves show the contribution of the first indicated ℓ-value for mixed-ℓ distributions. . 28

Figure Page

12. Experimental angular distributions for states in ^{36}Cl as observed in the $^{37}Cl(p,d)^{36}Cl$ reaction at 35 MeV. The solid curves are fits of the DFRNL calculations to the data in the angular range from 3° to 35°. The dotted curves show the contribution of the first indicated ℓ-value for mixed-ℓ distributions. . 72

13. Experimental angular distributions for states in ^{36}Cl as observed in the $^{37}Cl(p,d)^{36}Cl$ reaction at 35 MeV. The solid curves are fits of the DFRNL calculations to the data in the angular range from 3° to 35°. The dotted curves show the contribution of the first indicated ℓ-value for mixed-ℓ distributions. . 74

14. Experimental angular distributions for states in ^{36}Cl as observed in the $^{37}Cl(p,d)^{36}Cl$ reaction at 35 MeV. The solid curves are fits of the DFRNL calculations to the data in the angular range from 3° to 35°. The dotted curves show the contribution of the first indicated ℓ-value for mixed-ℓ distributions. . 76

15. Experimental angular distributions for states in ^{36}Cl as observed in the $^{37}Cl(p,d)^{36}Cl$ reaction at 35 MeV. The solid curves are fits of the DFRNL calculations to the data in the angular range from 3° to 35°. The dotted curves show the contribution of the first indicated ℓ-value for mixed-ℓ distributions. . 78

16. Experimental angular distributions for states in ^{36}Cl as observed in the $^{37}Cl(p,d)^{36}Cl$ reaction at 35 MeV. The solid curves are fits of the DFRNL calculations to the data in the angular range from 3° to 35°. The dotted curves show the contribution of the first indicated ℓ-value for mixed-ℓ distributions. . 80

17. Experimental angular distributions for states in ^{36}Cl as observed in the $^{37}Cl(p,d)^{36}Cl$ reaction at 35 MeV. The solid curves are fits of the DFRNL calculations to the data in the angular range from 3° to 35°. The dotted curves show the contribution of the first indicated ℓ-value for mixed-ℓ distributions. . 82

Figure Page

18. A spectrum from the $^{39}K(p,d)^{38}K$ reaction, measured at 35 MeV and 30°, as recorded on nuclear emulsion plates. The resolution of the deuteron groups is 10 keV, FWHM. All ^{38}K excitation energy values are from the present work. 102

19. A comparison of fits to representative angular distributions from the $^{39}K(p,d)^{38}K$ reaction at 35 MeV with the three chosen types of DWBA calculations. All fits were performed over the 3° to 35° angular region. The curves are identified as follows: ———DFRNL, ----FRNL, and — —ADIABATIC. . . 115

20. A comparison of ADIABATIC, FRNL, and DFRNL calculations (see text and Table 12) with ℓ=0 transitions in the $^{34}S(p,d)^{33}S$ reaction at 35 MeV. 117

21. Experimental angular distributions for states in ^{38}K, as observed in the $^{39}K(p,d)^{38}K$ reaction at 35 MeV. The solid curves are fits of the DFRNL calculations to the data in the angular range from 3° to 35°. The dotted curves show the amount of the ℓ=0 component in mixed ℓ=0-ℓ=2 distributions. 121

22. Experimental angular distributions for states in ^{38}K, as observed in the $^{39}K(p,d)^{38}K$ reaction at 35 MeV. The solid curves are fits of the DFRNL calculations to the data in the angular range from 3° to 35°. The dotted curves show the amount of the ℓ=0 component in mixed ℓ=0-ℓ=2 distributions. 123

23. Experimental angular distributions for states in ^{38}K, as observed in the $^{39}K(p,d)^{38}K$ reaction at 35 MeV. The solid curves are fits of the DFRNL calculations to the data in the angular range from 3° to 35°. The dotted curves show the amount of the ℓ=0 component in mixed ℓ=0-ℓ=2 distributions. 125

Figure Page

24. Experimental angular distributions for states in ^{38}K, as observed in the $^{39}K(p,d)^{38}K$ reaction at 35 MeV. The solid curves are fits of the DFRNL calculations to the data in the angular range from 3° to 35°. The dotted curves show the amount of the $\ell=0$ component in mixed $\ell=0$-$\ell=2$ distributions. 127

B1. Proton elastic scattering spectra recorded at 40° with a single-wire proportional counter. B-3

B2. Measured proton elastic scattering differential cross-sections for the ^{23}Na-^{35}Cl target. B-5

B3. Observed proton elastic scattering cross-sections for the ^{23}Na-^{37}Cl target. B-7

B4. Measured proton elastic scattering cross-sections for the ^{39}K target. B-9

I. INTRODUCTION

The nuclear shell-model assumes that a given number of nucleons occupy specified orbitals about an inert "core" much the same as atomic electrons move in orbitals in the electro-magnetic field of the nucleus. These "active" particles are assumed to be responsible for most observable properties of the nucleus. Indeed, spins, parities, and magnetic moments of many nuclei may be predicted solely on the basis of the number and kind of nucleons which occupy the last, or highest energy, subshell consistent with a systematic stacking of nucleons in the lowest unfilled orbitals.

A detailed theoretical description of the nucleus is assumed to be obtainable in terms of a Hamiltonian characterized by a sum of one and two-body matrix elements, which result from interactions of individual nucleons with the core and a two-body interaction between pairs of active nucleons, respectively.

Nuclei with mass numbers between 17 and 40 are members of the s-d shell, i.e., the last nucleons occupy the $1d_{5/2}$, $2s_{1/2}$, or $1d_{3/2}$ orbitals in the simplest picture. Shell-model calculations for these nuclei have shown considerable advancement in the last decade. Early works considered couplings only in the highest occupied orbit, with all other subshells comprising the core. Considerations of this sort led to predictions for only a small number of low-lying excited states. Calculations allowing two-orbital excitations

showed better agreement with available experimental data on spin, parity, and energy assignments for low-lying levels. Sophisticated computer codes and calculational techniques have allowed recent theoretical studies in which the basis states have been expanded to include the entire s-d shell. Both empirical and least-squares adjusted single particle energy parameterizations have been used for the one-body matrix elements, while theoretical and empirical two-body interactions have been studied. In general, the recent results show good correspondence with the data, particularly for those nuclei with either odd-even or even-even combinations of protons and neutrons. Calculated spectra for the odd-odd nuclei, however, are often in even qualitative disagreement with experimental results. The structure of these nuclei appears to be most sensitive to the details of the nuclear Hamiltonian and, therefore, any descriptive theory for the s-d shell would be severely tested in its attempt to reproduce sound experimental data for the odd-odd systems.

A critical comparison of recent Hamiltonians most certainly relies on accurately observed properties of the odd-odd s-d shell nuclei. Excitation energies, spins and parities of nuclear energy levels and spectroscopic factors for single-nucleon transfer may be observed via direct reaction nuclear spectroscopy. Direct reactions take place in a time interval comparable to the time necessary for the projectile to traverse the target nucleus ($\sim 10^{-23}$ seconds)

and therefore, do not "see" collective effects in the target nucleus and are assumed to involve only one-step processes, i.e., the target nucleus is not excited above a ground state configuration before any particle transfer occurs. Those in which the incident projectile absorbs a nucleon from the target nucleus (pick-up) or deposits a nucleon in the target nucleus (stripping) are called single nucleon transfer reactions. The target nucleus, therefore, undergoes a change in mass number (A) of ± 1 and the resulting residual nucleus may be left in any of its energetically and quantum mechanically allowed energy levels. In reality, any nuclear state may be described as a sum of weighted components, each corresponding to the probability that given shell model orbitals are populated by specified numbers of nucleons in particular angular momentum couplings. The spectroscopic factors observed in transfer reaction experiments are a measure of the overlap, a quantum mechanical correspondence, of initial and final state configurations. When only one nucleon is transferred, therefore, one expects to probe specific shell-model wave function components for the initial and final nuclear states.

The choice of an appropriate reaction for nuclear spectroscopy studies depends on the available projectiles, targets, and detection and analysis apparatus. The Michigan State University cyclotron provides high resolution proton beams with currents sufficient to allow experimental runs of

reasonable brevity. Several of the odd-odd s-d shell nuclei which can be reached through single-neutron pick-up from stable targets are ^{22}Na, ^{34}Cl, ^{36}Cl, and ^{38}K. Natural ^{23}Na and ^{39}K metals and isotopically enriched ^{23}Na-^{35}Cl, ^{7}Li-^{35}Cl, and ^{23}Na-^{37}Cl compounds are commerically available. All are easily evaporated at moderate temperatures and thin targets may be routinely produced. The properties of the MSU cyclotron and split-pole magnetic spectrograph allow charged reaction product groups of closely similar energy to be clearly separated, detected and analyzed. The structures of ^{22}Na, ^{34}Cl, ^{36}Cl, and ^{38}K are, therefore, subject to study via the (p,d) reaction.

Precise excitation energies for these four nuclei have previously been assigned only to those states below the 3-4 MeV region. Any extension of the experimental understanding of these nuclei naturally includes a precise determination of higher lying energies. Accurate extraction peak centroids is allowed by the high particle group resolution (8-10 keV, FWHM) obtained on nuclear emulsion plates in the present work. A comprehensive spectrograph calibration scheme and least-squares fitting procedures have made possible the assignment of excitation energies in the residual nuclei to accuracies of $\lesssim$1 keV/MeV of excitation. This represents a significant improvement over previous charged particle studies, allowing a more critical comparison with calculated spectra and the rationalization of the results

of different kinds of experiments. The spectrum analysis for these studies was performed with the computer code MONSTER2 (see APPENDIX A) on the MSU Sigma-7 computer.

In the direct reaction process, one may attempt to picture the nucleus as a sum of several spherically-symmetric potentials. This approximation is the basis of the Distorted Wave Born Approximation (DWBA) predictions with which the present data are compared. Parities of energy levels in the residual nuclei, orbital angular momenta of the neutrons transferred in (p,d) reactions and spectroscopic factors may be assigned on the basis of such comparisons of individual experimental angular distributions with DWBA predicted distributions calculated for given neutron quantum numbers and appropriate final-state excitation energies. Shape comparisons yield the transferred neutron orbital angular moemtnum quantum numbers (ℓ) and, hence, the parities of the residual states ($\pi_{residual}=\pi_{target}\pi_{neutron}$ with $\pi_{neutron}=(-1)^{\ell}$). Magnitude comparisons indicate relative strengths for the ℓ-values involved in a given transition; hence, a measure of wave-function component amplitudes. Previous single neutron pick-up experiments ((p,d), (d,t), (^{3}He,α)) observed angular distributions which generally did not include angles smaller than 10^{o}-15^{o}. The present work measures distributions in to 3^{o}, providing a critical test of the forward angle DWBA shapes. The use of different currently popular proton optical model

parameters had little effect on the calculated (p,d) distributions. However, the DWBA-predicted differential cross-section shapes were found to be noticeably dependent on the choice of deuteron parameters. The experimentally observed shapes for pure ℓ=0 and ℓ=2 transfers in the A>30 nuclei were best reproduced when the interaction responsible for the reaction, V_{pn}, was damped by a simulated nuclear matter density dependence, and a broadly based set of optical-model potentials was used to describe the outgoing deuteron. The empirical Q-dependence of the $^{23}Na(p,d)^{22}Na$ shapes has not been successfully reproduced, particularly those for ℓ=0 neutron transfers. All of the DWBA calculations were performed with the computer code DWUCK using standard Q-dependence techniques.

The results of the present experiments are presented in three autonomous sections, one for the combined $^{23}Na(p,d)^{22}Na$ and $^{35}Cl(p,d)^{34}Cl$ works, and one each for $^{37}Cl(p,d)^{36}Cl$ and $^{39}K(p,d)^{38}K$. Each section includes a summary of pertinent previous experimental and theoretical studies, and the experimental and analytical techniques employed for the particular work under consideration. Theoretical implications of the present energy level, parity and single neutron pick-up spectroscopic factor assignments are discussed in conjunction with recently utilized shell-model Hamiltonians.

II. THE $^{23}Na(p,d)^{22}Na$ AND $^{35}Cl(p,d)^{34}Cl$ REACTIONS

II.1. Introductory Remarks

Recent shell-model analyses[1-4] of the nuclei in the regions A=18-24 and A=30-38 indicate that the nuclei whose structures depend most sensitively upon details of the model Hamiltonian are those which have odd numbers of both neutrons and protons. While the general features of the spectra of doubly-even and even-odd nuclei emerge more or less satisfactorily from such shell-model calculations, the calculated spectra of the doubly-odd nuclei are often even in qualitative disagreement with the observed level sequences. It thus appears that the definitive test of microscopic many-body theories of the spectroscopy of light-medium nuclei will come in the attempt to explain the rich store of details observed in the experimental study of these particular nuclei.

The nuclei ^{22}Na and ^{34}Cl are pivotal to understanding the structure of the s-d shell. In an s-d shell-model their wave functions are constructed of 6 particles and 6 holes, respectively. This number of active nucleons is large enough to allow the full consequences of the particularities of the two-particle component of the nuclear Hamiltonian to become manifest. At the same time, the dimensionalities of the model states are such that extensive theoretical work, in which the full s-d shell-model space is employed to describe the wave functions of these nuclei, is available. This

latter point is important because it allows the exclusion of the possibility that the theoretical results might be contaminated by effects arising from intra-shell basis truncation.

Shell-model calculations made with Hamiltonians of the Kuo-Brown[5] type or with two-body matrix elements derived from simple central potentials fail to reproduce many simple aspects of the ^{22}Na and ^{34}Cl energy level spectra, such as, for example, the spins of the ground states.[1,2] Hamiltonians derived in less straightforward fashion have been used to achieve some improvement in the agreement between theory and experiment, but it seems fair to say that a full understanding of these systems has not yet been achieved. The aim of the present experiment, part of a systematic study of doubly-odd nuclei in the s-d shell,[6-8] is to provide definitive experimental information on some aspects of ^{22}Na and ^{34}Cl so that a more rigorous critique of present and future structure calculations is possible. The hope is that a clarification of the structure of the A=22 and A=34 systems will facilitate progress in understanding the behavior of the nuclei in the middle of the s-d shell, A=24-32, where the correct details of the effective two-body nuclear interaction are essential.

We present in this report the results of a study of the (p,d) reaction on ^{23}Na and ^{35}Cl at 35 MeV. The principle results obtained relate to excitation energies and angular distributions of states in ^{22}Na and ^{34}Cl, and the ℓ-values and associated spectroscopic factors of the neutrons picked up

in the formation of these levels. There is considerable experimental knowledge[9-14] of the levels of ^{22}Na and a rapidly growing body of data[15-23] on ^{34}Cl. Work relevant to the characteristics of the T=1 states of these nuclei has also been done with the nuclei ^{22}Ne[24,25] and ^{34}S.[26,27] Since an extensive particle-transfer study with good energy resolution is available[10] for ^{22}Na, a large amount of fundamentally new information was not expected to emerge from our ^{23}Na(p,d)^{22}Na data. Rather, we aimed to obtain more precise experimental excitation energies for higher lying states, an alternate set of spectroscopic factors to complement those from the (^{3}He,^{4}He) reaction, and, with the aid of the higher energy resolution of the present work, a clarification of a few (but important) questions concerning the low-lying states.

Our results for ^{34}Cl make a considerably more significant contribution to the state of knowledge about this nucleus. We are able to resolve many more states than has been possible in previous experiments[22] and, even for easily resolved states, our extensive angular distributions provide evidence for reversing some previous ℓ-value assignments. These ℓ-values and their associated spectroscopic factors, and the precise excitation-energy assignment made in the 3-5 MeV region of excitation, serve to advance our experimental comprehension of the mass 34 system to a condition almost comparable with that of A=22.

The present data are of interest from a reaction theory standpoint also, in that the angular range, energy resolution, statistical accuracy, and large number of transitions combine to provide stringent criteria for evaluating the usefulness of ordinary DWBA calculations for the (p,d) reaction at these energies for medium-light nuclei. The value of this aspect of the present study is enhanced by the concurrent analyses of (p,d) data[6,8] on neighboring nuclei.

II.2. Experimental Procedures and Results

The present experiments were performed with the MSU Cyclotron[28] and Enge-type[29] split-pole magnetic spectrograph. The beam energies for the various experimental periods ranged from 34.9 to 35.0 MeV, and beam currents on target ranged between 300 and 800 nanoamps. The beam on target had a coherent energy spread of about 20 keV, but by using dispersion matching[30] in the spectrograph in conjunction with the techniques discussed by Blosser, et al.,[31] resolutions of better than 8 keV (FWHM) were obtained for 20-25 MeV deuterons at the focal plane under optimum conditions.

Particle detection at the focal plane was accomplished either with nuclear emulsions or with a position-sensitive wire proportional counter.[32] The latter type of data, limited to a resolution of about 50 keV by the characteristics of

the counter, was used to supplement and confirm the results obtained by scanning the nuclear emulsions.

Three different types of targets were used in the present experiment in order to circumvent the difficulty of obtaining a clean Cl target. Targets of LiCl (^{35}Cl enrichment $\geq$99%) were used to obtain spectra free from sharp states which would arise from other chlorine compound contaminants. However, the continuous background resulting from the (p,d) reaction on the Li isotopes lowered the quality of these spectra and made it difficult to obtain accurate cross-sections for weak transitions. Sodium chloride targets (^{35}Cl enrichment $\geq$99%) provided data on Cl transitions which nicely complement those from the LiCl targets. Finally, in order to remove ambiguities resulting from overlaps of peaks from Na and Cl levels, a target of Na metal was bombarded. All of these targets were fabricated by vacuum evaporation onto thin carbon foils.

Figure 1 displays spectra, measured at 14^{o} with nuclear emulsions, which result from bombardment of the three types of targets used. These targets were of moderate thickness and the combined spectrograph-cyclotron energy resolution was not fully optimized, resulting in peak widths at half-maximum intensity of 15-20 keV. Representative particle groups in Fig. 1 are labeled as to energy of excitation. Figure 2 displays a spectrum measured at 8^{o}, with a NaCl target, for

which the energy resolution for deuterons at the focal plane was at the best level obtained in this set of experiments.

The excitation energies measured for levels of ^{22}Na and ^{34}Cl in the present experiment are used to label the peaks in Fig. 2 and are presented in Tables 1 and 2. These energies are obtained primarily from spectra measured at 8°, 11°, and 16° with a resolution of $\sim$8 keV, FWHM. In the case of many weakly excited levels, these data were supplemented by the data from the thicker targets of all three compositions. The energies were assigned as follows. The nuclear emulsion plates were scanned with a computer-linked microscope system[33] in which a 25-cm-long precision screw served to position the plate under the microscope objective. A stepping motor on the screw served to increment both the plate position and a position signal which was read into the computer whenever a contact was activated to signal the observation of a track. In this way, the track-density spectra were generated with high accuracy and reliability as regards both peak positions and intensities. The dominant peaks in the spectra were then tentatively assigned to known levels in ^{22}Na, ^{34}Cl, ^{11}C, ^{15}O, ^{12}C, ^{35}Cl, and ^{23}Na for which accurate ($\leq$1 keV uncertainty) excitation energies exist. All of these residual nuclei were formed from the (p,d) and (p,p) reactions on ^{35}Cl, ^{23}Na, and on the ^{12}C and ^{16}O contaminants in the targets. The momenta of the deuteron and proton groups corresponding to

Figure 1. Complementary spectra from the (p,d) reaction on the ^{23}Na, ^{23}Na-^{35}Cl and Li-^{35}Cl targets, measured at 35 MeV and 14°, as recorded on nuclear emulsion plates. The resolution of the deuteron groups is 15-20 keV, FWHM. Selected peaks are labeled with excitation energy assignments from the present work, the "boxed" values indicating levels in ^{34}Cl.

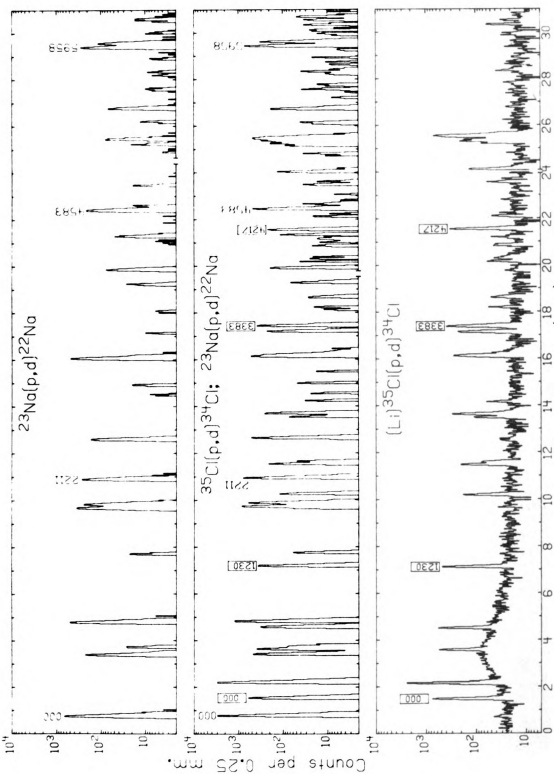
^{23}Na(p,d)^{22}Na
^{35}Cl(p,d)^{34}Cl; ^{23}Na(p,d)^{22}Na
(Li)^{35}Cl(p,d)^{34}Cl
Counts per 0.25 mm.
Plate Distance(cm.)
000
1230
2211
3383
4217
5358
4583
4217
3383
2211
1230
000

Figure 1

Figure 2. A spectrum from the (p,d) reaction on the ^{23}Na-^{35}Cl target, measured at 35 MeV and 8°, as recorded on nuclear emulsion plates. The resolution of the deuteron groups is 8 keV, FWHM. All excitation energy values are from the present work, with those "boxed" indicating levels in ^{34}Cl.

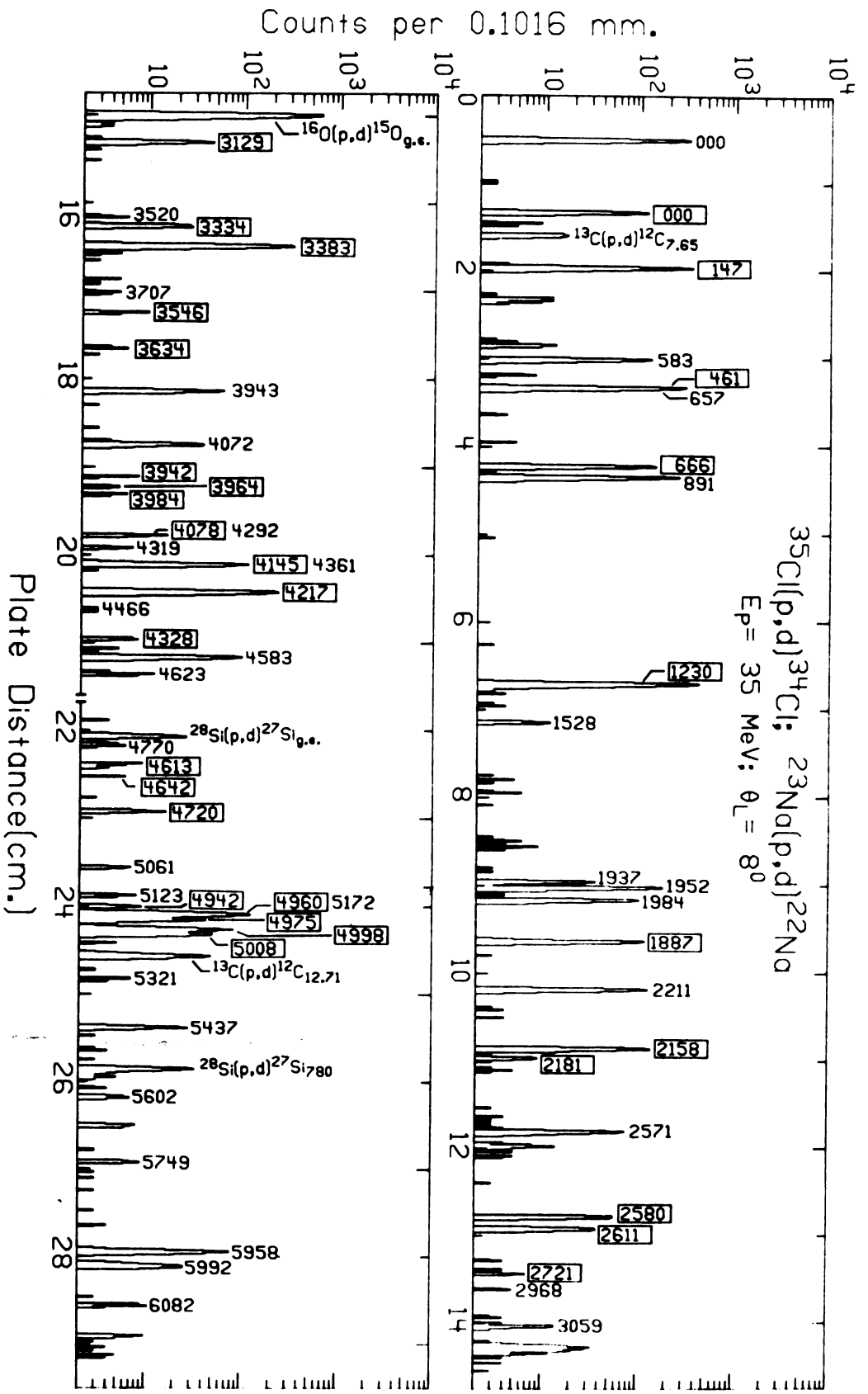
Counts per 0.1016 mm.
10
10²
10³
10⁴
Plate Distance(cm.)
16
18
20
22
24
26
28
0
2
4
6
8
10
12
14
$^{35}Cl(p,d)^{34}Cl$; $^{23}Na(p,d)^{22}Na$
E_p= 35 MeV; θ_L= 8°
$^{16}O(p,d)^{15}O_{g.s.}$
3129
3520
3334
3383
3707
3546
3634
3943
4072
3942
3964
3984
4078
4292
4319
4145
4361
4217
4466
4328
4583
4623
$^{28}Si(p,d)^{27}Si_{g.s.}$
4770
4613
4642
4720
5061
5123
4942
4960
5172
4975
4998
5008
$^{13}C(p,d)^{12}C_{12.71}$
5321
5437
$^{28}Si(p,d)^{27}Si_{780}$
5602
5749
5958
5992
6082
000
000
$^{13}C(p,d)^{12}C_{7.65}$
147
583
461
657
666
891
1230
1528
1937
1952
1984
1887
2211
2158
2181
2571
2580
2611
2721
2968
3059

Figure 2

population of these states were then calculated from the nominal settings and operating parameters of the cyclotron (beam energy) and spectrograph (scattering angle, magnetic field strength, position of emulsion plates, and non-linear corrections to the focal plane position vs. radius of curvature line) and from the nominal Q-values for the reactions. When the total spectrum spanned two emulsion plates the gap between the plates was also specified.

At this point all, or any desired subset, of the above parameters were adjusted so as to produce a least-squares fit between the set of precision energies used as input and the energies calculated to correspond to the measured peak positions. The changes in the nominal parameter values which occur when an adequately large data set is used as input are well within the experimental uncertainties associated with the various parameters. For example, typical beam energy changes are $\lesssim$10 keV out of 35 MeV, angle changes are $\leq 0.1^{o}$, and plate-gap changes are 0.0 to 0.1 mm. The appropriate final calculated excitation energies agree with the input values to $\pm$1 keV on the average. As input, we used essentially all level energies in ^{22}Na and ^{34}Cl below 3 MeV excitation[9,15,18,34] the ground[34] and first excited states[67,89] of ^{11}C and ^{12}C, the ground states[34] of ^{15}O and ^{16}O, and the ground[34] and first two excited states[68,97] of ^{23}Na and ^{35}Cl.

We found that a statistically significant better fit to the input energies could be obtained if the $^{35}Cl(p,d)^{34}Cl$ Q-value was changed from its nominal value[34] of -10.422 MeV to -10.420 MeV and the $^{23}Na(p,d)^{22}Na$ Q-value was changed from -10.193 MeV to -10.195 MeV. These changes are not inconsistent with the assigned uncertainties of the nominal Q-values,[34] and at any rate, the excitation energy assignments depend only slightly upon whether the nominal or the adjusted Q-values are used. The levels whose excitation energies are of primary interest fall in the middle 15 cm of the 50 cm (two adjacent 25 cm plates) of exposed emulsion. The 15 cm on either side of this region are thus simultaneously calibrated to many precisely known energies and this calibration is interpolated into the middle region, where it is confirmed by one or two additional known states.

The uncertainties we assign to the excitation energies listed in Tables 1 and 2 are consistent with the scatter obtained both in analyzing the same data with different variants of the analysis procedure described above and in analyzing data taken at different angles with the same procedural details. The uncertainties are compounded from jitter in the measured peak positions, irregularities in the detailed magnetic field and focal plane structure, and inaccuracies and incompleteness in the set of input energies.

The angular distributions we present for the $^{23}Na(p,d)^{22}Na$ and $^{35}Cl(p,d)^{34}Cl$ reactions were compounded from all of the

Table 1. Excitation energies, ℓ-values, J^π and T values, and pick-up spectroscopic factors for states of ^{22}Na. All C^2S values extracted from the present data have been normalized to yield 0.59 for the ground state.

Ex (keV)		J^π,T	ℓ(^{23}Na→^{22}Na)		100 x $C^2S(\ell),C^2S(\ell+2)$--(^{23}Na→^{22}Na)		
000[a]	000[b,c,d]	3^+,0[b,c,f]	2[a]	2[c]	,59[a]	,59[g]	,59[c]
583±1	583	1^+,0	0,2	2	2,19	1,22	,24
657±1	657	0^+,1	2	2	,2	, 1	,<7
891±1	891	4^+,0	2	2	,47	,58	,57
1528±1	1528	5^+,0					
1937±1	1937	1^+,0	0		3,	3, 3)	
1952±1	1952	2^+,1	2	2	,41	7,49)	,57
1984±1	1983	3^+,0	2	2	,26	,37	,29
2211±1	2211	1^-,0	1	1	27,		27,
2571±1	2572	2^-,0	1	1	20,		21,
2968±2	2969	3^+,0	(2)	(2)	, 1	,13	,<2
3059±1	3059	2^+,0	2	2	, 3	0, 3	, 3
3520±1	3521	3^-,0	(3)		,(2)		
3707±2	3708	6^+,0					
3943±2	3944	1^+,0	0,2	0	1, 3	2, 0	3,
4072±2	4069	4^+,1	2	2	,12	14,14	,17
4292±3	4294	,0					
4319±3	4319	1^+,0	0,2		<1, 1	1, 0	
4361±2	4360	2^+,0	0,2	0,2	1, 5	4, 3	2, 2
4466±3	4466	(4^-),0					
4525±4	4522	(7^+),0					
4583±2	4583	2^-,0	1	1	40,		34,
4623±2	4622	,0					
	4708	(5^+) 0					
4770±2	4770	$0-4^+$ 0		(2)			, 9
5061±4	5061	$1-2^+$,		0,2			1, 2
5096±4	5099						
5123±3	5117						
5172±3	5165	$(2)^+$,1	0,2	0,2	2,18	, 9	7 ,15
5321±3	5317						
5437±3	5440	-,	1	1	11,		8,
5602±3	5605	+,		0,2			1, 2
5719±4 / 5749±4	5740						
5826±6	5830			n.s.			
5861±5	5858			0,2			<1, 2
	5938						
5958±4	5953	,1	1	1	50,		58 ,
5992±4	5995		2	2	,15		,13
6082±4	6088						

[a] Present work.
[b] Reference 9.
[c] Reference 10.
[d] Reference 11.
[e] Reference 13.
[f] Reference 12.
[g] Reference 4.

Table 2. Excitation energies, ℓ-values, J^{π} and T values, and pick-up spectroscopic factors for states of ^{34}Cl. All C^2S values extracted from the present data are normalized such that $C^2S=0.35$ for the ground state.

Ex (keV)			J^{π},T	ℓ		$100 \times C^2S(\ell), C^2S(\ell+2)$--($^{35}Cl \rightarrow ^{34}Cl$)			
000[a]	000[b,c,d]	e	$0^+,1$[b,c,d]	2[a]	2[d]	, 35[a]	,43[f]	, 31[g]	, 45[h]
147±1	146		$3^+,0$	2	2	,105		,106	,120
461±1	461		$1^+,0$	0,2	0,(2)	11, 23		18, 15	0, 28
666±1	666		$1^+,0$	0,2	2,(0)	4, 28		1, 32	16, 0
1230±1	1230		$2^+,0$	0,2	0	23, 20		18, 9	50, 0
1887±1	1888		$2^+,0$	0,2	(0)	5, 11		2, 14	16, 0
2158±1	2159	2127	$2^+,1$	0,2	2	8, 11	12,	5, 11	32, 0
2181±1	2181		$2,3^+,0$	2		, 4		, 0	assume J=2
2377±3	2377		$4^+,0$	(2)		, 3		, 0	
2580±1	2579		$1^+,0$	0,2	(0)	5, 5		0, 4	
2611±1	2611		,0	2	(2)	, 25		0, 42	assume J=4
2721±2	2722		$2^-,0$	3	3	, 3			
3129±2	3126		$1^+,0$	0,2	2	1, 20		4, 6	
3334±2	3332		,0	2	(2)	, 25		, 34	assume J=3
3383±2	3381	3303	$2^+,1$	0,2	2	26, 25	35,	25, 12	75, 0
3546±2	3545		$3^-,0$		1				
3602±3	3601		$4^{(-)},0$						
3634±3	3632		$5^-,0$		3				
	3771		$1^-,0$		(1)				
3865±5									
3942±4	394(0)	3914	$0^+,1$					, 1	
3964±4									
3984±4	3982		$3^-,0$		3				
4078±4	4075		$4^-,0$		3				
4145±4	4140		$2^-,0$		1,3				
		4072	$1^+,1$					17, 4	
4217±2		4115	$2^+,1$	0,2		16,20	30,	0, 18	30,0
4328±4									
	4352		$(1)^-,0$		1				
	4416		$(1-3)^-,0$		1				
4465±5	4460		$(2,3)^-,0$		1				
	4514		$(2)^-,0$		1				
4613±4	4605		$(1-3)^-,0$		1				
4642±5	4636	4622	$(1-3)^-,1$		1				
4720±5	4720	4687	$4^+,1$	2		, 21	,21	, 5	
4860±6		(4875)	(3^+)						
4942±5		(4891)	(2^+)						
4960±5									
4975±5	497(0)	5227	$0^+,1$				,40		
4998±3									0,170
5008±3		5318							
5560±6		5380							

[a]Present Work.

[b]Reference 15.

[c]Reference 16.

[d]Reference 17.

[e]Energies for states in ^{34}S; References 26,27.

[f]Spectroscopic factors for $^{35}Cl(d,^3He)^{34}S$; Reference 25.

[g]Reference 2.

[h]Reference 22.

data accumulated from the different targets and with the different detection mechanisms. Of course, when lack of resolution prevented unambiguous values from being obtained in particular cases, such data were rejected. Also, in some cases the track density of strongly excited levels was too high to permit accurate counting by the scanners, so that counter data alone was relied upon. The angular distributions for states in ^{22}Na are shown in Figs. 3, 4, and 5 and those for levels in ^{34}Cl in Figs. 6 and 7. Not all states listed in Tables 1 and 2 could be observed at enough angles to permit measurement of meaningful angular distributions. These states were at best weakly populated and are not included in Figs. 3-7.

The cross-section scales in Figs. 3-7 were assigned by comparing the (p,d) differential cross-sections as measured with the wire proportional counter to the (p,p) elastic differential scattering cross-sections in the vincity of the maximum in the 30^{o}-50^{o} region. The counting rates for the elastic scattering were manageable for the counter in this region and the Na and Cl peaks could be resolved clearly. The elastic scattering distributions were normalized to the predictions obtained from the Becchetti-Greenlees optical model potential formula[37] (see APPENDIX B). The experimental angular distributions for ^{23}Na and ^{35}Cl in this region are rather dissimilar and both were simultaneously well fit with the Becchetti-Greenlees predictions. We estimate a 10% uncertainty for the

accuracy of the optical model cross-sections in this region, and estimate a 10% probable error for the mechanics of relating the experimental (p,d) yields to the (p,p) yields. Thus, the combined total uncertainty in the overall cross-section normalization of our angular distributions is estimated to be in the range of 15%.

The relative uncertainties from distribution to distribution should be less than 2%. The chemical stability of sodium chloride appears to be maintained under evaporation and bombardment, so the relative Na to Cl cross-sections should also be good to 2%.

II.3. Analysis of the Angular Distributions

The angular distributions displayed in Figs. 3-7 were analyzed with the distorted-wave Born approximation (DWBA)[38] to obtain ℓ-values for the neutrons transferred in the (p,d) pick-up process and the associated strengths, or spectroscopic factors. This analysis was carried out by least-squares fitting a combination of $\ell=0$ and $\ell=2$ (or $\ell=1$ and $\ell=3$) curves, predicted for a transition of given Q-value, to the 3^{o}-35^{o} experimental data for each state. The solid curves in Figs. 3-7 show the combined-ℓ theoretical distribution fits from which the spectroscopic factors were obtained. The dotted curves indicate the contribution of the smaller ℓ-value pattern to the combined (solid line) distribution curves.

Figure 3. Experimental angular distributions for states in ^{22}Na as observed in the $^{23}Na(p,d)^{22}Na$ reaction at 35 MeV. The solid curves are fits of the DFRNL calculations to the data in the angular range from 3° to 35°. The dotted curves show the contribution of the first indicated ℓ-value for mixed-ℓ distributions.

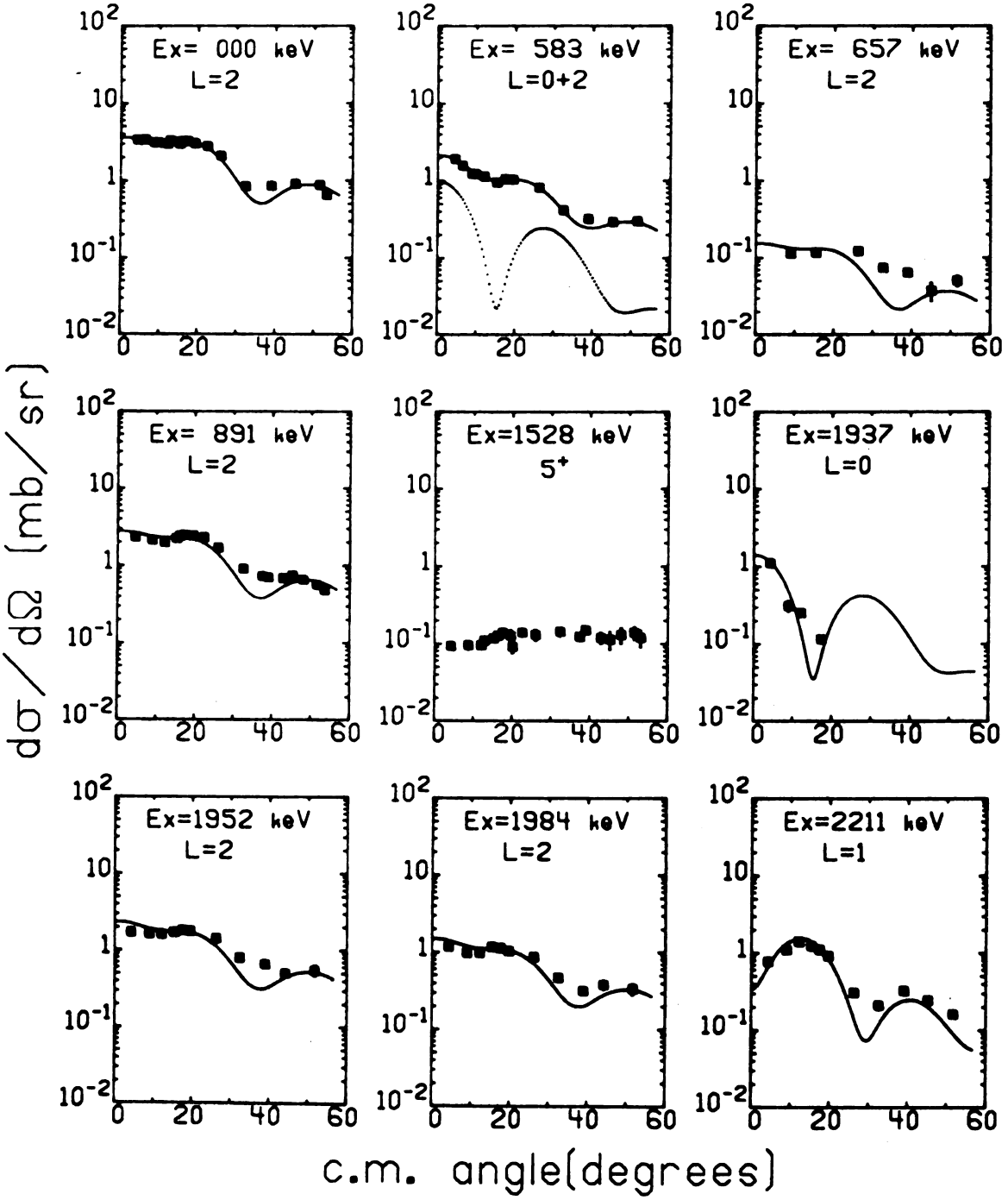
Ex= 000 keV
L=2
Ex= 583 keV
L=0+2
Ex= 657 keV
L=2
Ex= 891 keV
L=2
Ex=1528 keV
5+
Ex=1937 keV
L=0
Ex=1952 keV
L=2
Ex=1984 keV
L=2
Ex=2211 keV
L=1
dσ / dΩ (mb/sr)
c.m. angle(degrees)

Figure 3

Figure 4. Experimental angular distributions for states in ^{22}Na as observed in the ^{23}Na(p,d)^{22}Na reaction at 35 MeV. The solid curves are fits of the DFRNL calculations to the data in the angular range from 3° to 35°. The dotted curves show the contribution of the first indicated ℓ-value for mixed-ℓ distributions.

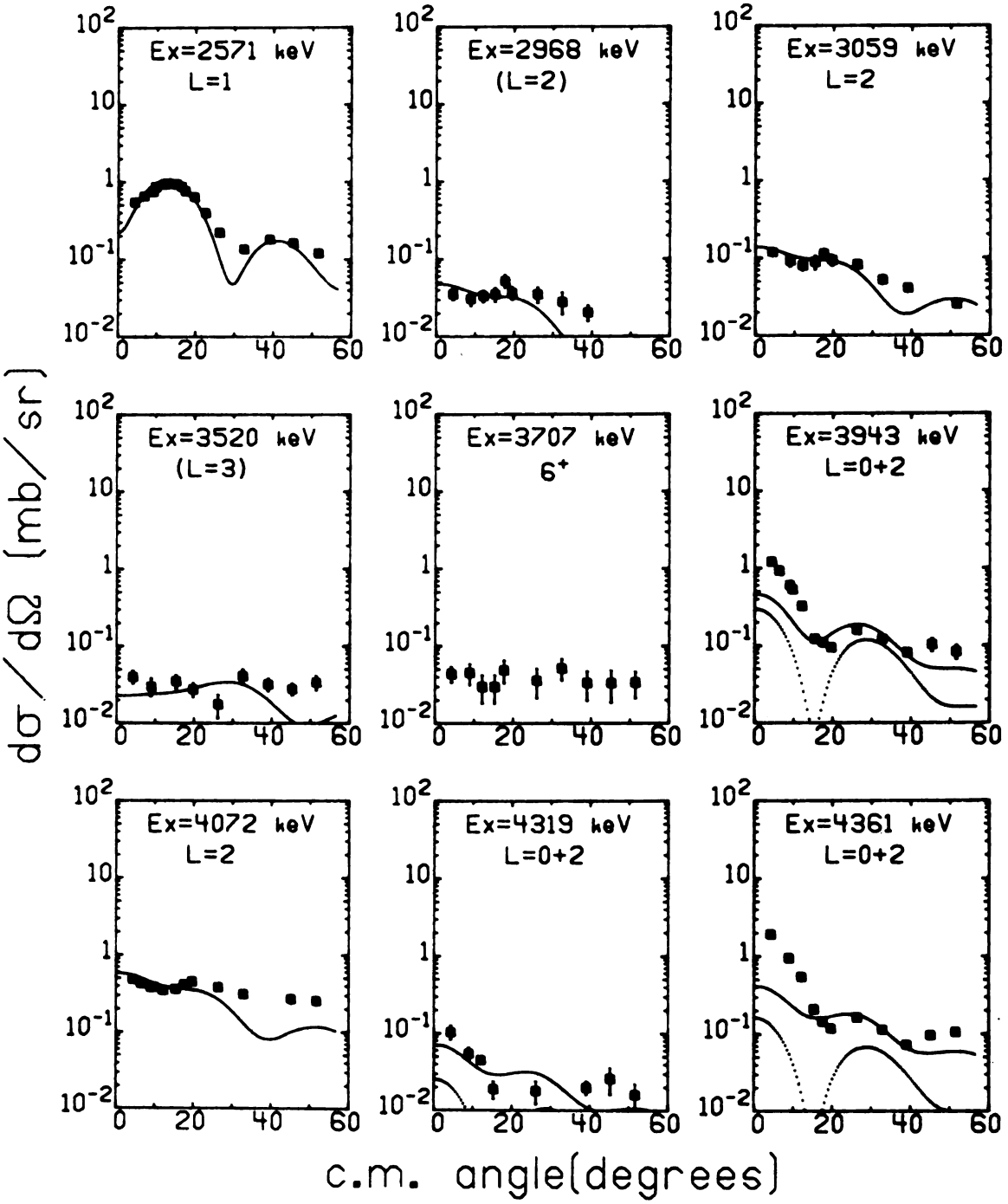
Ex=2571 keV
L=1
Ex=2968 keV
(L=2)
Ex=3059 keV
L=2
Ex=3520 keV
(L=3)
Ex=3707 keV
6+
Ex=3943 keV
L=0+2
Ex=4072 keV
L=2
Ex=4319 keV
L=0+2
Ex=4361 keV
L=0+2
dσ / dΩ (mb/sr)
c.m. angle(degrees)

Figure 4

Figure 5. Experimental angular distributions for states in ^{22}Na as observed in the $^{23}Na(p,d)^{22}Na$ reaction at 35 MeV. The solid curves are fits of the DFRNL calculations to the data in the angular range from 3^{o} to 35^{o}. The dotted curves show the contribution of the first indicated ℓ-value for mixed-ℓ distributions.

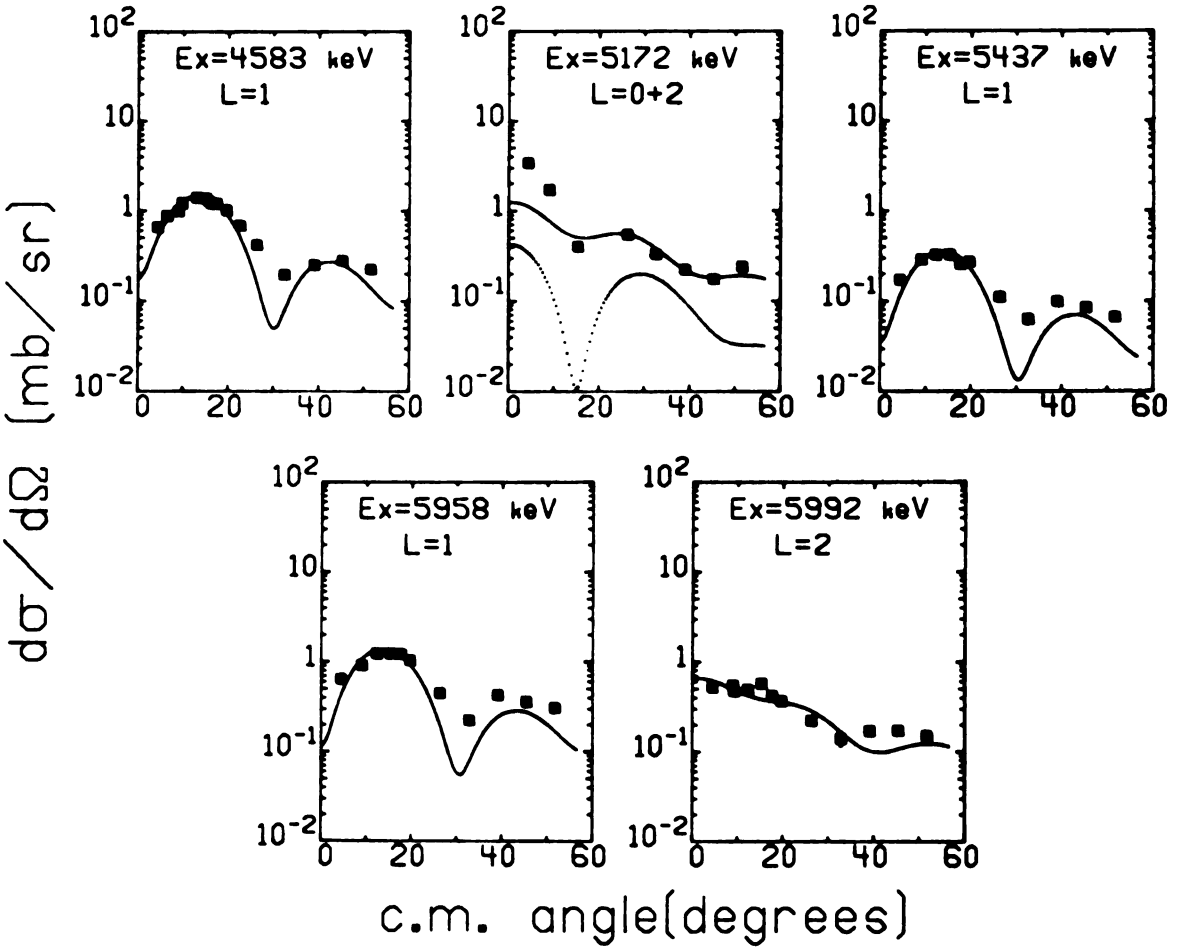
Ex=4583 keV
L=1
Ex=5172 keV
L=0+2
Ex=5437 keV
L=1
Ex=5958 keV
L=1
Ex=5992 keV
L=2
dσ/dΩ (mb/sr)
c.m. angle(degrees)

Figure 5

Figure 6. Experimental angular distributions for states in ^{34}Cl, as observed in the $^{35}Cl(p,d)^{34}Cl$ reaction at 35 MeV. The solid curves are fits of the DFRNL calculations to the data in the angular range from 3° to 35°. The dotted curves show the contribution of the first indicated ℓ-value for mixed-ℓ distributions.

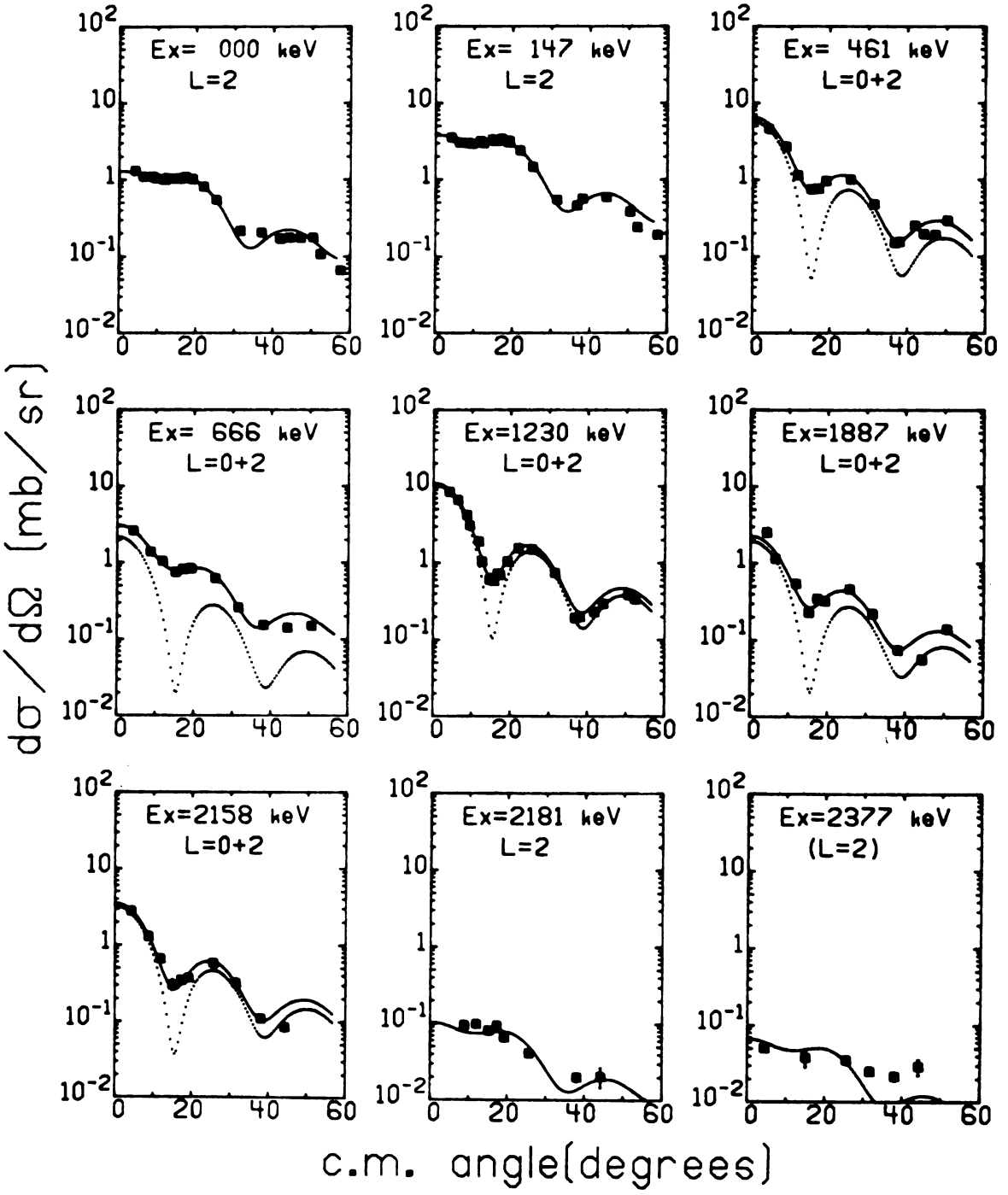
Ex= 000 keV
L=2
Ex= 147 keV
L=2
Ex= 461 keV
L=0+2
Ex= 666 keV
L=0+2
Ex=1230 keV
L=0+2
Ex=1887 keV
L=0+2
Ex=2158 keV
L=0+2
Ex=2181 keV
L=2
Ex=2377 keV
(L=2)
dσ/dΩ (mb/sr)
c.m. angle(degrees)

Figure 6

Figure 7. Experimental angular distributions for states in ^{34}Cl, as observed in the $^{35}Cl(p,d)^{34}Cl$ reaction at 35 MeV. The solid curves are fits of the DFRNL calculations to the data in the angular range from 3° to 35°. The dotted curves show the contribution of the first indicated ℓ-value for mixed-ℓ distributions.

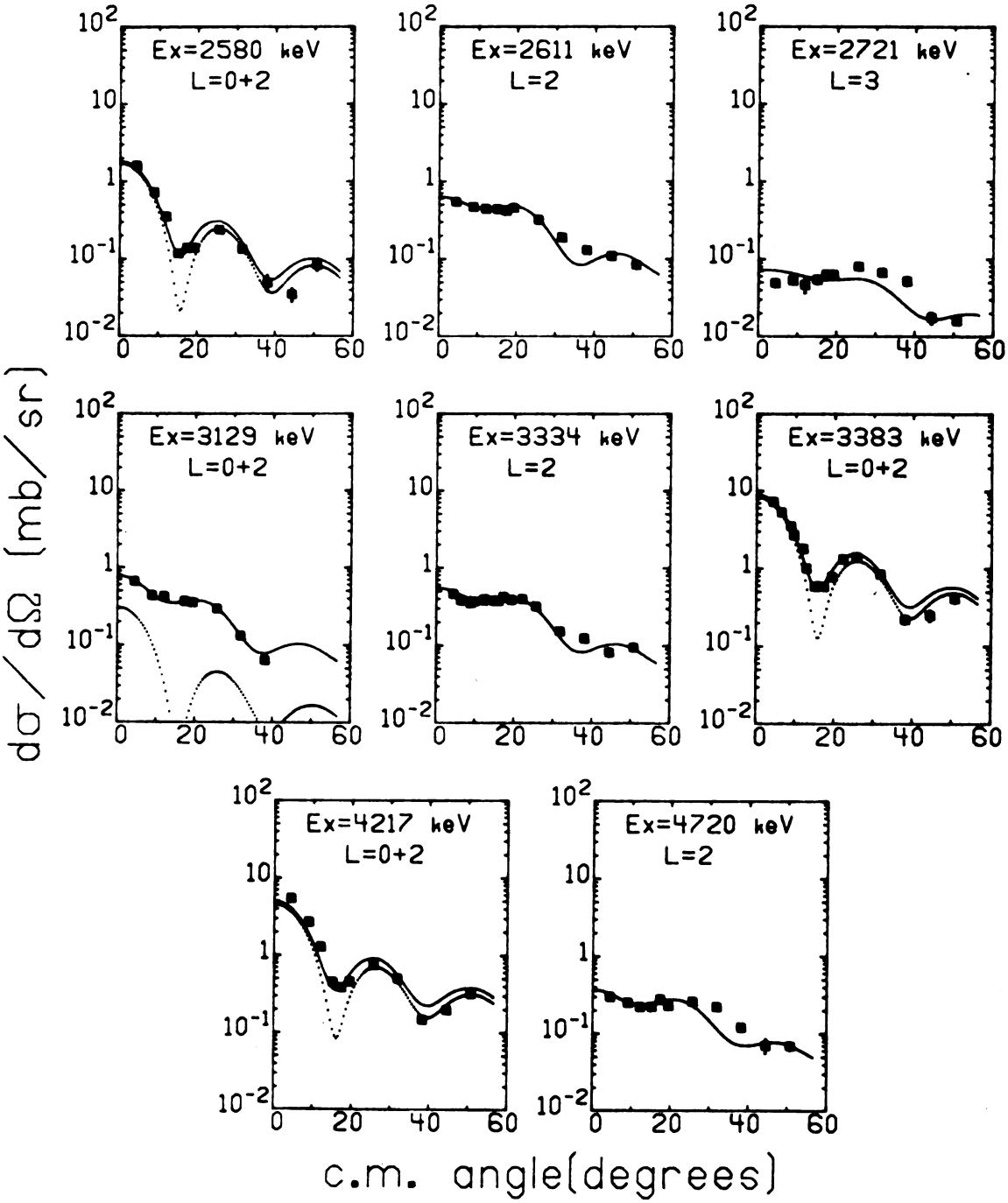
Ex=2580 keV
L=0+2
Ex=2611 keV
L=2
Ex=2721 keV
L=3
Ex=3129 keV
L=0+2
Ex=3334 keV
L=2
Ex=3383 keV
L=0+2
Ex=4217 keV
L=0+2
Ex=4720 keV
L=2
dσ/dΩ (mb/sr)
c.m. angle(degrees)

Figure 7

Many previous studies of the (p,d) and (d,p) reactions in the 15-40 MeV range of particle energies have experienced serious difficulties in analyzing the experimental angular distributions with the DWBA. Detailed studies[39,40] on ^{208}Pb and ^{16}O are particular examples. The difficulties involved obtaining good fits to given ℓ-value transitions at particular energies and maintaining stable, good fits and consistent spectroscopic factors over a range of ℓ-values, beam energies, and Q-values. Problems specifically involving the relationship between DWBA predictions and experiment as a function of the Q-value of the reaction (corresponding to different bindings of the transferred neutron to the core) have been studied extensively[41,42] in the f-p shell with the aid of sum-rule arguments.

A general feature of past DWBA analyses of (p,d) angular distributions has been that the local, zero-range predictions were improved, vis a vis the experimental shapes, by introducing a cut-off in the radial integration somewhere near the nuclear surface. It has been proposed[43] and demonstrated[44-47] that an alternate prescription, the "adiabatic" deuteron, to the usual elastic-scattering-based deuteron optical model potential can, in a more physically motivated way, provide all of the benefits obtained by the use of cut-offs. A second alternative, also more plausible and successful than the sharp cut-off technique, involves making finite-range and

non-locality approximation corrections and, in addition, introducing a density-dependent damping of the V_{pn} interaction.[48]

The many angular distributions obtained in the present experiment, measured with good statistical accuracy and energy resolution in the 4^{o}-40^{o} angular range, provide the basis for a very thorough critique of current DWBA procedures for (p,d) reactions on medium-light nuclei. We have carried out DWBA calculations using a variety of different prescriptions for the various input parameters and have compared the results with our data.

The present DWBA calculations were all made with the computer code DWUCK.[49] The parameters of the optical model potential for 35 MeV protons were obtained from the formulae of Becchetti and Greenlees.[37] The formulae of Fricke, et al.,[50] predict discernably different elastic scattering angular distributions for s-d shell nuclei, but the DWBA predictions for (p,d) seem largely insensitive to changing from one proton potential to the other.

When any of the conventional[51-55,98] deuteron optical-model potentials are used, the calculated shapes of the ℓ=0 and ℓ=2 distributions agree much better with our experimental test cases in the finite-range, non-local (FRNL) approximation than in the local, zero-range (LZR) approximation. (The non-locality parameters used were the standard values of 0.85 and 0.54 for the proton and deuteron, respectively.) The best

results obtained with any of these various potentials appear to be obtained with the "Set I" values of Hinterberger, et al.[51] (see Table 3), which is gratifying since this potential is probably the best grounded in terms of mass and energy dependence. The Hinterberger et al. "Set II" and the Newman, et al.[52] potentials yielded results very similar to each other and not too different from those of "Set I".

The critical success of Hinterberger "Set I", relative to potentials of different origins, lies in its correct reproduction of the forward angle ($\theta_{cm} \leq 20^{o}$) $\ell=0$ and $\ell=2$ shapes. Its principle failing, shared by all the others to a greater or lesser extent, is its overestimation of cross-sections at larger angles ($\theta_{cm} \geq 30^{o}$), a failing which grows more pronounced as the Q-values become more negative (excitation energies increase). Previous investigations led us to expect that both the "adiabatic"[43] and the "density-dependent"[46] alterations to the conventional DWBA procedure would improve the predictions at these larger angles. The "adiabatic" potential, designed to account for effects resulting from disassociation of the deuteron, is put together from proton and neutron optical model potentials (taken from Ref. 37 in the present instance) according to a particular prescription.[43,44] The adiabatic-potential calculations were carried out in the LZR approximation, since the FRNL corrections did not yield significantly different results.

Table 3. Optical-model parameters used in the analysis of the $^{23}Na(p,d)^{22}Na$ and $^{35}Cl(p,d)^{34}Cl$ data.

Particle	V_R (MeV)	r_R (fm)	a_R (fm)	W_V (MeV)	r_V (fm)	a_V (fm)	W_{SF} (MeV)	r_{SF} (fm)	a_{SF} (fm)	V_{SO} (MeV)	r_{SO} (fm)	a_{SO} (fm)	r_c (fm)
$^{23}Na(p,d)^{22}Na$:													
Proton[a]	45.39	1.17	0.75	5.0	1.32	0.54	3.57	1.32	0.54	6.2	1.01	0.75	1.17
Deuteron[b] (FRNL and DFRNL)	84.89-0.35 E_{cm}	1.25	0.743				13.0	1.25	0.723	6.0	1.25	0.743	1.30
Deuteron[c] (ADIABATIC)	102.59[d]	1.17	0.779	1.17[d]	1.29	0.589	17.33[d]	1.29	0.583	6.2	1.01	0.75	1.17
$^{35}Cl(p,d)^{34}Cl$:													
Proton[a]	45.57	1.17	0.75	5.0	1.32	0.53	3.39	1.32	0.53	6.2	1.01	0.75	1.17
Deuteron[b] (FRNL and DFRNL)	86.92-0.35 E_{cm}	1.25	0.733				13.0	1.25	0.755	6.0	1.25	0.733	1.30
Deuteron[c] (ADIABATIC)	103.41[d]	1.17	0.779	1.13[d]	1.29	0.589	17.41[d]	1.29	0.583	6.2	1.01	0.75	1.17
Neutron Bound State[e]	Adjusted to match separation energy	1.24	0.65							λ=25			1.24

[a] Reference 37.

[b] Reference 51.

[c] Reference 43; proton and neutron parameters from Reference 37.

[d] Values shown are for E_x=0.00 MeV only; Q-dependence is as given in Reference 37.

[e] For both reactions.

The "density-dependent damping" of the V_{pn} interaction[48] provides an alternate means to reduce cross-sections at larger angles. We use here the damping factor $F(r)=(1.0-1.845\rho(r)^{2/3})$, where $\rho(r)=0.17[1+\exp(x)]^{-1}$, $x=(r-r_oA^{1/3})/a$ and "r_o" and "a" are the radius and diffusivity of the neutron bound-state well. The density-dependent V_{pn} damping was studied in conjunction with FRNL calculations which used the Hinterberger, et al. "Set I" deuteron potentials.

We have analyzed our data in detail with the following DWBA calculations (see Table 3): (1) The Becchetti-Greenlees[37] proton parameters and Hinterberger, et al.[51] "Set I" deuteron parameters, using the FRNL approximation. These calculations, henceforth referred to as FRNL, are thus completely orthodox and unadjusted. (2) This same combination of proton and deuteron parameters and computational approximations, but with the addition of the density-dependent damping of the V_{pn} interaction, henceforth referred to as DFRNL, and (3) The Becchetti-Greenlees proton parameters and the adiabatic deuteron parameters in the LZR approximation, henceforth referred to as ADIABATIC.

The results of these three types of DWBA calculations are compared with each other and with some of our experimental data for the $^{35}Cl(p,d)^{34}Cl$ reaction in Fig. 8. The virtue of the DFRNL shapes is clearly evident over the range of excitation energy in ^{34}Cl shown therein.

Figure 8. A comparison of fits to representative angular distributions from the $^{35}Cl(p,d)^{34}Cl$ reaction at 35 MeV with the three chosen types of DWBA calculations. All fits were performed over the angular range from 3° to 35°. The curves are identified as follows: ———DFRNL, -----FRNL, and — —ADIABATIC.

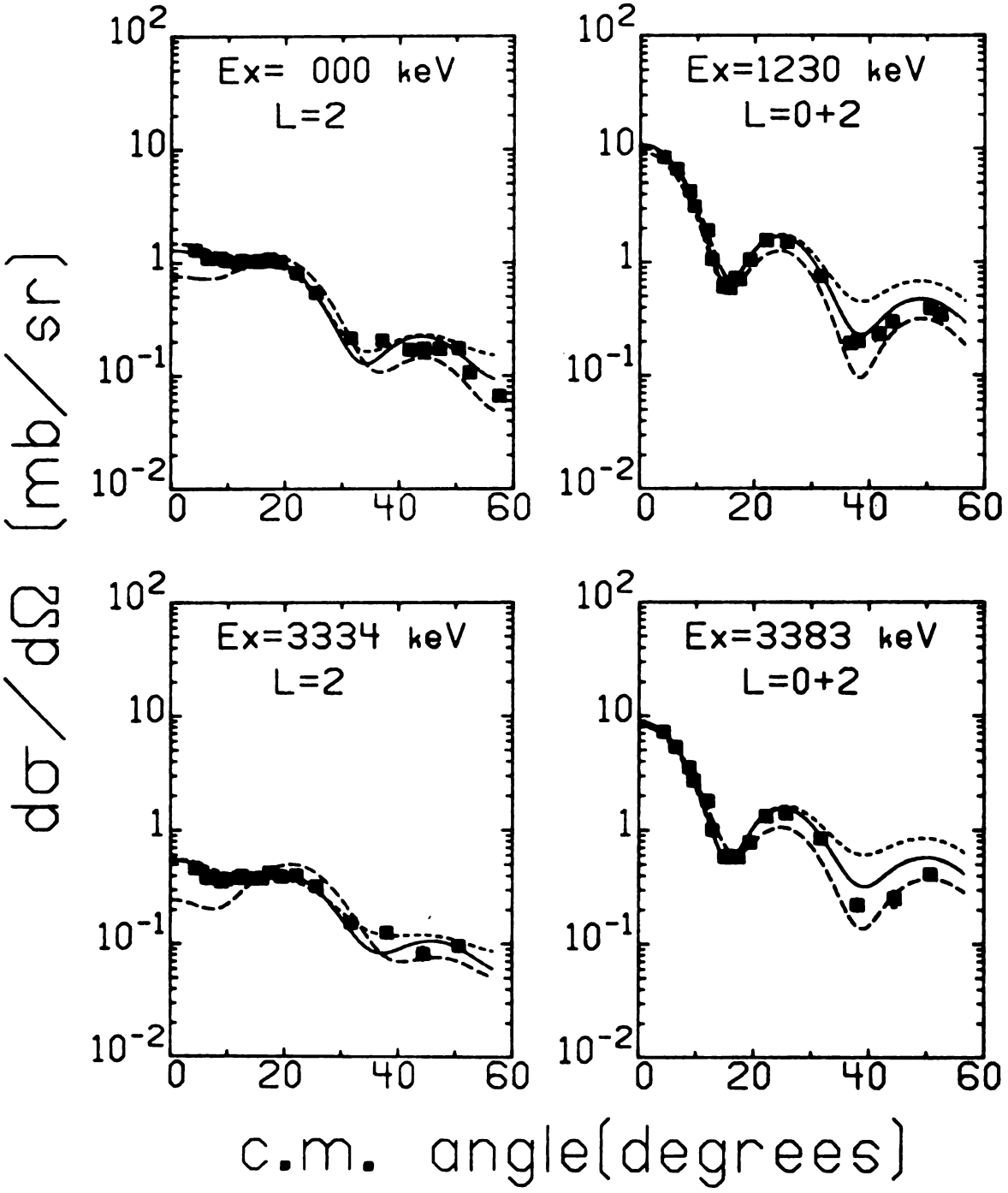
Ex= 000 keV
L=2
Ex=1230 keV
L=0+2
Ex=3334 keV
L=2
Ex=3383 keV
L=0+2
dσ / dΩ (mb / sr)
c.m. angle(degrees)

Figure 8

II.4. Discussion of Results

II.4.A. Levels of ^{22}Na

Experimental evidence on the energies, spins, parities, and other properties of levels in ^{22}Na has been accumulated principally at Brookhaven (see the literature cited in Ref. 9) via studies of the gamma-ray decays of these levels, and at the University of Pennsylvania via charged particle transfer studies. These works have resulted in precise excitation energy assignments to all of these low-lying levels plus some higher excited states, and a rather complete catalog of what levels exist up through 6 MeV excitation. With the (p,d) reaction at 35 MeV, we observe evidence for the existence of all but 2 of the 38 previously identified levels below 6 MeV excitation in ^{22}Na (see Table 1). The two unobserved levels are very weakly excited in analogous reactions. We observe one new level, at 5.719 MeV, unresolved in previous work. Our assigned excitation energy values agree with previous assignments to within the 1-2 keV combined uncertainties up through 4 MeV excitation. Between 4 and 5 MeV, agreement in excitation energies between the present and previous results is still good, although uncertainties and deviations are both in the 2-4 keV range for that region. From 5 to 6 MeV, there are some significant discrepancies between the present assignments and previous values, which, in this region, have all resulted from

magnetic analysis of charged particle reactions. These discrepancies seem to involve spacings between levels rather than more understandable systematic deviations of scale.

The present assignments (Table 1) for the ℓ-values of the various transitions are, in all cases, consistent with the consensus assignments of J^{π} and with the results of the analysis of $^{23}Na(^{3}He,^{4}He)^{22}Na$ data.[10] The relative values for spectroscopic factors extracted from the present data agree qualitatively with the numbers obtained from the $(^{3}He,^{4}He)$ work. However, the failure to obtain a good $\ell=0$ fit to the data with the present DWBA calculations leaves a large uncertainty in our values for $C^{2}S$ $(\ell=0)$. There are some individual deviations between present and previous spectroscopic factors, such as the different ratios of the strengths of the first 3^{+} state to the first 4^{+} state, which might indicate some differences either in the behavior of the DWBA for these two kinds of reactions or in which alternate reaction mechanism is the most significant contributor to the direct single-step process. The results of the analysis of (p,d) data taken at 17.5 MeV for the lowest few states[35] are also consistent with the present analysis.

The observed features of the positive-parity levels of ^{22}Na, as regards electromagnetic decay and single-nucleon transfer population, have been extensively interpreted in the framework of the Nilsson model.[10,36] The most detailed

shell-model analysis of this system,[4] carried out with complete consistency for the A=19, 20, 21, and 22 systems, treats all of the same observables with a uniformly higher degree of success. The spectroscopic factors predicted for $^{23}Na \rightarrow ^{22}Na$ transitions are listed in Table 1. The shell-model predictions agree with the experimental results for spectroscopic factors within reasonable uncertainties for the first six states. The $\ell=0$ spectroscopic factor for the first 2^+, T=1 state, predicted to be $C^2S=0.07$, is observed to be less than 0.01. Even though the magnitudes are rather small, this might be an important clue to a failing of the wave functions involved. Larger $\ell=2$ spectroscopic factors are predicted for the second and third 3^+ states than are observed, in particular for the third, at 2.968 MeV excitation.

II.4.B. Results for ^{34}Cl

The energies of the levels in ^{34}Cl have been assigned by a combination of gamma-ray decay and single nucleon stripping experiments. The combined uncertainties of the two kinds of experiments are such that unique identification of states above 3.5 MeV excitation is not always possible. We present in Table 2 a composite of the results of these previous experiments, but do not attempt to quote errors. The uncertainties in the energies of levels below 3.5 MeV are all based on gamma ray measurements and should be good to the order of a kilovolt, or better.

The level energies extracted from the analysis of our data, and their assigned uncertainties, are in agreement with the existing values up through 3.5 MeV excitation. The largest deviation, 3 keV, occurs for the "3129" keV state. All levels previously well established to lie in the 0.0-3.5 MeV region are seen in the present data. The level located by Erskine, et al.[17] at 1924 keV, and not seen in any other work, is not observed here. Nonetheless, its existance is not implausible in the context of theoretical spectra for ^{34}Cl, which predict a few low-lying levels with vanishing spectroscopic factors. Above 3.5 MeV we fail to observe several states seen in previous work. All of these levels would be expected to be weakly populated via pick-up. This, together with the high density of peaks in this region, makes observation of these levels at enough angles to insure unambiguous identification difficult. At the same time, we excite several levels in the 3.5-5.0 MeV region which have not been previously reported. Most of these are also weakly excited, but a few have significant strengths and are hence of special interest in the present spectroscopic picture.

The third 2^+ and the first 1^+ levels are known to lie close to 4.1 MeV excitation in ^{34}S (see Table 2) and should occur at about the same energy in ^{34}Cl. All theoretical calculations predict a significant $\ell=2$ pick-up spectroscopic factor for this 2^+ and a strong $\ell=0$ strength for the 1^+. The

"level" we observe at 4217 keV has both of these properties. The 1^+ and 2^+ levels in ^{34}S are separated by 43 keV, the 1^+ lying lower. The first two 2^+, T=1 states in ^{34}Cl are raised in excitation energy relative to their positions in ^{34}S by 32 and 78 keV, respectively. The second of these levels has three times the ℓ=0 pick-up strength of the first, and we may consider it, crudely, as a $s_{1/2}^{-1}d_{3/2}^{3}$ state relative to the $d_{3/2}^{2}$ nature of the first 2^+ level. The difference in energy shift is quite probably associated with this empirically established difference in the wave functions.

The first 1^+, T=1 state should be $(s_{1/2}^{-1}d_{3/2}^{3})$ in nature also. All structure calculations agree on this point, and the stripping data in consistent, though not confirmatory, with these predictions. The third 2^+ level is empirically determined to be mainly $d_{3/2}^{2}$ in character. Thus, if the energy shifts observed for the lowest two 2^+ states were to be replicated by the third 2^+ and the first 1^+, the 1^+ level would move up by 46 keV more than the 2^+. This difference would almost exactly cancel out the 43 keV gap between the corresponding states in ^{34}S. Hence, the very close degeneracy of these levels in ^{34}Cl would not be a completely unreasonable possibility. However, it must be noted that the total shift of these levels, which must occur if they together form the 4.217 MeV peak, is greater than that observed for the lower two excited T=1 states. Nonetheless, if this peak is not a doublet we have a rather clear-cut discrepancy with theory on our hands as regards spectroscopic factors.

The excited 0^+, T=1 states, populated strongly via the $^{36}Ar(p,^3He)^{34}Cl$ reaction, should be very weakly populated in the present single nucleon pick-up experiment. We have tentatively assigned the 3942 keV state as 0^+, T=1, but this is based solely on energy proximity. Likewise, we associate some of the other T=1 states observed in ^{34}S with levels we observed in the 4-5 MeV region. We do not believe that either of the two strongly excited levels at 5 MeV excitation (4998 and 5008 keV is the third 0^+, T=1 state, but suggest the 4975 keV level as a possibility.

The ℓ-values we assign are all consistent with the consensus spin assignments and stripping ℓ-values. Our results are in repeated disagreement with the previous neutron pick-up study[22] as regards dominant ℓ-value assignments and spectroscopic factors for all but the most trivial cases in the low-lying spectrum. Results are compared in Table 2. At higher energies, the lack of adequate resolution in the previous work resulted in a failure to realize several doublets, such as those at 3334 and 3383 keV, and at 4998 and 5008 keV. It should also be noted, parenthetically, that the comparison between experiment and theory in Ref. 22 is further vitiated by an inconsistent treatment of the isospin coupling factor.

There are striking similarities between the $(sd)^{-6}$-configuration spectrum of ^{34}Cl and the $(sd)^6$-configuration spectrum of ^{22}Na. Despite the formal theoretical identity and the resemblance of the sequences of the first few levels,

it must be remembered that the single particle energies and the Pauli Principle limits on orbital occupation dictate that states in ^{22}Na are dominantly formed out of $d_{5/2}$ configurations while the features of the low-lying levels of ^{34}Cl arise from some mixture of $d_{3/2}$ and $s_{1/2}$ couplings. The first step to understanding the structure of these latter levels is to determine the way in which $s_{1/2}$ and $d_{3/2}$ particles contribute to each of the individual wave functions.

The two kinds of reactions which most directly relate to this issue are single-nucleon stripping from ^{33}S and one nucleon pick-up from ^{35}Cl. The (^{3}He,d) and (d,p) reactions[17,26] on ^{33}S have been studied with good energy resolution.

The results of the ℓ-value assignments from these works are noted in Table 2. If a simple $d^1_{3/2}$ model is assumed for ^{33}S, the measured stripping spectroscopic factors indicate that the "$d^2_{3/2}$" states of J^π,T = 0^+,1, 3^+,0, and 1^+,0 are the ground, first, and third excited states, with the 1^+ strength being slightly fragmented into neighboring 1^+ levels. The $(d^2_{3/2})$ 2^+,1 configuration seems to be spread over the 2158 and 3383 states in a ratio of about 2 to 1. Many of the levels show some ℓ=0 strength, indicating a significant lack of closure in the $s_{1/2}$ orbit. A much more realistic shell-model treatment, allowing all three s-d shell orbitals to be active, accounts for a large portion of the details of the stripping results (see Ref. 3, FPSDI Hamiltonian results).

If we assume the simplest model, $(d_{3/2}^3)$, for the ^{35}Cl ground state, then the present pick-up results express the following qualitative picture. Again, the 0^+,1 and 3^+,0 states resemble $(d_{3/2}^2)$ states. The $(d_{3/2}^2)$ configuration is spread almost equally over the first three 1^+,0 states and is again split between the 2^+,1 states at 2.158 and 3.383 MeV. This time, however, the ratio is 1 to 2. The dominant impression yielded by the spectroscopic factor results is, however, one of complexity. Simple shell-model pictures are only faintly suggestive of the complex structure of the low-lying levels revealed in pick-up and stripping. This detailed structure observed in pick-up is also, however, quite well reproduced by the same three-orbit shell-model calculation just mentioned.

The predictions this calculation yields for pick-up spectroscopic factors for the levels of ^{34}Cl are presented in Table 2 for comparison with the experimental results. The correspondences between the lowest eight or so states, and for a few selected higher levels, are quite good. This, together with the almost comparable success obtained for stripping, indicates that the complex shell-model wave functions for these levels have many of the properties required of a realistic and thorough description of the physical states. There are several discrepancies between theory and experiment for higher-lying states. The lack of spin assignments for some of these higher states prevents a more definitive critique of the model results. In Table 2 we have therefore entered

some theoretical states which have significant spectroscopic factors and appropriate energies in line with states of unknown spin.

The spectroscopic factor predictions from this shell-model calculation are actually more successful than are the predictions for energies. There are some inversions in level orderings and a serious compression of the theoretical spectrum. These features, as well as the spectroscopic factor failings at higher excitations, clearly indicate the need for still better calculations. The present experimental results verify, however, that the present calculations form a secure foundation upon which more advanced theoretical work may be based.

II.5. Conclusions

The DWBA analysis of the $^{35}Cl(p,d)^{34}Cl$ transitions yields good fits to the angular distributions and stable spectroscopic factors. The $^{23}Na(p,d)^{22}Na$ data is not fit so well. In particular, no formulation of parameters and adjustments we attempted yielded an acceptable $\ell=0$ shape for Na while preserving a reasonable $\ell=2$ prediction for Na and simultaneous good fits to the Cl data.

The spectroscopic factors extracted from the data are well reproduced by recent shell model calculations in the domain of approximately the lowest 10 levels. The spectroscopic

factors also facilitate identification of T=1 levels by comparison with $^{35}Cl(d,^{3}He)^{34}S$ results. Several strongly populated states still remain without a unique spin assignment, and when these are fixed, the final combined experimental picture of ^{34}Cl will offer a challenging and hopefully rewarding problem to structure theorists.

III. THE $^{37}Cl(p,d)^{36}Cl$ REACTION

III.1. Introductory Remarks

The simplest shell-model description of ^{36}Cl arises from the couplings of three $d_{3/2}$ neutrons and one $d_{3/2}$ proton. An obvious model extension is the inclusion of $s_{1/2}$ excitations.[56-58] Recently, the set of configuration basis states has been further expanded to include the $1d_{5/2}$, as well as the $2s_{1/2}$, and $1d_{3/2}$ orbits,[3,59] and initial calculations involving excitations to the f-p shell have also been made for various s-d shell nuclei.[60-61] Several residual interactions and model Hamiltonians have been used in the recent studies, yielding different results for some predicted observables. There is an obvious need for accurately determined experimental quantities in any attempt to critically evaluate, and suggest improvements for, these various models. Since calculated spectra for the odd-even and doubly-even s-d shell nuclei show good correspondence with available data while predictions for the odd-odd nuclei are often in qualitative disagreement with experiment, sound experimental knowledge of the doubly-odd systems is essential to a useful critique of recent theoretical studies.

Although many levels have been previously observed in ^{36}Cl, excitation energies have not been assigned to high accuracy and the spins of several low-lying levels are not as yet unambiguously determined. Only a few single-neutron

pick-up experiments leading to states in ^{36}Cl have been performed.[22,62-65] Spectroscopic information is consequently sparse, with the bulk of the experimental spectroscopic factors available for the strongly populated positive parity levels below 4 MeV excitation and only one negative parity state. The present work is a continuation of a comprehensive study of doubly-odd s-d shell systems via the (p,d) reaction at 35 MeV.[6-8] We have attempted to observe and catalogue as many levels in ^{36}Cl as possible, assigning them precise excitation energies and extracting spectroscopic factors for the neutron transfers which populate them. Deuteron spectra recorded on nuclear emulsion plates with a total energy resolution of 10-18 keV, FWHM, allowed the assignment of excitation energies in ^{36}Cl to $\sim$8.2 MeV with an overall accuracy of $\lesssim$1 keV/MeV. Angular distributions for states up to 8.2 MeV have been taken over a 3^{o} to 55^{o} range, with spectroscopic factors extracted and ℓ-values assigned for transitions producing analyzable distribution patterns. The forward-angle data allowed essentially parameter-free ℓ=0 spectroscopic factor extraction and a critical test of theoretical ℓ=2 shapes. The present results will be compared with previous experimental works, and their implications for theoretical studies in the upper s-d shell will be discussed.

III.2. Experimental Procedure

Targets for the present experiment were made by evaporating a sodium-chloride compound (enriched to 96.5% in the ^{37}Cl isotope) onto 30 $\mu gm/cm^2$ carbon foil backings. The targets were kept under vacuum. Consequently, target thicknesses (20-120 $\mu gm/cm^2$) were estimated from deuteron yields and assumed scattering chamber geometry. 35 MeV protons from the Michigan State University sector-focussed cyclotron were used to induce the (p,d) reaction leading to states in ^{36}Cl and ^{22}Na. Reaction products were analyzed in the MSU split-pole magnetic spectrograph, deuteron spectra being recorded both with a single-wire proportional counter[32] and on 25 micron thick nuclear emulsion plates.

Spectra were recorded with the counter at closely spaced laboratory angles from 3^o to 55^o with a total resolution of 50 keV, FWHM. The spectrograph acceptance aperature was 0.6 msr for the angular region of greatest importance (3^o to 30^o) and 1.4 msr for angles greater than 30^o. Data acquisition and particle identification is this portion of the experiment were accomplished in the MSU Sigma-7 computer. These data allowed extraction of complete angular distributions for the levels in ^{36}Cl below 2 MeV excitation. The $^{37}Cl(p,d)^{36}Cl$ and $^{23}Na(p,d)^{22}Na$ Q-values[34] dictate an overlap of their separate deuteron spectra for excitations greater than approximately 2 MeV in ^{36}Cl. Consequently, for higher

excitations the counter data generally provided useable cross-section measurements only for those ^{36}Cl levels separated from others in ^{36}Cl, and from any in ^{22}Na, by more than the deuteron peak resolution.

Protons elastically scattered from ^{37}Cl and ^{23}Na were observed in an experimental configuration identical to that used in the (p,d) measurements, except for an appropriate adjustment of the spectrograph magnetic field. The $^{37}Cl(p,p_o)^{37}Cl$ and $^{23}Na(p,p_o)^{23}Na$ data were recorded at laboratory angles from 25^o to 50^o, and assumed to have the values predicted by optical-model calculations using the Becchetti-Greenlees proton parameters[37] (see Table 6 and Appendix B). Normalization for the (p,d) data was made relative to these elastic cross-sections. A total uncertainty of 15% is assumed to arise from uncorrelated 10% uncertainties in the optical-model predictions and the normalization procedure itself. The $^{23}Na(p,d)^{22}Na$ angular distributions observed in this experiment show complete consistency in both shape and absolute magnitude with those obtained in another, independent study at this laboratory.[7] When peaks from the ^{37}Cl and ^{23}Na reactions coincided, the cross-section associated with the transition to a ^{36}Cl level was, therefore, deduced by subtraction of the independently measured $^{23}Na(p,d)^{22}Na$ cross-section for the appropriate energy level and angle. Similar corrections for those cases where levels

in ^{34}Cl, strongly populated via $^{35}Cl(p,d)^{34}Cl$, coincided with those in ^{36}Cl were made after an appropriate consideration of the enrichment factor.

Deuteron spectra were also recorded at angles from 4^{o} to 45^{o} on nuclear emulsion plates. Various runs yielded total particle group resolutions of 10 to 18 keV, FWHM. An example of the best resolution spectra is shown in Fig. 9. The spectrograph acceptance apertures were the same as those used in recording the counter data. The plates were shielded from ^{3}He and ^{4}He particles by 10 mil Mylar strips and levels in ^{36}Cl to approximately 8.2 MeV excitation were observed. At each angle, the deuteron spectrum to roughly 4.8 MeV excitation in ^{36}Cl was recorded on one 10 inch long emulsion plate, with the remainder of the deuteron groups and the proton groups from scattering on ^{12}C, ^{16}O, ^{23}Na, and ^{37}Cl falling on a second, abutting plate. Elastic proton spectra recorded with a NaI monitor detector at 90^{o} to the beam, and a beam-current integrator were used to achieve relative normalization of all proton and deuteron spectra. Normalization of the plate data to the counter data was accomplished by cross-section comparisons for selected low-lying levels in ^{36}Cl and ^{23}Na at several forward angles.

Figure 9. A spectrum from the (p,d) reaction on the ^{23}Na-^{37}Cl target, measured at 35 MeV and 14°, as recorded on nuclear emulsion plates. The resolution of the deuteron groups is 10 keV, FWHM. All excitation energy values are from the present work, with those "boxed" indicating levels in ^{36}Cl.

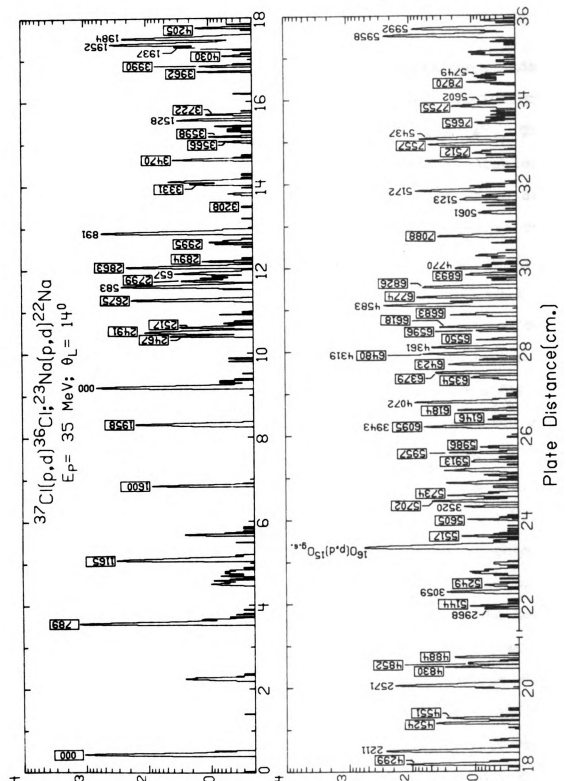
37Cl(p,d)36Cl;23Na(p,d)22Na
Ep= 35 MeV; θL= 14°
16O(p,d)15O g.s.
Counts per 0.1016 mm.
Plate Distance(cm.)

Figure 9

III.3. Excitation Energies

Excitation energy analysis and assignments were made on the basis of centroids extracted from the best resolution nuclear emulsion spectra recorded at 4^{o}, 8^{o}, and 14^{o}. The energy levels in ^{36}Cl presented in Table 5 are a weighted average of the results of two analyses involving these data.

The first method involved much the same procedure used in the analysis of the $^{39}K(p,d)^{38}K$ reaction. The low-lying excitation energies in ^{36}Cl have not been reported to 1 keV accuracy. Consequently, any energy calibration in the present work must rely heavily on the precisely determined energies in ^{22}Na.[66] The energy analysis involved a fit to these and other reference energies via a least-squares adjustment of the beam energy, scattering angle, and the constant, linear and quadratic coefficients of a $B\rho$ vs. focal-plane-position relationship[67] for the 8^{o} and 14^{o} spectra (see APPENDIX A). At angles $<8^{o}$, effective use of this fitting procedure is greatly hindered by the overlap of all elastic proton levels on the nuclear emulsions. The second plate was assumed to be directly adjacent to the first. Table 4 displays the reference peaks chosen. These levels were used only where accurate, unambiguous centroids could be extracted. Appropriate target loss corrections were made for all reference levels. The best overall results were obtained

Table 4. States used for the energy calibration of the $^{37}Cl(p,d)^{36}Cl$ reaction data. Some energies in ^{22}Na extracted in the present work and in a previous (p,d) study are shown to illustrate calibration consistency.

Reaction	Excitation Energy (keV) in the Residual Nucleus[a]	Levels in ^{22}Na(keV) from previous work[b]	Levels in ^{22}Na(keV) from this work
$^{37}Cl(p,d)^{36}Cl$	ground state[c]		
$^{23}Na(p,d)^{22}Na$	ground state[c]	000^{+}	000^{+}
	583.05 ± 0.1[d]	$583\pm1^{+}$	$583\pm1^{+}$
	657.0 ± 0.14[d]	$657\pm1^{+}$	$658\pm1^{+}$
	890.89 ± 0.2[d]	$891\pm1^{+}$	$890\pm1^{+}$
	1951.8 ± 0.3[d]	$1952\pm1^{+}$	$1952\pm2^{+}$
	1983.5 ± 0.5[d]	$1984\pm1^{+}$	$1984\pm2^{+}$
	2211.4 ± 0.32[d]	$2211\pm1^{+}$	$2211\pm2^{+}$
	2571.5 ± 0.3[d]	$2571\pm1^{+}$	$2571\pm2^{+}$
	2968.6 ± 0.6[d]	$2968\pm2^{+}$	$2971\pm4^{+}$
	3059.4 ± 0.6[d]	$3059\pm1^{+}$	$3061\pm4^{+}$
		$3943\pm2^{+}$	$3944\pm4^{+}$
		$4072\pm2^{+}$	$4072\pm4^{+}$
		$4583\pm2^{+}$	$4581\pm4^{+}$
		$5958\pm4^{+}$	$5959\pm5^{+}$
		$5992\pm4^{+}$	$5993\pm5^{+}$
$^{16}O(p,d)^{15}O$	ground state		
$^{12}C(p,d)^{11}C$	ground state		
$^{37}Cl(p,p)^{37}Cl$	ground state		
$^{23}Na(p,p)^{23}Na$	ground state		
	441.0 ± 1.0[e]		
$^{16}O(p,p)^{16}O$	ground state		
$^{12}C(p,p)^{12}C$	ground state		

[a] Used for present calibration.

[b] See Sec. II.2.

[c] Adjusted as described in text.

[d] Reference 66.

[e] Reference 68.

when the mass table Q-values for the $^{23}Na(p,d)^{22}Na$ and $^{37}Cl(p,d)^{36}Cl$ reactions[34] were manually adjusted by -2 and -1 keV, respectively. This is consistent with the adjustment of the $^{23}Na(p,d)^{22}Na$ Q-value required in the analysis of $^{35}Cl(p,d)^{34}Cl$ data (see Sec. II.2.) and within the Q-value errors quoted in the latest mass tables for both reactions. The corrections to the nominal beam energy required by the fit for both angles was +9 keV, with scattering angle corrections $<0.3^{o}$ in both cases. These changes are within the accuracy to which the experimental apparatus and analysis systems yield precise experimental parameters for any given run.

In an effort to obtain the best possible overall excitation energies from the present data, a second fitting procedure was employed for the 4^{o}, 8^{o}, and 14^{o} spectra. The beam energy and scattering angle corrections and the geometrical calibration parameters found in the above analysis were used for the 8^{o} and 14^{o} spectra. Close approximations to these parameters were used for the 4^{o} spectrum since the experimental configuration was essentially the same. This time, a linear, least-squares fit to the deuteron momenta for appropriate reference levels in ^{36}Cl and ^{22}Na (see APPENDIX A and Table 4) was required. Again, the appropriate Q-value and target loss corrections were made. The excitation energies shown in Table 5 are an average of the results of these two calibration procedures. The errors quoted

include jitter arising from the two calibration methods employed and estimated systematic errors.

Table 4 also indicates some excitation energies in ^{22}Na returned in the present study, and a comparison with those found from a previous investigation via the (p,d) reaction (Sec. II.2.). The overall consistency in the energy calibration schemes is clearly evident and, consequently, there was little motivation to alter the previous ^{22}Na excitation energy assignments based on the ^{23}Na(p,d)^{22}Na reaction. Therefore, all ^{22}Na energies shown in Fig. 9 are those assigned in Sec. II.2.

III.4. Angular Distributions

III.4.A. General Discussion

All orbital angular momentum quantum numbers (ℓ) for the transferred neutrons and corresponding spectroscopic factors have been assigned to transitions observed in the present work on the basis of fits to distorted-wave Born approximation (DWBA) angular distributions calculated using the computer code DWUCK.[49] The optical model potentials are of the standard form:

$$U(r) = V_R f(r_R,a_R)+i\left(W_V f(r_V,a_V)-4W_{SF}a_{SF}\frac{d}{dr}f(r_{SF},a_{SF})\right)$$

$$+ \left(\frac{h}{m_\pi c}\right)^2 V_{SO}\frac{1}{r}\frac{d}{dr}f(r_{SO},a_{SO})\ \vec{\ell}\cdot\vec{\sigma}$$

Table 5. Energy levels in ^{36}Cl observed in the present study and in other works.

Excitation Energy (keV)								
$(p,d)^a$	$(d,p)^b$	$(n,\gamma)^c$	$(n,\gamma)^d$	$(n,\gamma)^e$	$(^3He,\alpha)^f$	$(^3He,\alpha)^g$	$(p,d)^h$	$(p,d)^i$
000	000	000	000	000	000	000	000	000
789±1	789±4	790	790±2	788	78(0)	793±15	780±15	787
1165±1	1163±4	1166	1167±2	1165	116(0)	1165±15	1160±15	1163
1600±1	1599±5	1608	1605±4	1599	160(0)	1608±15	1600±15	1599
				1951				
1958±1	1954±5	1962	1959±3	1959	196(0)	1970±15	1950±15	1956
		2164						
		2316						
2467±2	2472±6	2472	2472±3	2469				
2491±2	2497±6				250(0)	2497±15		2490
2517±2	2522±6							
		2617						
2675±1	2679±6	2683	2675±5		268(0)	2682±15		2673
2799±3	2816±6							
2863±1	2868±6	2867	2865±3		287(0)	2905±15		2858
2894±2	2900±6							
2995±2	3000±6	2999	2979±5					
		3065	3061±5					
	3103±7							
3208±4	3212±8							
3331±2	3338±6	3336						
3470±2	3474±7				350(0)	3492±25		3477
3566±4		3564						
3598±3	3606±7	3601						
	3640±6	3636						
(3661)	3670±8							
3722±3	3728±7				374(0)	3736±25		
	(3831)	3822						
		3852						
3962±3	3970±7	3970						
3990±3	4000±7	3989						
4030±4	4040±7	4030						
		4059						
	4146±7	4137						
4205±3								
	(4269)							
4299±2	(4300)				433(0)	4333±25		4297
4316±3	4323±7							
	4413±8							
		4445						
	4504±7	4497						
4524±3		4526						
4551±3	4560±8	4560			452(0)	4560±25		
	4607±8	4601				4590±25		
		4618						
		4693						
4720±3								
4738±4	4734±8					4740±25		
	4765±8	4760						
4830±4	4834±8	4838						
4852±4	4857±8							
4884±3	4887±8	4879			490(0)	4940±25		
	4919±8							
4953±4	4965±8	4972						
	5008±8	5009						
	5090±8							
5144±5	5160±8	5150						
	5213±8	5194						
		5231						

Table 5. (Cont'd)

Excitation Energy (keV)								
(p,d)[a]	(d,p)[b]	(n,γ)[c]	(n,γ)[d]	(n,γ)[e]	(^{3}He,α)[f]	(^{3}He,α)[g]	(p,d)[h]	(p,d)[i]
5249±4	5269±8	5250						
	5314±8							
	5339±8							
	5376±8							
	5469±8							
5517±4	5518±8	5510						
	5550±8							
	5584±8							
5605±4	5622±8							
5702±4	5701±8							
5734±5	5731±8						5730±25	
	5766±8				576(0)			
	5836±8							
	5871±8							
5913±4	5906±8							
5957±4	5952±8							
5986±4	5972±8						6000±25	
	6032±8							
6095±4	6090±8							
6146±5	6155±8						6150±25	
6184±4							6190±25	
					625(0)			
6354±5	6356±8							
6379±4								
6423±4	6445±8				644(0)		6450±25	
6480±6	6474±8						6490±25	
	6510±8							
6550±5	6546±8				653(0)		6540±25	
6596±6								
6618±5								
6683±4	6680±8						6680±25	
6750±5							6750±25	
6774±5								
6826±5					685(0)		6840±25	
6893±6							6890±25	
	7007±8							
7088±5					708(0)		7090±25	
7165±6					717(0)		7160±25	
7512±5								
7557±5					766(0)		7640±25	
7665±5								
7755±6								
7870±6								
8184±6								

[a] Present work.
[b] Ref. 73.
[c] Ref. 72.
[d] Ref. 70.
[e] Ref. 76.
[f] Ref. 64; (±20 keV).
[g] Ref. 63.
[h] Ref. 22.
[i] Ref. 65; (all levels ±20 keV except 4297±10 keV).

where $f(r_i,a_i) = -[1+\exp(\frac{r-r_iA^{1/3}}{a_i})]^{-1}$

V_R is the real well depth, while W_V and W_{SF} are the volume and surface imaginary well depths, respectively. V_{SO} is the strength of the spin-orbit potential. A standard, uniformly charged sphere of radius $R_c=r_cA^{1/3}$ was used for the Coulomb potential.

The proton optical model parameters of Becchetti and Greenlees[37] were chosen for use in all DWBA calculations presented here. Use of the parameter set presented by Fricke, et al.[50] had little or no effect on the predicted (p,d) angular distribution shapes. A lack of extensive deuteron elastic scattering data for the appropriate mass region and energy led to a search of the available literature in an effort to find a suitable set of optical-model parameters. Deuteron potentials proposed by Perey and Perey,[53] Newman, et al.,[52] Hinterberger, et al.,[51] Schwandt and Haeberli,[54] Mermaz, et al.,[55] and Cowley, et al.[98] were tested in an effort to reproduce pure $\ell=0$ and $\ell=2$ empirical angular distributions recorded for the (p,d) reaction on several nuclei in the $35\leq A\leq 39$ region at $E_p=35$ MeV.[6-8]

This investigation indicated that calculations in the local, zero-range (LZR) approximation for all of the standard deuteron potentials were clearly inferior to the shapes produced when finite-range and non-local corrections (FRNL) were introduced. The standard non-locality parameters[49] 0.85 and

and 0.54 were chosen for the proton and deuteron, respectively, while the finite-range parameter[49] for the neutron bound-state was chosen to be 0.621 in all cases. FRNL calculations using the "Set I" parameters of Hinterberger, et al.[51] provided the best overall fits throughout the mass region, although the pure ℓ=0 fits were found somewhat lacking in the observed Q-dependence and all calculations tended to predict cross-sections significantly greater than the data for $\theta > 35^{o}$. In some cases, the superiority of this parameter set was not overwhelming although the usefulness of this potential was most gratifying since it is the most broadly-based deuteron elastic scattering parameter set currently available.

The "adiabatic" deuteron model of Johnson and Soper,[43] used in (p,d) analyses in the oxygen[46,48] and lead[45] regions, was also investigated and found to produce poor forward-angle ℓ=2 shapes.

The shortcomings of the FRNL calculations were found to be at least partially alleviated with the introduction of a density-dependent damping of the V_{pn} interaction.[46,69] The damping factor used here and in the other concurrent s-d shell studies via the (p,d) reaction,[7,8] is a general Fermi form

$$F(r) = (1.0-1.845\ \rho(r)^{2/3}),$$

where $\rho(r)=0.17[1+\exp(x)]^{-1}$, $x=(r-r_{o}A^{1/3})/a$, and "r_{o}" and "a" are the radius and diffusivity of the neutron bound-state well.

The normalization factor suggested by nuclear matter considerations[69] produces an overall renormalization of the calculated DWBA cross-sections, and has been omitted. A more thorough treatment of this deuteron parameter investigative procedure may be found in Sec. IV.

The present data has been analyzed in detail using: (1) the Hinterberger "Set I" deuteron parameters (FRNL), (2) the same parameter set and calculational approximations as (1) with the aforementioned damping correction to the V_{pn} interaction (DFRNL), and (3) the adiabatic deuteron prescription in the LZR approximation, henceforth referred to as ADIABATIC. These parameters are shown in Table 6. Angular distributions resulting from these three calculations are compared with each other and with the distributions observed in the present experiment for transitions to four levels in ^{36}Cl in Fig. 10. The virtue of the DFRNL calculations is clearly evident over a wide Q-value range for the present data.

III.4.B. Analysis of Experimental Angular Distributions

DFRNL fits to the angular distributions observed in this study for the population of states in ^{36}Cl via the ^{37}Cl(p,d)^{36}Cl reaction are shown in Figs. 11, 12, 13, 14, 15, 16, and 17. States observed at an insufficient number of angles to allow plausible ℓ-value assignments are not shown.

Table 6. Optical-model parameters used in the analysis of the $^{37}Cl(p,d)^{36}Cl$ data.

Particle	V_R (MeV)	r_R (fm)	a_R (fm)	W_V (MeV)	r_V (fm)	a_V (fm)	W_{SF} (MeV)	r_{SF} (fm)	a_{SF} (fm)	V_{SO} (MeV)	r_{SO} (fm)	a_{SO} (fm)	r_C (fm)
Proton[a]	46.79	1.17	0.75	5.0	1.32	0.57	4.02	1.32	0.57	6.2	1.01	0.75	1.17
Deuteron[b] (FRNL and DFRNL)	$86.73-0.35E_{cm}$	1.25	0.73				13.0	1.25	0.761	6.0	1.25	0.73	1.30
Deuteron[c] (ADIABATIC)	102.76[d]	1.17	0.779	1.60[d]	1.29	0.603	16.91[d]	1.29	0.597	6.2	1.01	0.75	1.17
Neutron Bound State	Adjusted to match separation energy	1.24	0.65							$\lambda=25$			1.24

[a]Ref. 37.

[b]Ref. 51.

[c]Ref. 43; proton and neutron parameters from Reference 37.

[d]Values shown are for $E_x=0.000$ MeV only; Q-dependence is as given in Reference 37.

Figure 10. A comparison of fits to representative angular distributions from the $^{37}Cl(p,d)^{36}Cl$ reaction at 35 MeV with the three chosen types of DWBA calculations. All fits were performed over the angular range from 3° to 35°. The curves are identified as follows: ———DFRNL, ----FRNL, and — — —ADIABATIC.

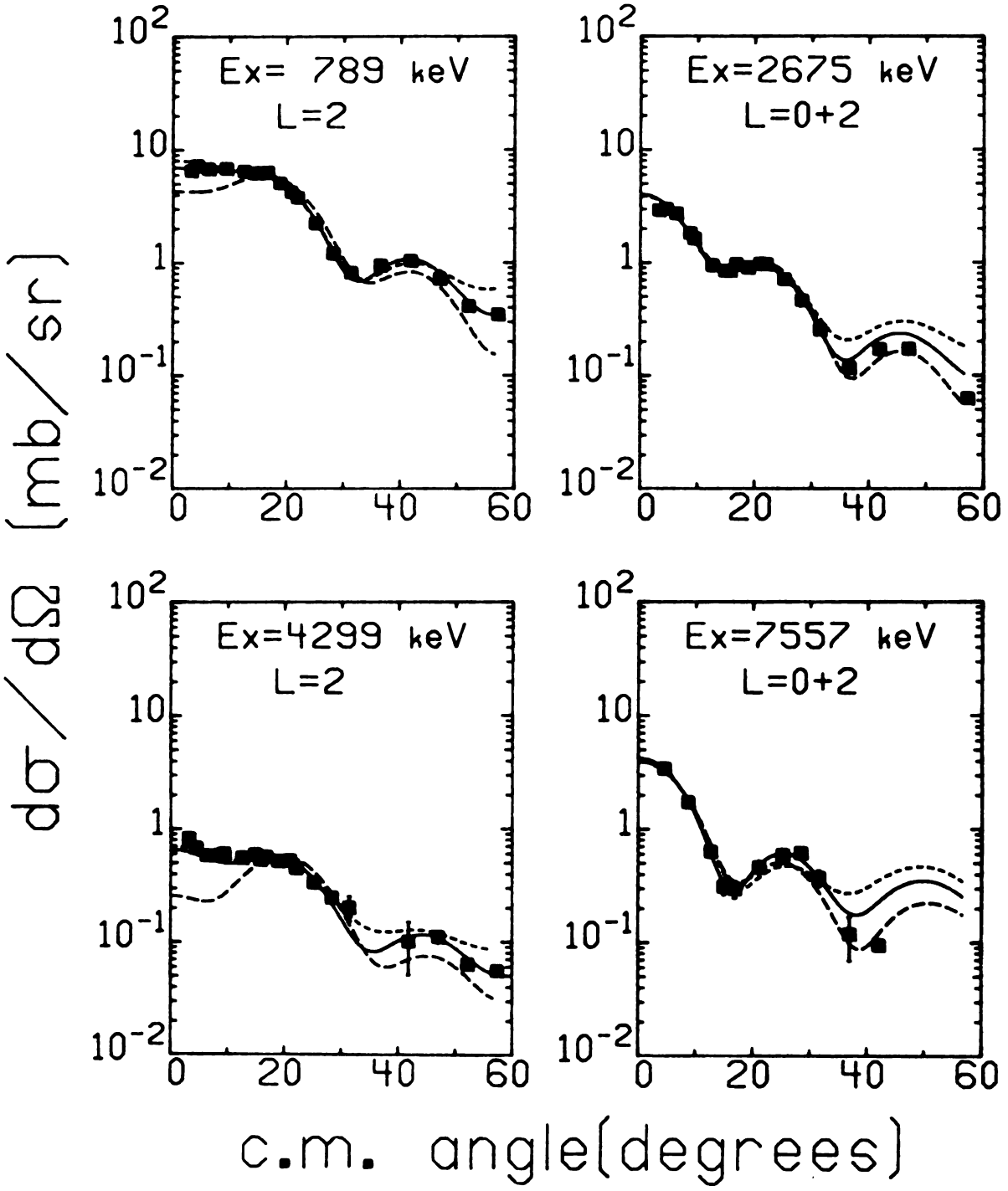
Ex= 789 keV
L=2
Ex=2675 keV
L=0+2
Ex=4299 keV
L=2
Ex=7557 keV
L=0+2
dσ / dΩ (mb/ sr)
c.m. angle(degrees)

Figure 10

Figure 11. Experimental angular distributions for states in ^{36}Cl as observed in the $^{37}Cl(p,d)^{36}Cl$ reaction at 35 MeV. The solid curves are fits of the DFRNL calculations to the data in the angular range from 3^{o} to 35^{o}. The dotted curves show the contribution of the first indicated ℓ-value for mixed-ℓ distributions.

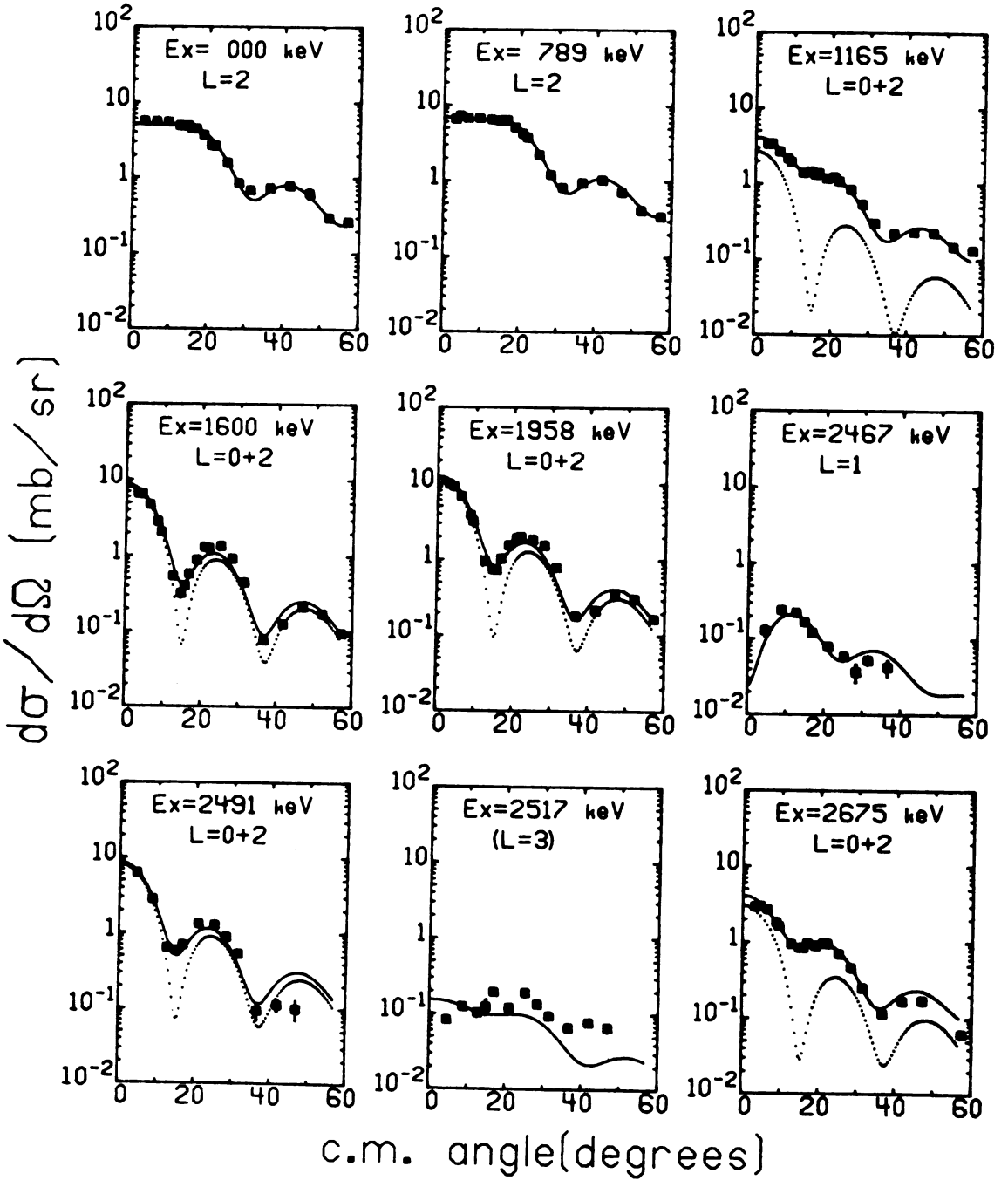
Ex= 000 keV
L=2
Ex= 789 keV
L=2
Ex=1165 keV
L=0+2
Ex=1600 keV
L=0+2
Ex=1958 keV
L=0+2
Ex=2467 keV
L=1
Ex=2491 keV
L=0+2
Ex=2517 keV
(L=3)
Ex=2675 keV
L=0+2
dσ/dΩ (mb/sr)
c.m. angle(degrees)

Figure 11

Figure 12. Experimental angular distributions for states in ^{36}Cl as observed in the $^{37}Cl(p,d)^{36}Cl$ reaction at 35 MeV. The solid curves are fits of the DFRNL calculations to the data in the angular range from 3° to 35°. The dotted curves show the contribution of the first indicated ℓ-value for mixed-ℓ distributions.

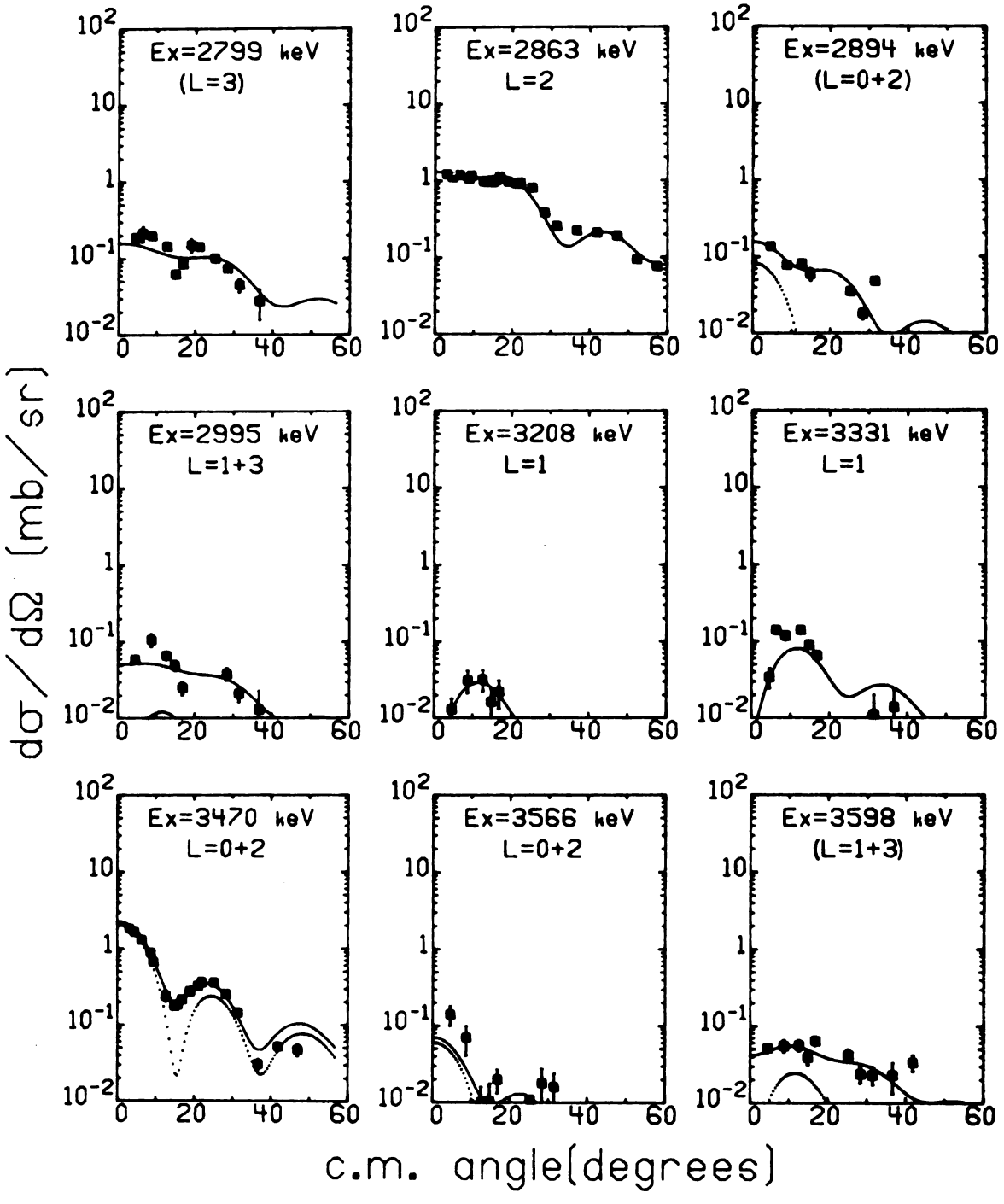
Ex=2799 keV
(L=3)
Ex=2863 keV
L=2
Ex=2894 keV
(L=0+2)
Ex=2995 keV
L=1+3
Ex=3208 keV
L=1
Ex=3331 keV
L=1
Ex=3470 keV
L=0+2
Ex=3566 keV
L=0+2
Ex=3598 keV
(L=1+3)
dσ/dΩ (mb/sr)
c.m. angle(degrees)

Figure 12

Figure 13. Experimental angular distributions for states in ^{36}Cl as observed in the $^{37}Cl(p,d)^{36}Cl$ reaction at 35 MeV. The solid curves are fits of the DFRNL calculations to the data in the angular range from 3^{o} to 35^{o}. The dotted curves show the contribution of the first indicated ℓ-value for mixed-ℓ distributions.

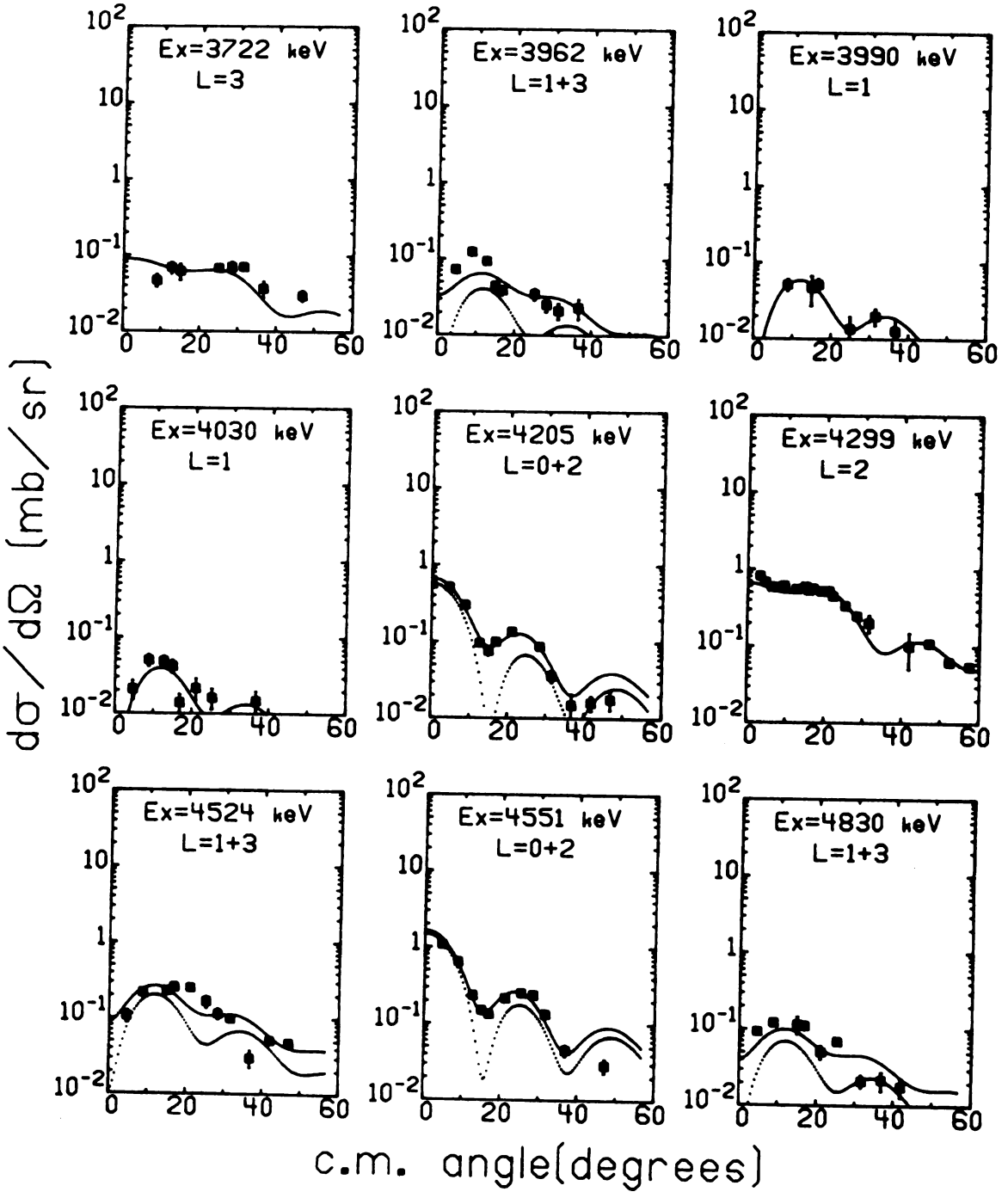
Ex=3722 keV
L=3
Ex=3962 keV
L=1+3
Ex=3990 keV
L=1
Ex=4030 keV
L=1
Ex=4205 keV
L=0+2
Ex=4299 keV
L=2
Ex=4524 keV
L=1+3
Ex=4551 keV
L=0+2
Ex=4830 keV
L=1+3
dσ/dΩ (mb/sr)
c.m. angle(degrees)

Figure 13

Figure 14. Experimental angular distributions for states in ^{36}Cl as observed in the $^{37}Cl(p,d)^{36}Cl$ reaction at 35 MeV. The solid curves are fits of the DFRNL calculations to the data in the angular range from 3^{o} to 35^{o}. The dotted curves show the contribution of the first indicated ℓ-value for mixed-ℓ distributions.

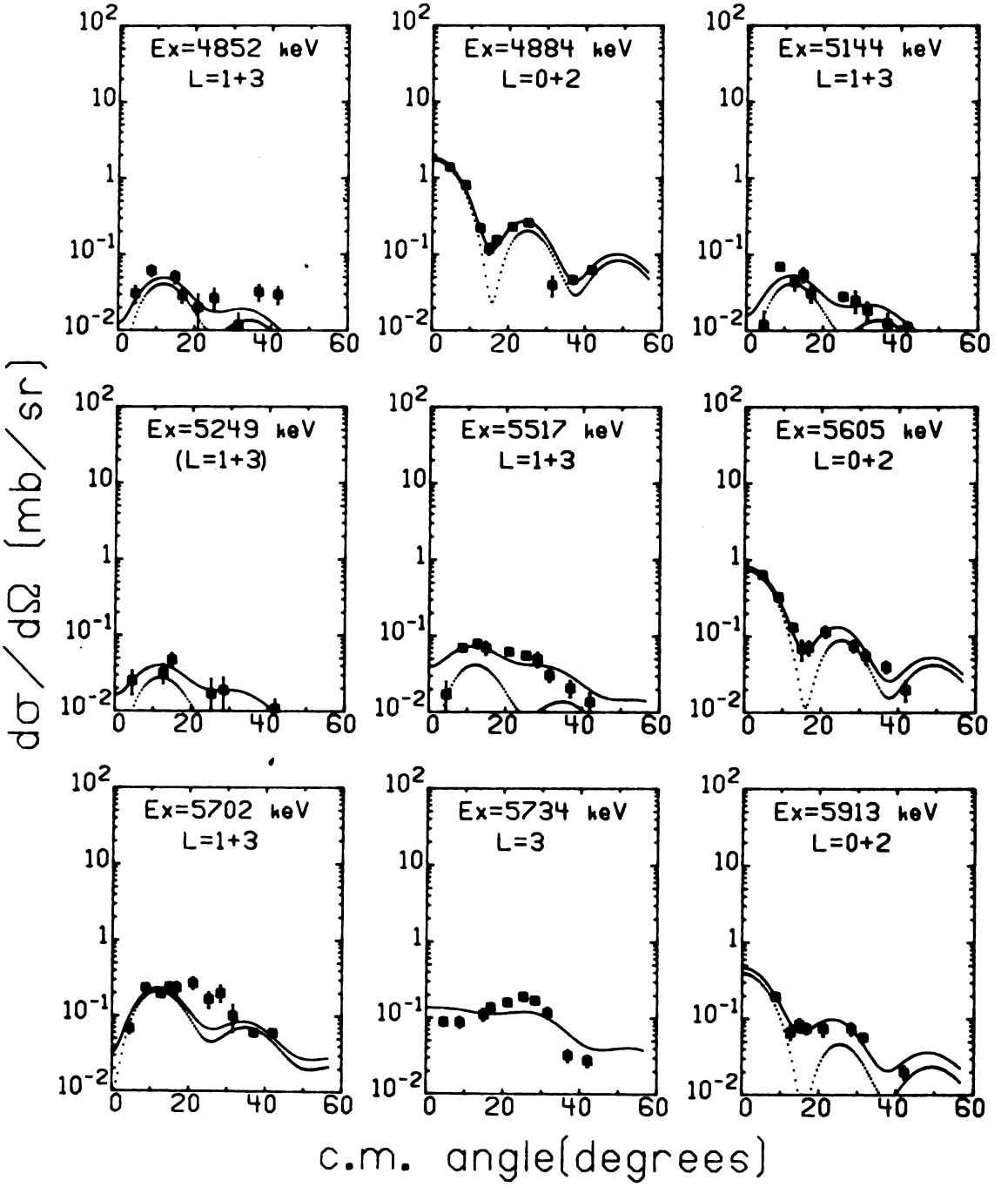
Ex=4852 keV
L=1+3
Ex=4884 keV
L=0+2
Ex=5144 keV
L=1+3
Ex=5249 keV
(L=1+3)
Ex=5517 keV
L=1+3
Ex=5605 keV
L=0+2
Ex=5702 keV
L=1+3
Ex=5734 keV
L=3
Ex=5913 keV
L=0+2
dσ / dΩ (mb/sr)
c.m. angle(degrees)

Figure 14

Figure 15. Experimental angular distributions for states in ^{36}Cl as observed in the $^{37}Cl(p,d)^{36}Cl$ reaction at 35 MeV. The solid curves are fits of the DFRNL calculations to the data in the angular range from 3° to 35°. The dotted curves show the contribution of the first indicated ℓ-value for mixed-ℓ distributions.

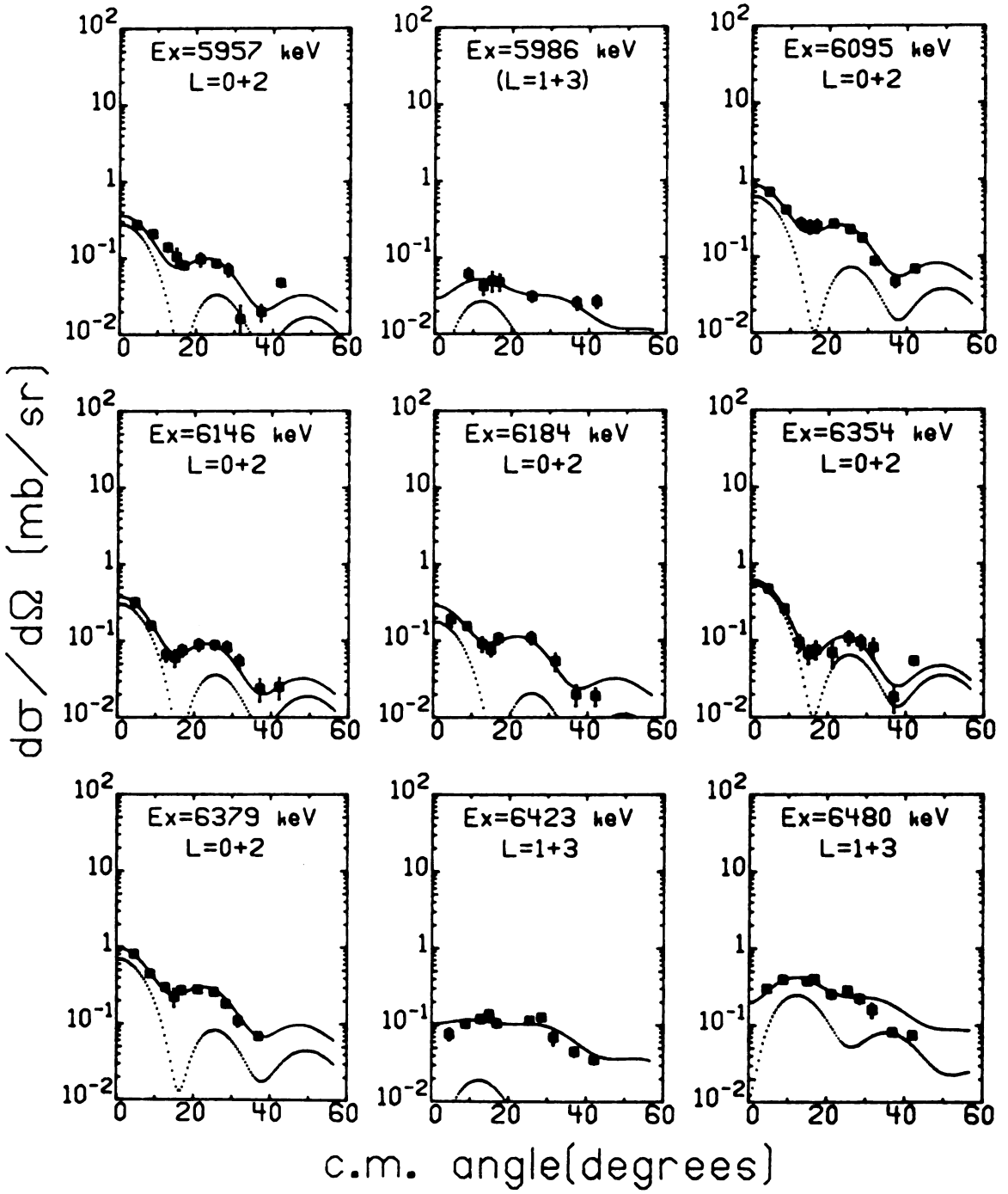
Ex=5957 keV
L=0+2
Ex=5986 keV
(L=1+3)
Ex=6095 keV
L=0+2
Ex=6146 keV
L=0+2
Ex=6184 keV
L=0+2
Ex=6354 keV
L=0+2
Ex=6379 keV
L=0+2
Ex=6423 keV
L=1+3
Ex=6480 keV
L=1+3
dσ/dΩ (mb/sr)
c.m. angle(degrees)

Figure 15

Figure 16. Experimental angular distributions for states in ^{36}Cl as observed in the $^{37}Cl(p,d)^{36}Cl$ reaction at 35 MeV. The solid curves are fits of the DFRNL calculations to the data in the angular range from 3° to 35°. The dotted curves show the contribution of the first indicated ℓ-value for mixed-ℓ distributions.

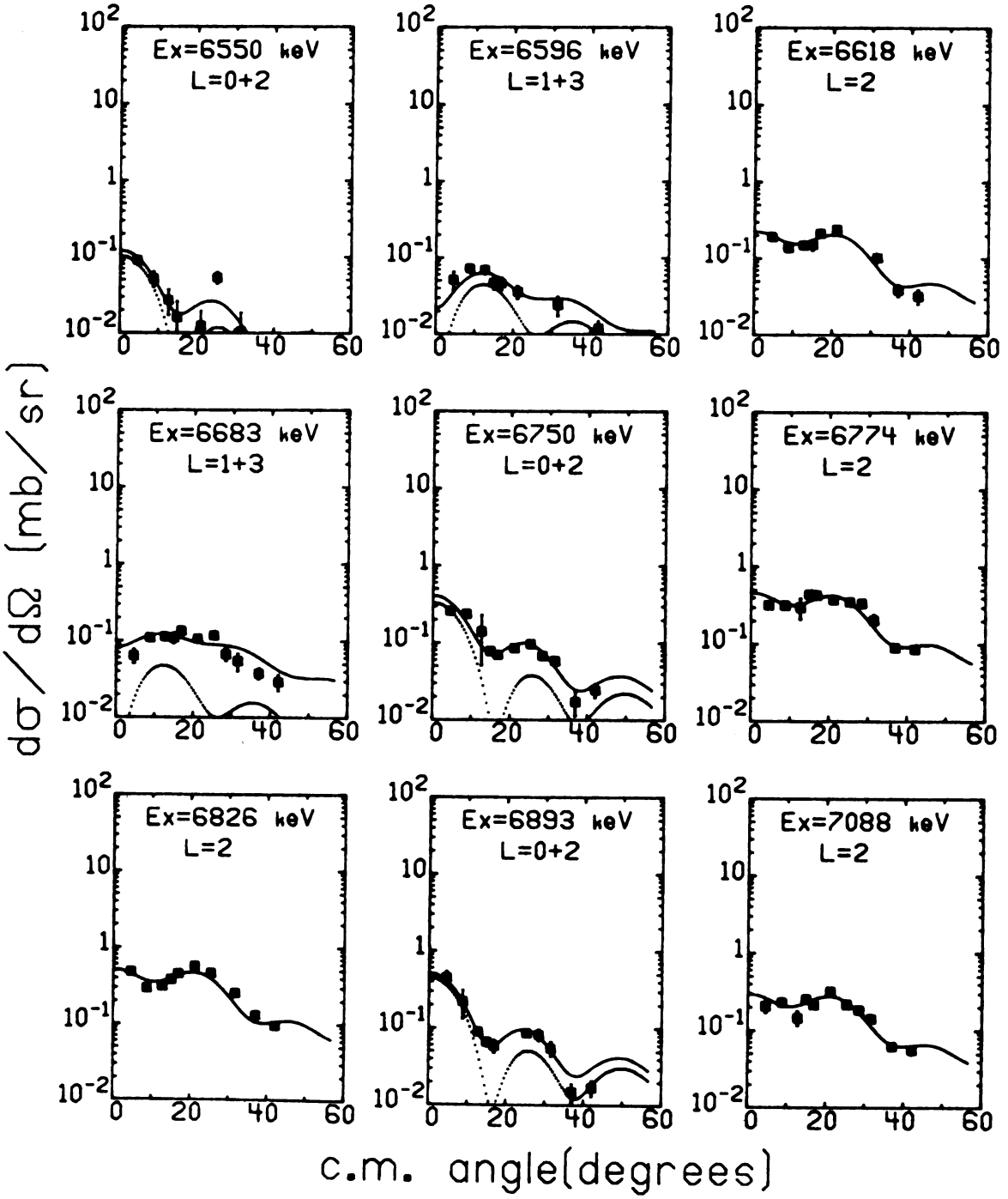
Ex=6550 keV
L=0+2
Ex=6596 keV
L=1+3
Ex=6618 keV
L=2
Ex=6683 keV
L=1+3
Ex=6750 keV
L=0+2
Ex=6774 keV
L=2
Ex=6826 keV
L=2
Ex=6893 keV
L=0+2
Ex=7088 keV
L=2
dσ/dΩ (mb/sr)
c.m. angle(degrees)

Figure 16

Figure 17. Experimental angular distributions for states in ^{36}Cl as observed in the $^{37}Cl(p,d)^{36}Cl$ reaction at 35 MeV. The solid curves are fits of the DFRNL calculations to the data in the angular range from 3° to 35°. The dotted curves show the contribution of the first indicated ℓ-value for mixed-ℓ distributions.

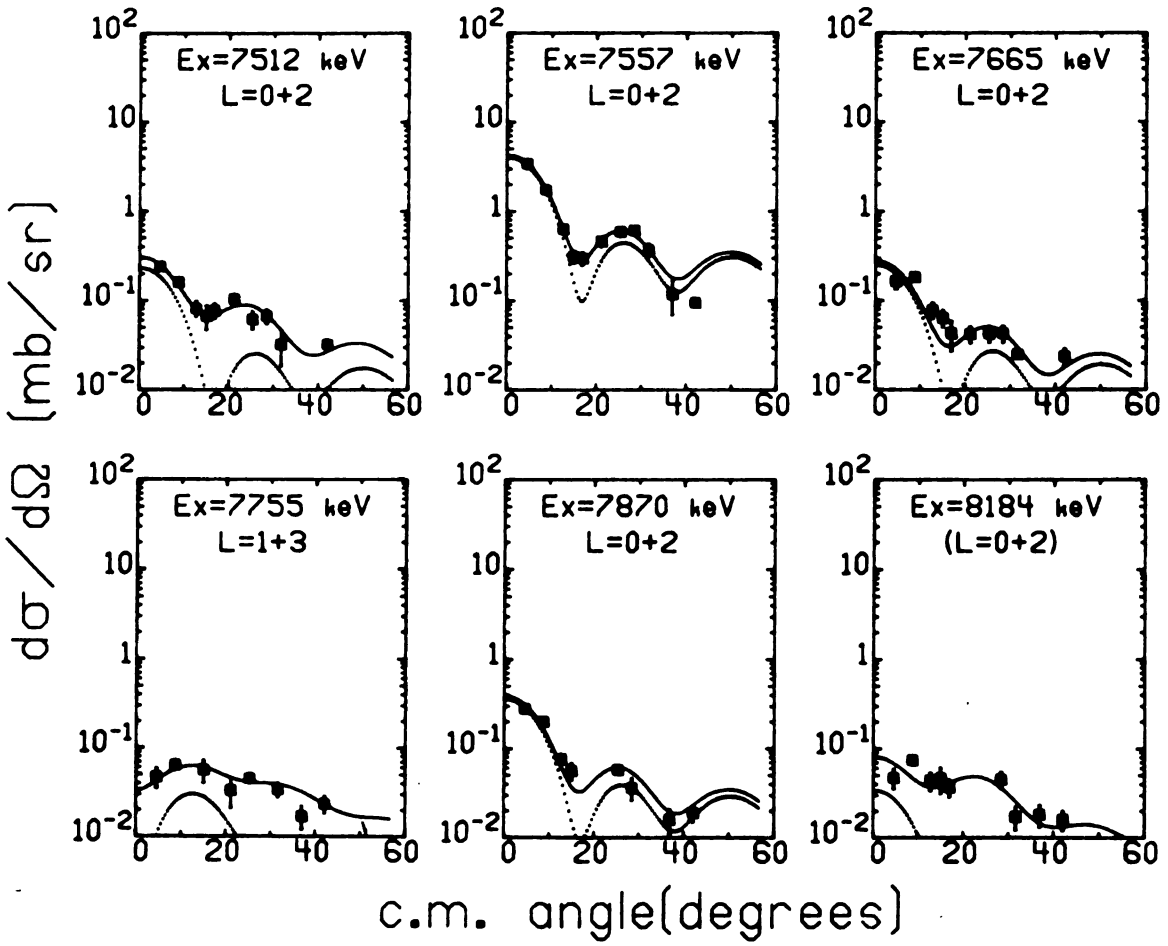
Ex=7512 keV
L=0+2
Ex=7557 keV
L=0+2
Ex=7665 keV
L=0+2
Ex=7755 keV
L=1+3
Ex=7870 keV
L=0+2
Ex=8184 keV
(L=0+2)
dσ/dΩ (mb/sr)
c.m. angle(degrees)

Figure 17

Minimization of the quantity

$$X^2 = \frac{1}{N} \sum_{i=1}^{N} [(A_{\ell j} \frac{d\sigma}{d\Omega} (\Theta_i)_{\ell j,DWBA} - \frac{d\sigma}{d\Omega}(\Theta_i)_{exp})/\Delta\sigma_i]^2$$

where $A_{\ell j}=2.29\ C^2S_{\ell j}$, with C and $S_{\ell j}$ the appropriate isospin Clebsch-Gordon coefficient and spectroscopic factor, respectively, was required for all fits. $\frac{d\sigma}{d\Omega}(\Theta_i)_{\ell j,DWBA}$, $\frac{d\sigma}{d\Omega}(\Theta_i)_{exp}$, and $\Delta\sigma_i$ are the DWBA calculated differential cross-section at the i^{th} experimental angle, the experimental value of the differential cross-section at angle i and the total (statistical plus estimated systematic) error in the appropriate experimental number, respectively. N is the number of data points within the 3^o-35^o angular range. All fits were performed over this subset of experimental points in order to allow comparisons of the resulting spectroscopic factors which are reasonably independent of the great differences found at larger angles for the three calculations used in the present analysis.

Table 7 lists the spectroscopic factors and ℓ-values for all states for which useful angular distributions could be extracted from the present data. Attempts to fit two ℓj combinations were made for each distribution, except where known final state spins precluded a possible mixed-ℓ transition; for example, the known $J^\pi,T = 0^+,2$, 4299 keV level was fit only with a pure $\ell,j=2,3/2$ calculation. In other cases where only one ℓ-value is assigned to a transition, the addition of a

Table 7. Experimental values of ℓ and C^2S_ℓ for the $^{37}Cl(p,d)^{36}Cl$ reaction as observed in the present investigation. All assignments are based on the DFRNL analysis, with the spectroscopic factors normalized to yield C^2S_ℓ =1.10 for the transition to the ^{36}Cl ground state.

E_x(keV)	ℓ	C^2S_ℓ[a]	E_x(keV)	ℓ	C^2S_ℓ[a]
000	2	1.10	5249	(1,3)	<0.01,0.01
789	2	1.66	5517	1,3	<0.01,0.02
1165	0,2	0.05,0.36	5605	0,2	0.02,0.04
1600	0,2	0.16,0.11	5702	1,3	0.02,0.02
1958	0,2	0.23,0.24	5734	3	0.09
2467	1	0.01	5913	0,2	0.01,0.04
2491	0,2	0.17,0.19	5957	0,2	0.01,0.05
2517	(3)	0.05	5986	(1,3)	<0.01,0.02
2675	0,2	0.07,0.31	6095	0,2	0.02,0.15
2799	(3)	0.05	6146	0,2	0.01,0.05
2863	2	0.45	6184	0,2	0.01,0.07
2894	(0,2)	<0.01,0.03	6354	0,2	0.02,0.04
2995	1,3	<0.01,0.01	6379	0,2	0.03,0.18
3208	1	<0.01	6423	1,3	<0.01,0.08
3331	1	0.01	6480	1,3	0.02,0.15
3470	0,2	0.05,0.07	6550	0,2	0.01,0.01
3566	0,2	0.01,0.01	6596	1,3	<0.01,0.02
3598	(1,3)	<0.01,0.02	6618	2	0.15
3722	3	0.04	6683	1,3	<0.01,0.07
3962	1,3	<0.01,0.01	6750	0,2	0.01,0.05
3990	1	<0.01	6774	2	0.31
4030	1	<0.01	6826	2	0.36
4205	0,2	0.01,0.04	6893	0,2	0.02,0.04
4299	2	0.29	7088	2	0.22
4524	1,3	0.01,0.04	7512	0,2	0.01,0.06
4551	0,2	0.04,0.06	7557	0,2	0.18,0.18
4830	1,3	0.01,0.02	7665	0,2	0.01,0.02
4852	1,3	<0.01,0.01	7755	1,3	<0.01,0.04
4884	0,2	0.05,0.05	7870	0,2	0.02,0.02
5144	1,3	<0.01,0.01	8184	(0,2)	<0.01,0.04

[a]Values for ℓ=0,1,2,3 are for $2s_{1/2}$, $2p_{3/2}$, $1d_{3/2}$ and $1f_{7/2}$ calculations, respectively.

second failed to improve the overall fit significantly. In Table 8, a comparison of DFRNL, FRNL, and ADIABATIC results with those of other single neutron pick-up experiments is presented for previously observed transitions only.

III.5. Discussion

III.5.A. Energy Levels

To date, the excitation energies of levels in ^{36}Cl have not been reported to the precision of states in other s-d shell nuclei.[70-77] Table 5 serves to illustrate the existing disparity in energy assignments for even the low-lying levels. Nearly all of the levels observed in the (n,γ) studies[70,71] are observed in the present experiment. We observe only 24 of the 41 levels reported by Alves, et al.,[72] but several states not observed in that investigation are reported here and in other single neutron transfer experiments.[63-65] Much the same situation exists with regard to the (d,p) studies of Hoogenboom, et al.[73] and Decowski.[74] The doublet at 1958 keV is not resolved in the present or previous single neutron pick-up works, but the negative-parity state is in all probability very weak, compounding the experimental problem but simplifying interpretation of the resulting "doublet".

The assigned excitation energy of 4299 keV for the 0^+, T=2 analog of the ^{36}S ground state agrees very well with the 4297 and 4295 keV assignments of Refs. 65 and 78,

respectively. The energy levels extracted from the present work generally allow a reasonable correlation with those observed in previous studies, particularly for levels below 4 MeV excitation, and many states have been observed for the first time via a single neutron pick-up reaction.

III.5.B. ℓ and π Assignments

Orbital angular momentum quantum numbers (ℓ) for the neutrons transferred in the formation of 61 states in ^{36}Cl via single neutron pick-up can be at least tentatively assigned on the basis of the DFRNL fits to angular distributions observed in the present work. Since the ^{37}Cl ground state is known to have $J^{\pi}=3/2^{+}$, transitions involving even-ℓ transfers populate states in ^{36}Cl with positive parity. Likewise, odd-ℓ transfers lead to negative parity states. Assignments of $\ell=0+2$ were generally evidenced by a definite forward rise in the experimental angular distribution, characteristic of the DWBA $\ell=0$ shape. Separate fits involving $1d_{5/2}$ and $1d_{3/2}$ neutron transfer calculations yielded only slightly different chi-squared per point values over the prescribed angular range for the distributions of positive parity states. Consequently, the 35 positive parity assignments below 8.2 MeV excitation are made on the basis of fits to $\ell=0$ and/or $\ell=2$ DWBA calculations with $j=1/2$ and $j=3/2$, respectively.

As a result of the ℓ=2 spin-orbit splitting for the neutron bound-state, any ℓ=2, j=3/2 spectroscopic factor may be converted to the appropriate ℓ=2, j=5/2 value via multiplication by $\sim$0.85.

Transfers involving ℓ=1 neutrons yield experimental angular distributions with a characteristic "dip" at very forward angles. This is clearly evident in both $1p_{1/2}$ and $2p_{3/2}$ DWBA calculations for this mass region and bombarding energy. As in previous charged particle work[63,73,74] we observe evidence of ℓ=3 transfers leading to states in ^{36}Cl. The $1f_{7/2}$ transfer calculations appear somewhat similar to ℓ=2 DWBA shapes for forward angles but do not fall off as quickly. Therefore, we assign negative parities to 25 levels in ^{36}Cl on the basis of the ℓ=1 forward angle fall-off and/or the relatively high ℓ=3 cross-section around 30°. For all levels, single ℓ-values are assigned when the addition of a second ℓ either resulted in a negative contribution to the cross-section or failed to produce a significant improvement in chi-squared per point values, or when known final state J values excluded mixed-transitions.

The ℓ assignments made on the basis of the present study are shown in Table 7. Parentheses denote levels for which the fit was only slightly preferable to one involving opposite parity ℓ-values. Our parity assignments agree with those made from previous single neutron pick-up experiments, except for

the $\pi=(+)$ observation for the 5.76 MeV level made by Rosin, et al.[64] We assume a correspondence with the negative parity 5734 keV state observed in this work. The recent $^{35}Cl(p,d)^{36}Cl$ study by Decowski[74] assigned at least tentative negative parities to the 2675, 2863, and 2894 keV levels. However, previous pick-up experiments[63-65] have observed positive parity transitions to these levels. The characteristic forward angle $\ell=0$ shape for the 2675 keV state and the excellent $\ell=2$ fit to the 2863 keV level observed in the present work confirm the positive parity assignments to each of these levels and limit their J^π values to $(1,2)^+$ and $(0-3)^+$, respectively. The present data also indicates a rise in cross-section at forward angles for the 2894 keV state, again indicative of a positive parity transition. Also based on the forward angle data, we assign positive parities to the 3470, 5605, 5906, and 6095 keV states as opposed to the $\pi=(-)$ assignments of Hoogenboom, et al.[73] All other present parity assignments for levels showing reasonable energy correspondences agree with those based on previous (d,p) works.

III.5.C. Experimental C^2S Values

In Table 8 we present a comparison of the spectroscopic factors obtained from the DFRNL, FRNL, and ADIABATIC fits and from the previously performed single neutron pick-up experiments leading to states in ^{36}Cl. Only previously observed levels are

Table 8. Experimental values of C^2S_ℓ for transitions from ^{37}Cl to ^{36}Cl. Absolute values for the ground state are presented in parentheses. All other values are normalized such that C^2S_ℓ =1.10 for the ground state.

E_x(keV)[a]	J^π,T	ℓ[a]	DFRNL[a]	FRNL[a]	ADIABATIC[a]	(p,d)[b]	(^{3}He,α)[c]	(^{3}He,α)[d]	(d,t)[e]	(p,d)[f]
			(2.36)	(1.85)	(2.08)		(0.92)	(1.30)	(1.00)	(0.90)
000	2^+,1	2	1.10	1.10	1.10	1.10	1.10	1.10	1.10	1.10
789	3^+,1	2	1.66	1.59	1.62	1.59	1.52	1.62	1.70	1.65
1165	1^+,1	0	0.05	0.05	0.06	0.07	<0.13		0.025	0.18
		2	0.36	0.35	0.35	0.35	0.35	0.37	0.42	0.49
1600	$(1,2)^+$,1	0	0.16	0.19	0.14	0.28	0.28-0.11	0.19	0.061	0.31
		2	0.11	0.06	0.15	<0.11	<0.15		0.42	
1958	2^+,1	0	0.23	0.27	0.20	0.47	0.37-0.20	0.42	0.17	0.79
		2	0.24	0.16	0.31	<0.19	0.15-0.31		0.42	
2491	$(1,2)^+$,1	0	0.17	0.20	0.14	0.34	0.32-0.16	0.38	0.085	
		2	0.19	0.12	0.23	<0.14	0.21-0.25		0.51	
2675	$(1)^+$,1	0	0.07	0.07	0.07					
		2	0.31	0.27	0.32	0.34	0.41	0.37		
2863	$(0\text{-}4)^+$,1	0			0.02					
		2	0.45	0.38	0.41	0.47	0.37	0.38		
3470	$(1,2)^+$,1	0	0.05	0.06	0.04	0.11	0.08	0.15		
		2	0.07	0.05	0.09	<0.04	0.08			
3722	$(2\text{-}5)^-$,1	3	0.04	0.03	0.03		0.10[g]	0.05		
4299	0^+,2	2	0.29	0.24	0.27	0.31	0.45	0.30		
4884	$(1,2)^+$,1	0	0.05	0.06	0.04		0.14			
		2	0.05	0.02	0.07		0.09			
5734	$(2\text{-}5)^-$,1	3	0.09	0.07	0.08		0.25[h]			
6826	$(0\text{-}3)^+$,1	2	0.36	0.26	0.41		0.43			
7557	2^+,2	0	0.18	0.18	0.13		0.28			
		2	0.18	<0.01	0.27					

[a]Present work.
[b]Reference 65.
[c]Reference 64.
[d]Reference 63.
[e]Reference 62.
[f]Reference 22.
[g]ℓ=1
[h]ℓ=2

included. Relative to the DFRNL values, the FRNL calculations yield somewhat lower ℓ=2 spectroscopic factors in the ℓ=0+2 mixtures, that disparity increasing with excitation energy. In contrast, the ADIABATIC ℓ=2 values tend to be higher in these mixtures. These deuteron parameter and calculational differences appear to be a direct result of the basic ℓ=0 Q-dependences, i.e., the FRNL and ADIABATIC shapes retain less and more of the first minimum, respectively, with increasing excitation energy.

The DFRNL spectroscopic factors are generally in good agreement with those obtained from previous studies. However, significantly more total strength is assigned to the 1165, 1600, and 1958 keV states by Vignon, et al.,[22] and to several of the low-lying levels in the (d,t) study by Puttaswamy and Yntema.[62] The present experiment also allows the observation of mixed ℓ=0 and ℓ=2 contributions to several levels for which pure ℓ=0 or ℓ=2 transfers have previously been assigned. A particularly interesting example is the 2675 keV state. The previous pick-up experiments in which this level was observed[63-65] assigned a pure ℓ=2 transfer to the transition. However, the present data for $\theta<10^{o}$, a region not explored in any of those works, definitely indicates the characteristically ℓ=0 forward angle rise (see Fig. 13). The inclusion of an ℓ=2 contribution to several previously assigned pure ℓ=0 transitions seems justified on the basis of DWBA ℓ=0 shape comparisons discussed in Sec. IV.

We observe only one strongly populated positive parity state in the 4 MeV excitation region, with $C^2S_{2,3/2}=0.29$. The $^{37}Cl(d,^3He)^{36}S$ work of Gray, et al.[79] and Puttaswamy and Yntema[80] yield values of 0.27 and 0.33, respectively, for the transition to the 0^+ ground state. Therefore, we concur with Refs. 63-65 in the assignment of $J^\pi,T=0^+,2$ for the 4299 keV level, as the analog of the ^{36}S ground state. The two $(d,^3He)$ works also show considerable spectroscopic strength for the 3.3 MeV, 2^+ level in ^{36}S. The 7557 keV state in $^{36}Cl(C^2S(\ell=0)=0.18, C^2S(\ell=2)=0.18)$ appears to be the most likely candidate for the analog of that level, based on its total strength relative to the other levels observed in that energy region and the spectroscopic factors of $C^2S(\ell=0)=0.22$, and $C^2S(\ell=0)=0.30$ for the 3.3 MeV ^{36}S state reported in Refs. 79 and 80, respectively.

III.5.D. Comparison with Shell-Model Calculations

The spectroscopic factors extracted from the present data (DFRNL) and those calculated from various shell-model Hamiltonians are presented in Table 9. The results of the Tabakin interaction calculations[59] have been renormalized to facilitate a relative comparison with the present results. The MSDI and 12.5 pA studies conducted by Wildenthal, et al.[3] tend to be less successful for upper s-d shell nuclei and have been omitted.

Table 9. A comparison of $C^2S(\ell)$ values obtained in the present study with those from various shell model calculations.

E_x(keV)[a]	J^π,T	ℓ[a]	$C^2S(\ell)$[a]	11.0h+ASPE[b]	12.5p+^{17}O[b]	TABAKIN[c]	2-shell[d]
000	2^+,1	2	1.10	1.11	1.08	1.10	1.10
789	3^+,1	2	1.66	1.57	1.52	1.58	1.50
1165	1^+,1	0	0.05	0.03	0.05	0.04	<0.01
		2	0.36	0.26	0.44	0.18	0.27
1600	$(1)^+$,1	0	0.16	0.13	0.05	0.09	0.34
		2	0.11	0.14	0.04	0.13	0.05
1958	2^+,1	0	0.23	0.06	0.28	0.06	0.2
		2	0.20[f]	0.05[e]	0.36[e]	0.04[e]	0.02
2491	$(2)^+$,1	0	0.17	0.42	0.05		0.50
		2	0.16[f]	0.16[e]	0.02		0.06
2675	$(1)^+$,1	0	0.07	0.00	0.01		
		2	0.31	0.14	0.03[e]		0.2
2863	$(3)^+$,1	2	0.38[f]	0.50[e]	0.81[e]		
3470	$(1)^+$,1	0	0.05	0.23	0.25		
		2	0.07	0.13	0.05		
4299	0^+,2	2	0.29	0.22	0.23	0.24	0.22
7557	2^+,2	0	0.18	0.28	0.27		
		2	0.15[f]	<0.01[e]	0.01[e]		0.3

[a] Present Work.

[b] Reference 3; $1d_{3/2}$ and $1d_{5/2}$ contributions are summed for ℓ=2 transitions.

[c] Reference 59; absolute C^2S_2=0.85 for ground state; all values have been renormalized for comparison; $d_{3/2}$ and $d_{5/2}$ contributions summed for ℓ=2.

[d] $2s_{1/2}$, $1d_{3/2}$ calculations using the wave functions of Reference 56 reported in Reference 64.

[e] Predominantly $d_{5/2}$.

[f] $C^2S_{2,5/2}$(=0.85 $C^2S_{2,3/2}$); see text.

Nine T=1 levels have been included in Table 9, with firm spin assignments having been made to four. The other spins have been tentatively assigned on the basis of the neutron orbital angular momentum transfers observed in this work (the presence of ℓ=0 components limiting final state spins to 1 or 2) and the general trends of recent shell-model level sequencing. It is evident that the ground state and 789 keV level spectroscopic factors for all of the calculations are in good agreement with present results. This is not surprising since, in isospin formalism, the wave functions for these two levels are dominated by a $(d_{5/2})^{12}(s_{1/2})^{4}(d_{3/2})^{4}$ configuration, the simplest of shell-model pictures for ^{36}Cl. The agreement is also good for the second excited state, although the Tabakin calculations[59] exhibit only about one-half the observed ℓ=2 strength. For higher excited states, the predicted spectroscopic factors are very sporadic, with no clear choice of a preferred set of wave functions. However, there is some indication of an over-estimation of the ℓ=2 strength and the ℓ=0 strength for transitions to the second 3^+ level and the fourth 1^+ level, respectively. The full s-d shell calculations of Wildenthal, et al.[3] predict a weakly populated 3^+ level near 4 MeV excitation, but no pure ℓ=2 transitions of appropriate strength are observed in that region. A 3^+ level populated by predominatly $d_{5/2}$ transfer is predicted for the 5-6 MeV

region ($C^2S(\ell=2)=0.2$), which may correspond to the observed 6618 keV level ($C^2S(\ell=2)=0.13$). The only other T=1 state predicted to carry significant pick-up strength is a 4^+ level at approximately 7 MeV excitation ($C^2S(\ell=2)=1.24$). Three levels with significant pure $\ell=2$ strength are observed near 7 MeV (6774, 6826, and 7088 keV) with total $C^2S(\ell=2)=0.77$.

The spectroscopic factors extracted from the present data for the 4299 and 7557 keV levels agree with the 2 and 3 orbital shell-model predictions except for the experimentally observed $\ell=2$ strength of the transition to the latter state. Since they are the only strongly populated levels in the appropriate energy regions and exhibit the correspondingly correct ℓ-values, we concur with previous pick-up works in their identification as the analog states of the $(J^\pi,T)=(0^+,2)$ ground state and $(2^+,2)$ 3.30 MeV levels in ^{36}S, but assign the excitation energies in ^{36}Cl much more accurately.

Single-shell sum rules for spectroscopic factors dictate a T=1 contribution to the total $d_{3/2}$ strength of 3.75 with the T=2 levels adding 0.25 for a total $d_{3/2}$ shell-model limit of 4.0. The summed $\ell=2,j=3/2$ spectroscopic strength observed for transitions to the ground state, 789, 1165, 1600, 2675, and 3470 keV levels in ^{36}Cl is 3.61. These states indeed show a majority of the predicted $d_{3/2}$

strength for the T=1 levels in recent shell-model studies. The observed ℓ=2 spectroscopic factor for the 4299 keV level would indicate that appropriate transitions to that state carry essentially all of the $d_{3/2}$ strength for the A=36,T=2 system. A total $d_{5/2}$ spectroscopic strength of 2.61 may then be assigned to the single neutron transfers to states in ^{36}Cl below 8.2 MeV, after the ℓ=2 values in Table 7 have been properly normalized to correspond to $d_{5/2}$ transitions.

Erne[60] has predicted 24 T=1, negative parity levels in ^{36}Cl between 2.0 and 6.5 MeV excitation. In the present study, 25 levels between 2.0 and 8.2 MeV are assigned at least a tentative negative parity, in excellent agreement with theory. The summed observed spectroscopic strengths are 0.15 and 0.69 for $2p_{3/2}$ and $1f_{7/2}$ neutron transfers, respectively.

III.6. Summary

Excitation energies have been assigned to many levels in ^{36}Cl with a precision heretofore unmatched in many previous studies of that nucleus. Spectroscopic factors for single neutron pick-up leading to many negative parity states in ^{36}Cl have been reported for the first time. Essentially all of the $d_{3/2}$ strength and nearly one-half the expected total $d_{5/2}$ transition strength have been observed below 8 MeV

excitation, with the approximate distributions among the T=1 and T=2 levels agreeing well, in total, with recent shell-model calculations. Approximately 60% of the shell-model limit for ℓ=0 strength is also observed in this energy region. The summed negative parity (ℓ=1,3) spectroscopic factors indicate small but significant f-p shell components in the ^{37}Cl ground state wave function. A level-by-level comparison of the present results with recent predictions indicates a need for the inclusion of f-p shell excitations in any attempt to fully describe the levels in ^{36}Cl above 2 MeV excitation.

IV. THE $^{39}K(p,d)^{38}K$ REACTION

IV.1. Introductory Remarks

In the simplest shell-model picture, the lowest energy states of ^{38}K should arise from the couplings of two $d_{3/2}$ holes, yielding J^{π},T values of 3^+ and 1^+, T=0, and 0^+ and 2^+, T=1. The incorporation of $s_{1/2}$-hole excitations into this picture is the most logical first improvement, a step taken by Glaudemans, Wiechers, and Brussaard.[56] Their shell-model provides a description for many aspects of the low-lying positive parity states in ^{38}K. However, much as appears to be the case for the two-particle nucleus in the s-d shell, ^{18}F, the mixing of the $d_{3/2}$ and $d_{5/2}$ orbits may be important even in the lowest few energy levels. Several calculations which consider excitations in all three s-d shell orbits have been reported,[3,59,81] and appear to yield still further improvement in the agreement between theory and experiment. Finally, again in analogy with ^{18}F and excitations from the p shell, the structure of ^{38}K cannot be explained in final detail without recourse to excitations from the s-d shell to the f-p shell. Some initial investigations along these lines have also been reported.

We attempt in the present work to provide an accurate and complete experimental summary of two aspects of the structure of ^{38}K. The first of these involves making a catalog of as many of the levels in the low-energy region

as possible, and assigning them precise excitation values. To this end, we have measured multiple spectra, using the (p,d) reaction on ^{39}K, with a resolution (10 keV, FWHM) that is at least three times better than that achieved in any of the previous particle-detection work on this nucleus[82,83] and ten times better than that achieved in previous single-neutron transfer experiments[64,84-86] leading to ^{38}K. The second aspect of our study involves measuring the ℓ-values of the neutron transfers which populate these states, and the associated spectroscopic factors. This has been done by a carefully cross checked DWBA analysis of the experimental angular distributions of the observed transitions, which were measured all the way in to $\theta_L=3^o$. We will discuss our results in their relation to the previous experimental situation and in their implications for the current theoretical pictures for this and neighboring nuclei.

IV.2. Experimental Procedure

Thin ($\sim$70 $\mu gm/cm^2$) targets were made by evaporating natural potassium metal (93% ^{39}K, 7% ^{41}K) onto thin carbon backings (30 $\mu gm/cm^2$). These targets were kept under vacuum throughout the experiment and thicknesses were estimated from the (p,d) yields and scattering chamber geometry. The targets were bombarded with 35 MeV protons from the MSU Cyclotron, and reaction products were analyzed in an Enge-type split-pole

magnetic spectrograph. Deuteron spectra were obtained both with a single-wire proportional counter[32] and with 25 micron-thick nuclear emulsion plates. The counter data yielded angular distributions at closely spaced angles from 3^{o} to 55^{o} for the strongly populated levels separated from their neighbors by more than the counter resolution of 50 keV, FWHM. The spectrograph acceptance aperture was 0.6 msr for angles than 30^{o} and 1.4 msr for angles greater than 30^{o}. Particle identification and data acquisition in this part of the experiment were accomplished in the MSU Sigma-7 computer.

An appropriate change of the spectrograph magnetic field allowed observation of protons elastically scattered from ^{39}K in an experimental configuration otherwise identical to that used for the (p,d) measurements. Data for $^{39}K(p,p_o)^{39}K$ were taken at angles from 25^{o} to 45^{o} and the cross-section normalization for the (p,d) data was taken relative to these elastic cross-sections, after an appropriate adjustment of the measured proton yields accounting for the 7% ^{41}K target contamination. The measured proton elastic scattering cross-sections were assumed to have the values predicted from an optical-model calculation using the Becchetti-Greenlees[37] parameters (see APPENDIX B). We estimate an uncertainty of 10% in the optical model prediction for this mass and angular range, and an additional 10% uncertainty in the mechanics of our normalization procedures.

Spectra were also taken with nuclear emulsions at laboratory angles from 4^{o} to 42^{o}. A typical example is shown in Fig. 18. The average resolution obtained for the deuteron groups here was approximately 10 keV, FWHM. The spectrograph acceptance apertures were the same as those used for the counter data and levels in ^{38}K up to 6 MeV of excitation were recorded. For each angle, the deuteron spectrum to approximately 4.5 MeV was collected on one 25 cm-long emulsion plate, with the remainder of the deuteron groups and the proton groups from scattering on ^{12}C, ^{16}O, and ^{39}K falling on a second abutting plate. The upper limit of 6 MeV for the energy range presented here was determined by the position of the elastic proton groups at forward angles. Relative normalization of all deuteron and proton spectra was accomplished by the use of a NaI monitor detector which recorded elastic protons scattered at 90^{o} to the beam. A beam-current integrator was also used to check normalization consistency.

IV.3. Excitation Energies

Centroids of the deuteron and proton groups which were used in the analysis and assignment of excitation energies were extracted from the spectra recorded with nuclear emulsions at 14^{o}, 18^{o}, and 20^{o}. The analysis involved the fitting of selected reference peak energies to precisely

Figure 18. A spectrum from the $^{39}K(p,d)^{38}K$ reaction, measured at 35 MeV and 30°, as recorded on nuclear emulsion plates. The resolution of the deuteron groups is 10 keV, FWHM. All ^{38}K excitation energy values are from the present work.

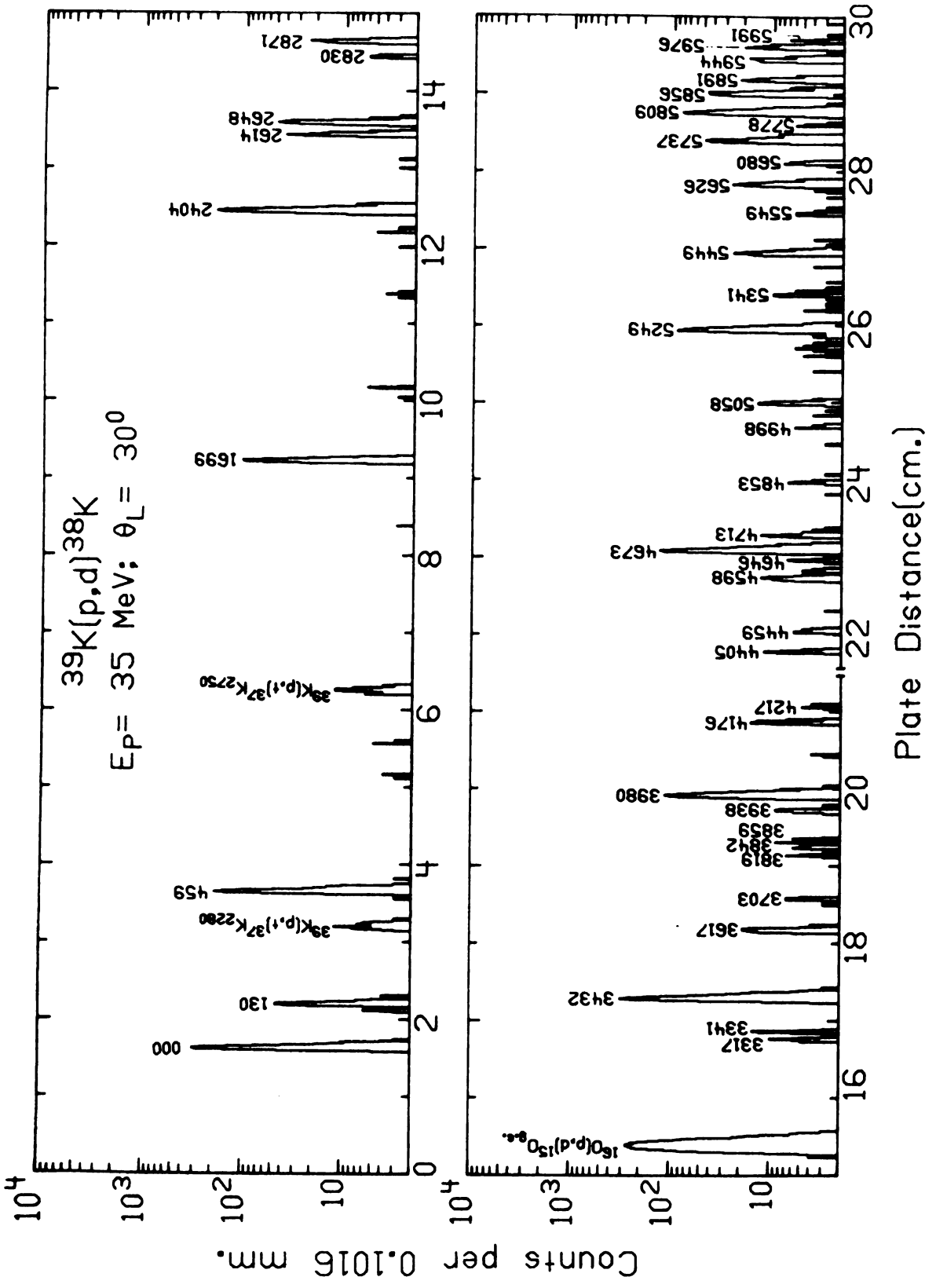
$^{39}K(p,d)^{38}K$
E_P= 35 MeV; θ_L= 30°
000
130
459
1699
2404
2614
2648
2830
2871
$^{39}K(p,\gamma)^{37}K_{2280}$
$^{39}K(p,\gamma)^{37}K_{2750}$
$^{16}O(p,d)^{15}O_{g.s.}$
3317
3341
3432
3617
3703
3819
3842
3859
3938
3980
4176
4217
4405
4459
4598
4646
4673
4713
4853
4998
5058
5249
5341
5449
5549
5626
5680
5737
5778
5809
5856
5891
5944
5976
5991
Counts per 0.1016 mm.
Plate Distance(cm.)

Figure 18

known values[34,67,87-89] via a least-squares iteration of the beam energy, the scattering angle, the small gap between the abutting plates, and the parameters appropriate to a quadratic Bρ vs. focal-plane-distance relationship.[67] The reference peaks chosen for this analysis (used only at those angles for which they yielded accurate, unambiguous centroids) are shown in Table 10. In all cases, appropriate target-loss corrections were taken into account. We found it impossible to obtain a good fit to the reference energies if we used the accepted $^{39}K(p,d)^{38}K$ Q-value of -10860 ± 8 keV.[34] An equal-weight, minimum chi-squared fit to all reference peaks was obtained by adjusting this accepted value by +9 keV. This same adjustment was required if all levels from $^{39}K(p,d)^{38}K$ except the ground state were omitted from the calibration data set. In all fits, the chi-squared-per-point value was $\sim$1. The greatest adjustments to the nominal beam energy and scattering angle which the fits required were 8 keV and 0.2°, respectively. These changes are compatible with the accuracy with which we set up the cyclotron beam line and the scattering chamber-spectrograph geometry.

The assignment of any given level to ^{38}K was made on the basis of a series of angle-to-angle comparisons of measured excitation energy. A level in ^{40}K (from $^{41}K(p,d)^{40}K$) misidentified at 14° as belonging to ^{38}K would, at 20°,

Table 10. States used in the energy calibration for the $^{39}K(p,d)^{38}K$ reaction data.

Reaction	Excitation Energy (keV) in Residual Nucleus
$^{39}K(p,d)^{38}K$	ground state[a]
	459.6 ± 1.2[b]
	1699.4 ± 1.3[b]
	2403.8 ± 1.2[b]
	2871.0 ± 1.2[b]
$^{16}O(p,d)^{15}O$	ground state[c]
$^{12}C(p,d)^{11}C$	ground state[c]
	1.9992 ± 1.0[d]
$^{39}K(p,p)^{39}K$	ground state
	2522.7 ± 0.3[e]
	3019.3 ± 0.2[e]
$^{16}O(p,p)^{16}O$	ground state
$^{12}C(p,p)^{12}C$	ground state
	4440.0 ± 0.5[f]

[a] Adjusted as described in text.
[b] Reference 87.
[c] Reference 34.
[d] Reference 67.
[e] Reference 88.
[f] Reference 89.

show a shift in assigned excitation energy of almost 4 keV because of the incorrect assumption made for the target mass. Shifts of this type, easily observed in the present high resolution data, naturally increase for larger angular differences, lighter nuclei and (p,t) reactions, allowing the unambiguous assignment of the various particle groups to specific residual nuclei.

The present analysis allowed the assignment of excitation energies to several levels in ^{40}K which fall close to the lowest few levels of ^{38}K in the spectrograph focal plane. Two of these levels, to which we make assignments of 2258 and 2575 keV, are known to have excitation energy values of 2260.6 ± 1.0 keV and 2574.7 ± 1.0 keV from Ge-Li detector studies of their gamma ray decays.[90] Since the Q-value for $^{41}K(p,d)^{40}K$ is known (-7871.3 ± 1.4 keV) to good accuracy[34] and our analysis indicates that $Q[^{41}K(p,d)^{40}K]-Q[^{39}K(p,d)^{38}K]=2980\pm2$ keV, we can assign $Q[^{39}K(p,d)^{38}K]=-10851\pm2$ keV either on the basis of this "local" comparison, which is essentially independent of the overall focal-plane calibration, or on the basis of the systematic calibration of 50 cm of the focal plane as described above.

The excitation energies we assign to levels of ^{38}K observed in the present study are presented in Table 11. The results of other studies of ^{38}K[82,83,85-87,91,92,64] are also presented in this table. It can be seen that almost all levels of ^{38}K observed in other reactions are found in the present

Table II. Energy levels of ^{38}K excited in the present investigation of the (p,d) reaction and in previous studies of other reactions.

Excitation Energy (keV)							
(p,d)[a]	(d,α,γ)[b]	(H.I.,γ)[c] and (β,γ)[d]	(d,α)[e]	(d,α)[f]	(d,t)[g]	(^{3}He,α)[h]	(^{3}He,α)[i]
000	000		000	000	000	000	000
130±1	131.4±1.2	130[c]	144	119	128	138	13(0)
459±1	459.6±1.2		459	43(0)	456	466	45(0)
1699±1	1699.4±1.3		1702	169(0)	1704	170(0)	170(0)
2404±1	2403.8±1.2		2403	241(0)	2405	240(0)	240(0)
2614±2	2514.1±1.4		2624	261(0)			
2648±1	2649.4±1.8	2646[c]		263(0)	2639	263(0)	264(0)
2830±1	2831.5±1.3			281(0)			
2871±1	2871.0±1.2		2864	284(0)		285(0)	287(0)
	2995 ±2		3000	297(0)			
				305(0)			
3317±1	3319 ±2		3327	333(0)			
3341±2	3347 ±3	3337[d]					
		3420[c]		342(0)			
3432±1	3432 ±2		3440	344(0)	3441	342(0)	344(0)
		3458[c]					
3617±1				360(0)			
	3670 ±2			365(0)			
3703±3			3691	367(0)			
				370(0)			371(0)
3819±2				379(0)			
3842±3				381(0)			
3859±3			3865	383(0)			
3938±2				391(0)			
3980±2			3980	394(0)	3989	397(0)	400(0)
4176±2				414(0)			420(0)
4217±2				418(0)			
4321±3							
4338±3							436(0)
4405±3							
4459±3							450(0)
4598±2							
4646±3							
4673±2					4660	460(0)	467(0)
4713±3							
4853±3							
4998±3							
5058±3							508(0)
5249±3						523(0)	525(0)
5341±3							
5449±2						544(0)	545(0)
5549±4							
5626±2							562(0)
5680±3							
5737±2							
5778±4							
5809±3							578(0)
5856±3							585(0)
5891±3							
5944±3							
5976±3							
5991±3							

[a] Present Work.

[b] Reference 87.

[c] Reference 91.

[d] Reference 92 (±10 keV).

[e] Reference 82 (quoted to only the nearest 10 keV).

[f] Reference 83.

[g] Reference 85 (±15 keV).

[h] Reference 86 (quoted to only the nearest 10 keV).

[i] Reference 64 (quoted to only the nearest 10 keV).

work. Below 4 MeV excitation there appear to be six levels observed in (d,α)[82,83] particle-detection experiments or in (d,α)[87] and heavy-ion initiated[91] gamma-detection experiments which we do not see in the (p,d) spectra. Reasonably sure correspondences can be established between the nineteen levels we do observe in this region and previously reported levels. Of the six levels we do not observe, three are seen by at least two other investigations, while two are reported only by Jänecke[83] and one only by Engelbertink.[91] There is reason to think[91] that the 3420 keV and 3458 keV levels have $J \geq 5$, which is consistent with their being very weakly populated via the (p,d) reaction. There are no such simple explanations available for our non-observance of the other four levels. In the 4-5 MeV region of excitation Jänecke again reports two or three more levels than we observe, but the discrepancies between his and our energy calibrations make it difficult to be sure which levels are which in that region.

Of the forty-six levels below 6 MeV excitation observed in the present study, only twenty have been observed in the various previous studies of single-nucleon transfer reactions leading to ^{38}K. All of the levels reported in these earlier investigations are observed in the present work.

The excitation energy assignments made in the present study agree well with the results of the most precise previous investigations.[82,87,91,92] The only significant discrepancy is the 6 keV gap between the (p,d) recorded energy of 3341 ± 2 keV

and the (d,αγ) recorded energy of 3347±3 keV. Some of the energies quoted in Ref. 93 differ widely from our values, but these discrepancies are probably not outside the uncertainties, arising from lack of resolution, in that particular study.

The uncertainties quoted for our excitation energies are the total estimated probable errors, compounded from the reproducibility of peak positions inherent in the scanning of the emulsions, uncertainties in the calibration energies, and uncertainties in the details of the spectrograph calibration. They are consistent with the scatter observed in analyzing several different spectra with several variations of the way in which the energy-analysis program is applied. Values of the differences in excitation energy between pairs of states 50 to 1000 keV apart should always be good to 1-2 keV as long as both were populated with reasonable strength.

IV.4. Angular Distributions

IV.4.A. Discussion of DWBA Calculations

The DWBA calculations[49] we discuss here were all made with the proton optical-model parameters of Ref. 37. Although another parameter set[50] produces discernibly different proton elastic scattering predictions for s-d shell nuclei at E_p=35 MeV, the DWBA (p,d) predictions are quite insensitive to the differences between these two proton potentials.

There is a lack of extensive deuteron elastic scattering data for the mass region of the s-d shell at energies appropriate to the present experiment. This necessitated an extensive survey of the relevant literature in an attempt to find a suitable set of such parameters. The criterion of suitability was, of course, a reasonable reproduction of our observed angular distribution shapes. The criterion for a good $\ell=2$ prediction was a match to known pure $\ell=2$ distributions obtained in the present work and in simultaneously performed measurements of the $^{35}Cl(p,d)^{34}Cl$ reaction.[7] Correspondence to the pure $\ell=0$ transitions leading to the 0.842 MeV and 5.49 MeV levels in ^{33}S, observed via the $^{34}S(p,d)^{33}S$ reaction at $E_p=35$ MeV, was used as the criterion for a good $\ell=0$ DWBA shape.

We have investigated the efficacy of deuteron potentials proposed by Hinterberger, et al.,[51] Perey and Perey,[53] Newman, et al.,[52] Schwandt and Haeberli,[54] Mermaz, et al.,[55] and Cowley, et al.[98] in both the local, zero-range (LZR) and the finite-range, non-local (FRNL) versions of the DWBA. The non-locality parameters used for the proton and deuteron channels were, respectively, the standard[49] values 0.85 and 0.54. The geometry of the neutron bound-state wave function had the standard Woods-Saxon form, $r_o=1.24$ fm, $a=0.65$ fm, and a Thomas spin-orbit term with $\lambda=25$. The depth of the bound-state potential well was always adjusted to match the experimental neutron separation energies corresponding to the various excited states of ^{38}K. The finite-range parameter was 0.621.[49]

All calculations were carried out with no lower cut-off in the radial integration.

In addition, we investigated the "adiabatic" prescription for deuteron-proton transfer reactions, as proposed by Johnson and Soper[43] and shown to yield good results for reactions on lead,[45] f-p shell,[44] and oxygen,[46-48] targets, and a "density-dependent" damping of the V_{pn} interaction as proposed by Preedom.[48]

When any of the conventional[51-55,98] deuteron optical-model potentials was used, the calculated shapes of ℓ=0 and ℓ=2 distributions were in much better agreement with our experimental test cases in the FRNL approximation than in the LZR approximation. The best results obtained with any of the various potentials[51-55] appear to be obtained with the "Set I" parameters of Hinterberger, et al.[51] (see Table 12), which is gratifying, since this potential set is probably the best grounded in terms of mass and energy dependence. The Hinterberger, et al. "Set II" and the Newman, et al. potentials yielded results not too different from those of "Set I".

The critical success of the Hinterberger "Set I" parameters, relative to potentials of different origins, lies in its correct reproduction of the forward angle ($\theta_{cm}<20^{o}$) ℓ=0 and ℓ=2 shapes. Its principle failing, shared by all the others to a greater or lesser extent, is its overestimation of cross-sections at larger angles ($\theta_{cm}>30^{o}$), a failing which grows more pronounced as the Q-values become more negative (excitation

Table 12. Optical-model parameters used in the analysis of the $^{39}K(p,d)^{38}K$ data.

Particle	V_R (MeV)	r_R (fm)	a_R (fm)	W_V (MeV)	r_V (fm)	a_V (fm)	W_{sf} (MeV)	r_{sf} (fm)	a_{sf} (fm)	V_{so} (MeV)	r_{so} (fm)	a_{so} (fm)	r_c (fm)
Proton[a]	45.66	1.17	0.75	5.0	1.32	0.53	3.36	1.32	0.53	6.2	1.01	0.75	1.17
Deuteron[b] (FRNL and DFRNL)	87.48-0.35 E_{cm}	1.25	0.729				13.0	1.25	0.766	6.0	1.25	0.729	1.3
Deuteron[c] (ADIABATIC)	103.79[d]	1.17	0.779	1.08[d]	1.29	0589	17.53[d]	1.29	0.583	6.2	1.01	0.75	1.17
Neutron Bound State	Adjusted to match separation energy	1.24	0.65							λ=25			1.24

[a] Reference 37.

[b] Ref. 51 averaged parameter Set 1 of Hinterberger, et al.

[c] Ref. 43 neutron and proton parameters from Ref. 37.

[d] Values shown are for E_x=0.000 MeV only; Q-dependence as given in Ref. 37.

energies get higher, binding energies of transferred neutrons become larger). Experience led us to expect that both the "abiabatic"[43] and the "density-dependent"[48] alterations to the conventional DWBA procedure would improve the predictions at these larger angles. The "adiabatic" potential, designed to account for effects resulting from disassociation of the deuteron, is not related to actual deuteron elastic scattering data but is constructed from proton and neutron optical-model potentials (taken from Ref. 37 in the present instance) according to a particular prescription.[43,47] The adiabatic-potential calculations were carried out in the LZR approximation, since the FRNL corrections did not yield significantly different results.

The "density-dependent damping" of the V_{pn} interaction,[48] motivated by a paper by Green,[69] provides an alternate means to reduce DWBA cross-sections at larger angles. We have chosen the damping factor $F(r)=(1.0-1.845\rho(r)^{2/3})$, where $\rho(r)=0.17[1+\exp(x)]^{-1}$, $x(r-r_oA^{1/3})/a$ and "r_o" and "a" are the radius and diffusivity of the neutron bound-state well. The density-dependent V_{pn} damping was studied in conjunction with FRNL calculations which used the Hinterberger, et al. "Set I" deuteron potential.

We have analyzed our data in detail with the following DWBA calculations (see Table 12): (1) The Becchetti-Greenlees[37] proton parameters and Hinterberger, et al.[51] "Set I" deuteron parameters, using the FRNL approximation. These calculations,

henceforth referred to as FRNL, are thus completely orthodox and unadjusted. (2) This same combination of proton and deuteron parameters and computational approximations, but with the addition of the density-dependent damping of the V_{pn} interaction, henceforth referred to as DFRNL, and (3) The Becchetti-Greenlees proton parameters and the adiabatic deuteron parameters in the LZR approximation, henceforth referred to as ADIABATIC.

The results of these three types of DWBA calculations are compared with each other and with some of our experimental data in Figs. 19 and 20. The general characteristics of these calculations, relative to the experimentally observed ℓ=2 and ℓ=0 transfer distributions, are as follows. The FRNL calculations fit the pure ℓ=2,j=3/2 observed shapes from 3^{o} out to 50^{o} quite well; the indications are that from 50^{o} on out, the theoretical differential cross sections are too large. For ℓ=0 transitions, the observed shapes are reasonably well reproduced out over the second maximum, but from there on, the theoretical predictions are much too large. In addition, the structure of the theoretical distributions begins to be flattened out for states at higher excitation energies, while the observed shapes seem almost independent of the Q-value involved.

The DFRNL calculations fit the ℓ=2 observed shapes essentially perfectly throughout the experimental angular range covered. The agreement with the observed ℓ=0 shapes is considerably improved over the FRNL predictions, but cross-sections are still

Figure 19. A comparison of fits to representative angular distributions from the $^{39}K(p,d)^{38}K$ reaction at 35 MeV with the three chosen types of DWBA calculations. All fits were performed over the 3° to 35° angular region. The curves are identified as follows: ——DFRNL, ----FRNL, and — —ABIABATIC.

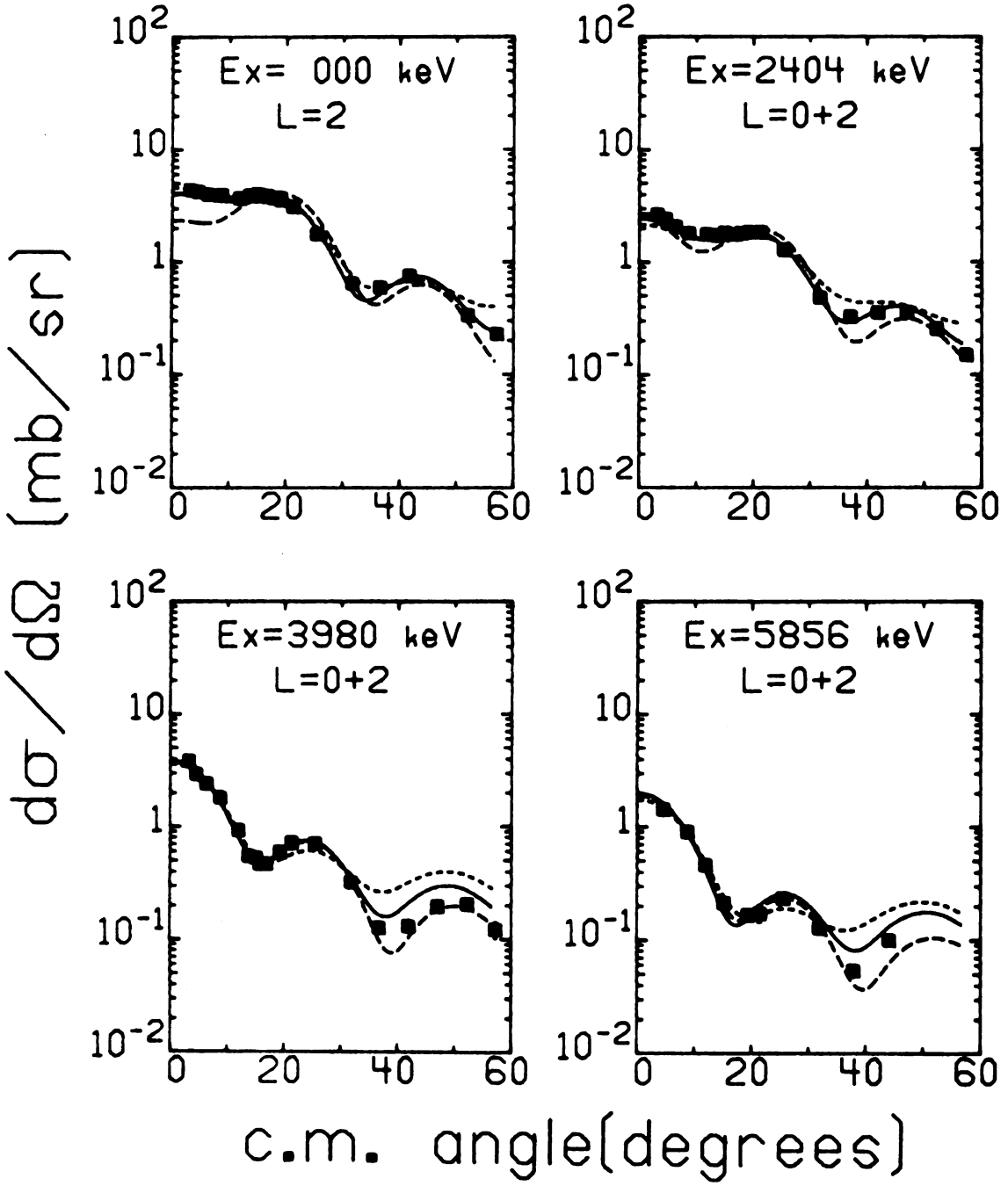
Ex= 000 keV
L=2
Ex=2404 keV
L=0+2
Ex=3980 keV
L=0+2
Ex=5856 keV
L=0+2
dσ / dΩ (mb / sr)
c.m. angle(degrees)

Figure 19

Figure 20. A comparison of ADIABATIC, FRNL, and DFRNL calculations (see text and Table 12) with ℓ=0 transitions in the $^{34}S(p,d)^{33}S$ reaction at 35 MeV.

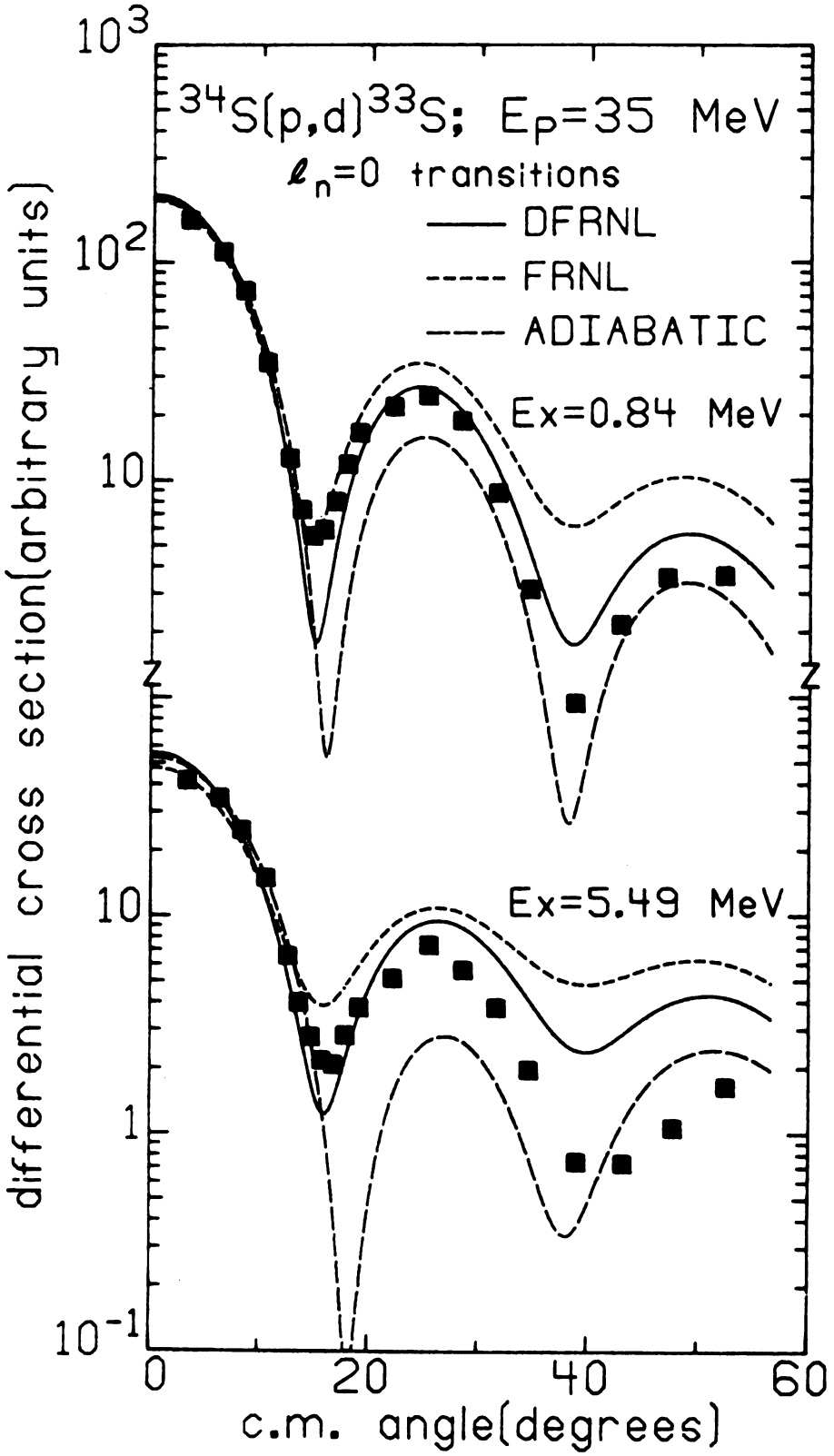
$^{34}S(p,d)^{33}S$; E_p=35 MeV
ℓ_n=0 transitions
DFRNL
FRNL
ADIABATIC
Ex=0.84 MeV
Ex=5.49 MeV
differential cross section(arbitrary units)
c.m. angle(degrees)
10^3
10^2
10
10
1
10^{-1}
0
20
40
60

Figure 20

somewhat too large beyond 30^{o}, and the undesired trend of shape with Q-value persists.

Finally, the ADIABATIC calculations do not match the forward angle ($\theta_{cm} < 15^{o}$) behavior observed for the $\ell=2$ distributions, although for $\theta_{cm} > 15^{o}$, the fits to the data are as good as the FRNL results (but still not as good as the DFRNL results). The differential cross sections predicted for $\theta_{cm} > 20^{o}$ for the $\ell=0$ distributions are indeed lower than those obtained with the FRNL and DFRNL calculations, but over the 3^{o}-40^{o} region, the agreement with experiment is worse for states at high excitation energy and only comparable for lower excited levels.

IV.4.B. Analysis of Experimental Angular Distributions

Our measurements of the angular distributions of the intensities with which states in ^{38}K are populated in the $^{39}K(p,d)^{38}K$ reaction at $E_p=35$ MeV are presented in Figs. 21-24. Some states included in the table of excitation energies are not shown because they were not observed at a sufficient number of angles. The solid curves through the data points are fits of the DFRNL calculations described above. These fits, and the resulting spectroscopic factors, were obtained by minimizing the quantity

$$\chi^2 = \frac{1}{N} \sum_{i=1}^{N} \left[\left(A_{\ell j} \frac{\frac{d\sigma}{d\Omega}(\theta_i)_{\ell j,DWBA}}{2j+1} - \frac{d\sigma}{d\Omega}(\theta_i)_{exp} \right) / \Delta\sigma_i \right]^2$$

through the adjustment of the coefficients $A_{\ell j}$. Here, $\frac{d\sigma}{d\Omega}(\theta_i)_{\ell j,DWBA}$ are the numbers output from the DWUCK program for angles θ_i, $\frac{d\sigma}{d\Omega}(\theta_i)_{exp}$ are the experimental differential cross-sections and $\Delta\sigma_i$ are the statistical plus estimated relative systematic errors in the experimental numbers. Values of ℓ=0 plus 2, or 1 plus 3, were used except in special cases where known spin assignments precluded mixing. The number of data points, N, included all observations in the angular range 3^o-35^o. The spectroscopic factors, weighted by the isospin Clebsch-Gordon factors, are then obtained from the relation

$$A_{\ell j} = 2.29\ C^2 S_{\ell j}.$$

In Table 13 we list the excitation energies, ℓ-value assignments and spectroscopic factors for all the states whose angular distributions we considered analyzable. The DFRNL DWBA calculations were used in extracting these numbers.

We carried out the same fitting procedure, again with the DFRNL predictions, including all data points out to 60^o. The maximum changes in the resulting spectroscopic factors were 10%. We also carried out the fitting procedure for all distributions, in the 3^o-35^o angular range, with the FRNL and ADIABATIC DWBA predictions. The DFRNL results are compared to the FRNL and ADIABATIC results and to results of previous experiments and analyses in Table 14. Only those states previously observed are included in this table, to keep the size

Figure 21. Experimental angular distributions for states in ^{38}K, as observed in the $^{39}K(p,d)^{38}K$ reaction at 35 MeV. The solid curves are fits of the DFRNL calculations to the data in the angular range from 3^{o} to 35^{o}. The dotted curves show the amount of the $\ell=0$ component in mixed $\ell=0$-$\ell=2$ distributions.

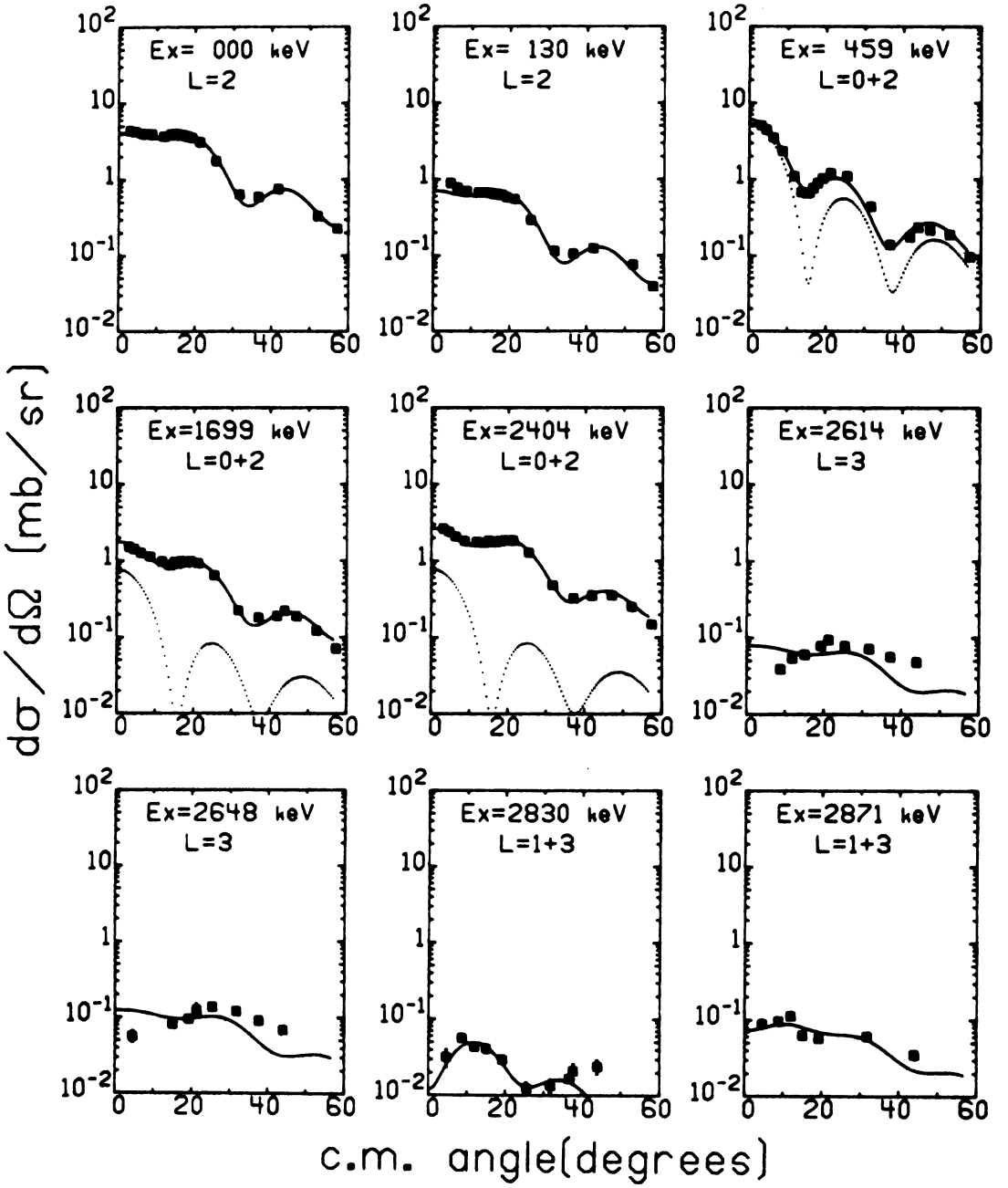
Ex= 000 keV
L=2
Ex= 130 keV
L=2
Ex= 459 keV
L=0+2
Ex=1699 keV
L=0+2
Ex=2404 keV
L=0+2
Ex=2614 keV
L=3
Ex=2648 keV
L=3
Ex=2830 keV
L=1+3
Ex=2871 keV
L=1+3
dσ/dΩ (mb/sr)
c.m. angle(degrees)

Figure 21

Figure 22. Experimental angular distributions for states in ^{38}K, as observed in the $^{39}K(p,d)^{38}K$ reaction at 35 MeV. The solid curves are fits of the DFRNL calculations to the data in the angular range from 3° to 35°. The dotted curves show the amount of the $\ell=0$ component in mixed $\ell=0$-$\ell=2$ distributions.

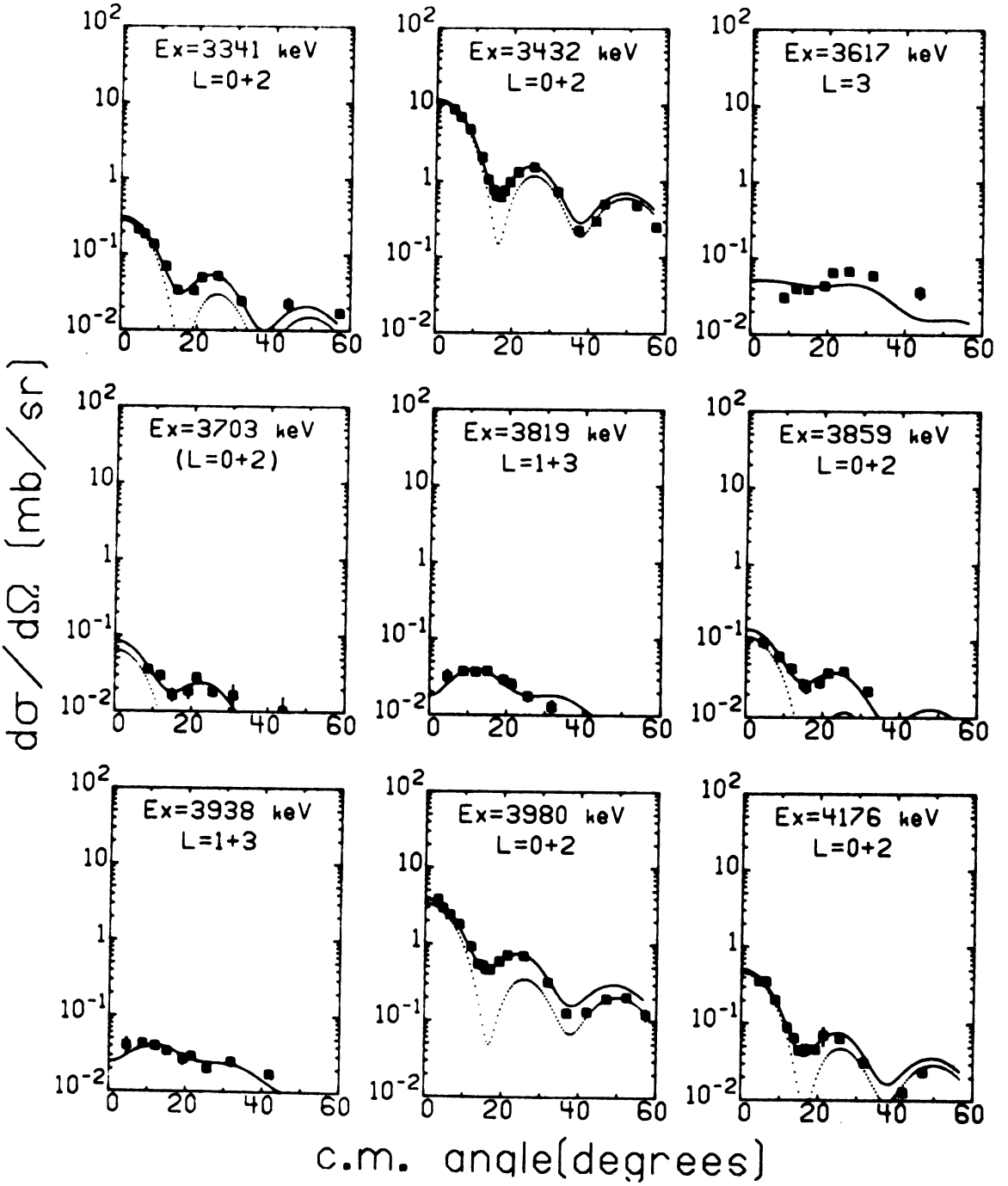
Ex=3341 keV
L=0+2
Ex=3432 keV
L=0+2
Ex=3617 keV
L=3
Ex=3703 keV
(L=0+2)
Ex=3819 keV
L=1+3
Ex=3859 keV
L=0+2
Ex=3938 keV
L=1+3
Ex=3980 keV
L=0+2
Ex=4176 keV
L=0+2
dσ/dΩ (mb/sr)
c.m. angle(degrees)

Figure 22

Figure 23. Experimental angular distributions for states in ^{38}K, as observed in the $^{39}K(p,d)^{38}K$ reaction at 35 MeV. The solid curves are fits of the DFRNL calculations to the data in the angular range from 3^{o} to 35^{o}. The dotted curves show the amount of the $\ell=0$ component in mixed $\ell=0$-$\ell=2$ distributions.

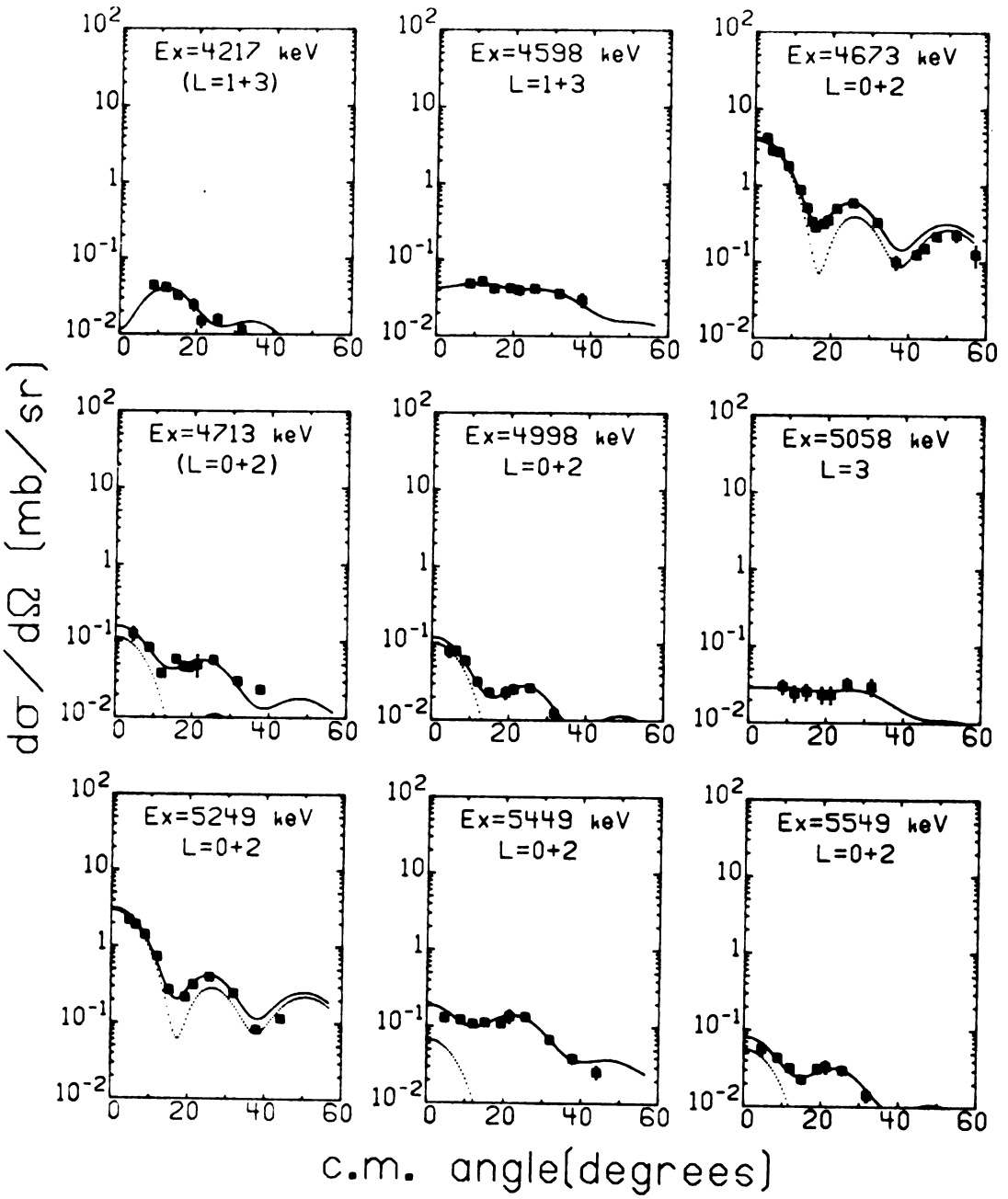
Ex=4217 keV
(L=1+3)
Ex=4598 keV
L=1+3
Ex=4673 keV
L=0+2
Ex=4713 keV
(L=0+2)
Ex=4998 keV
L=0+2
Ex=5058 keV
L=3
Ex=5249 keV
L=0+2
Ex=5449 keV
L=0+2
Ex=5549 keV
L=0+2
dσ/dΩ (mb/sr)
c.m. angle(degrees)

Figure 23

Figure 24. Experimental angular distributions for states in ^{38}K, as observed in the $^{39}K(p,d)^{38}K$ reaction at 35 MeV. The solid curves are fits of the DFRNL calculations to the data in the angular range from 3° to 35°. The dotted curves show the amount of the $\ell=0$ component in mixed $\ell=0$-$\ell=2$ distributions.

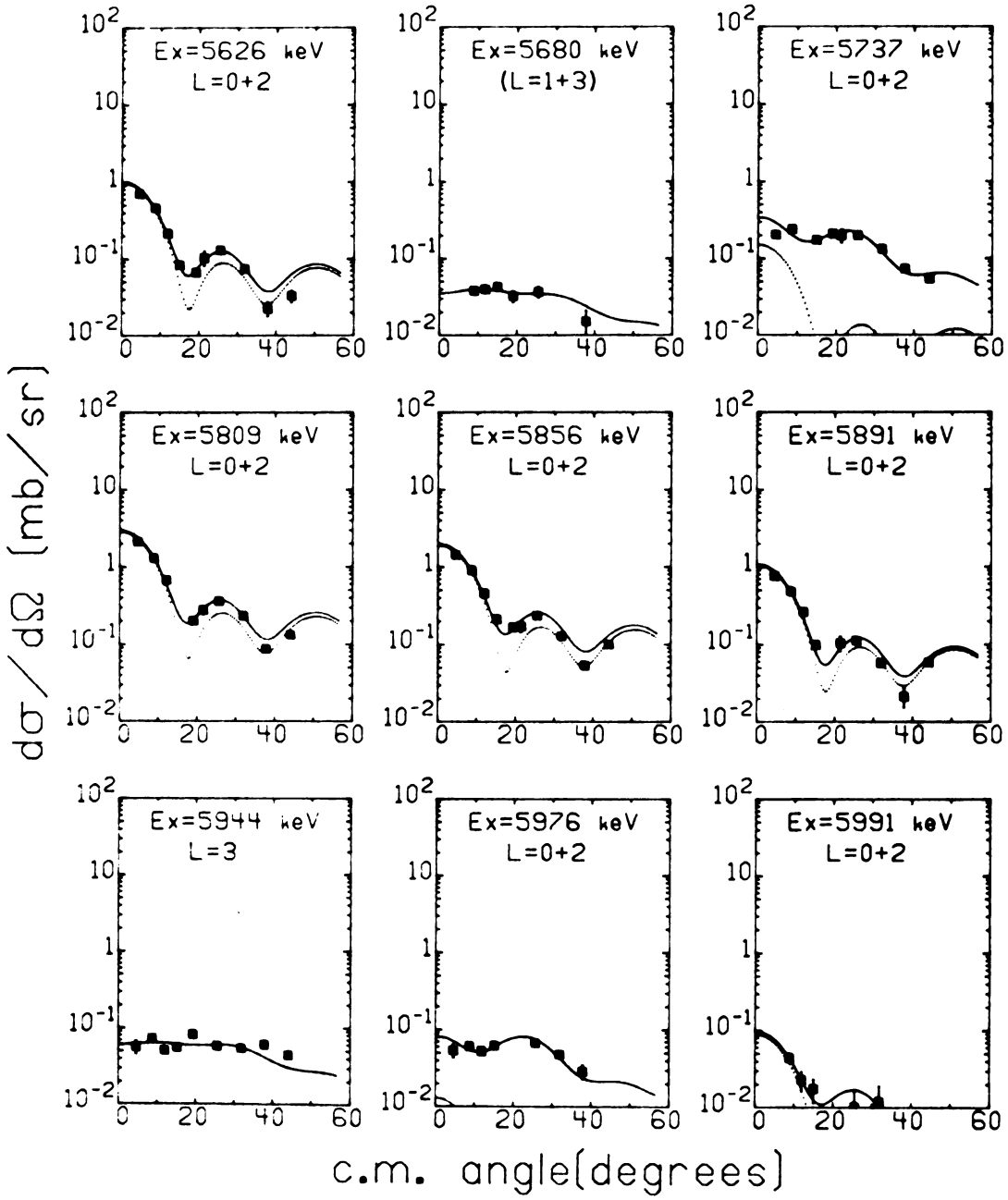
Ex=5626 keV
L=0+2
Ex=5680 keV
(L=1+3)
Ex=5737 keV
L=0+2
Ex=5809 keV
L=0+2
Ex=5856 keV
L=0+2
Ex=5891 keV
L=0+2
Ex=5944 keV
L=3
Ex=5976 keV
L=0+2
Ex=5991 keV
L=0+2
dσ/dΩ (mb/sr)
c.m. angle(degrees)

Figure 24

Table 13. Experimental values of ℓ and C^2S_ℓ, obtained from the DFRNL analysis for transitions from ^{39}K to ^{38}K as observed in the present investigation. All values are normalized so that C^2S_ℓ for the ground state is 1.75. The assumed j-values are 3/2 for ℓ=2, 3/2 (n=2) for ℓ=1, and 7/2 for ℓ=3.

E_x(keV)	J^π,T^a	ℓ	C^2S_ℓ	E_x(keV)	J^π,T^a	ℓ	C^2S_ℓ
000	$3^+,0$	2	1.75	4217		(1,3)	0.02 ,0.01
130	$0^+,1$	2	0.31	4598		1,3	0.005,0.04
459	$1^+,0$	0,2	0.13 ,0.32	4673	$(1,2)^+,1$	0,2	0.19 ,0.25
1699	$1^+,0$	0,2	0.02 ,0.57	4713		(0,2)	0.005,0.05
2404	$2^+,1$	0,2	0.03 ,1.26	4998		0,2	0.005,0.02
2614		3	0.05	5058		3	0.03
2648	$(2,3)^-$	3	0.08	5249	$(1,2)^+,1$	0,2	0.16 ,0.17
2830	$(0,3)^-$	1,3	0.02 ,0.01	5449		0,2	0.004,0.15
2871	$(0,3)^-$	1,3	0.01 ,0.05	5549		0,2	0.003,0.03
3341	$1^+,0$	0,2	0.01 ,0.02	5626		0,2	0.06 ,0.05
3432	$2^+,0$	0,2	0.43 ,0.43	5680		(1,3)	0.003,0.04
3617		3	0.04	5737		0,2	0.009,0.26
3703		(0,2)	0.003,0.02	5809	$(1,2)^+$	0,2	0.17 ,0.16
3819		1,3	0.01 ,0.02	5856	$(1,2)^+$	0,2	0.11 ,0.12
3859		0,2	0.005,0.03	5891	$(1,2)^+$	0,2	0.06 ,0.04
3938		1,3	0.01 ,0.02	5944		3	0.08
3980	$(2)^+,1$	0,2	0.14 ,0.42	5976		0,2	0.001,0.10
4176		0,2	0.02 ,0.03	5991		0,2	0.006,0.01

[a]References 84, 85, 87, 92, 93, 94.

manageable, but these suffice to indicate the trends and scatter of the spectroscopic factors as functions of the details of the DWBA calculations.

IV.4.C. Assignment of ℓ-values

Of the forty-six ^{38}K levels observed in the present investigation, thirty-six can be assigned at least tentative values for the orbital angular momentum quantum numbers of the neutrons transferred in the process of their formation (see Table 13). Twenty-four levels are assigned pure $\ell=2$ or a combination of $\ell=0$ and $\ell=2$ transfers. The basis for these assignments is typically an excellent and unambiguous fit to the the experimental distribution with a mixture of calculated $\ell=0$ and $\ell=2$ shapes. Most of the transitions having significant $\ell=0$ strength are also easily recognized simply on the basis of the differential cross-sections for this type of transfer, which is clearly evident in the 3^{o}-13^{o} portion of our angular distributions.

Assignments of negative-parity ℓ-values ($\ell=1$ and 3) could not, in general, be made with the assurance possible for the positive parity cases. This was because the experimental distributions were rather featureless (except for a few examples dominated by $\ell=1$) and because the calculated $\ell=3$ shape does not appear to fit the data as well as those for $\ell=0$, 1 and 2. Consequently, it is possible in many cases to get as reasonable

a fit to the data with ℓ=2+4 shapes as it is with ℓ=1+3 shapes. In addition, there is the uncertainty as to whether some of the weakest, flattest distributions observed are even characteristic of a single-step direct transfer. We have assigned a negative parity (ℓ=3 and/or 1) to twelve of the levels observed. Many of these assignments, however, are dependent upon an assumption which rules out the possibility of significant ℓ=4 transfer strength in the present experiment.

Questions involving the agreement of the present assignments with previous results, their relationship to theoretical studies, and the degree of certainty with which the presence or absence of a particular ℓ-value component can be detected in a given transition will be discussed in the following sections.

IV.4.D. Discussion of Values Extracted for C^2S

In the present study, we are not concerned with extracting the absolute magnitude of the single nucleon transfer spectroscopic factors. We are interested primarily in trying to get some measure of the reliability of relative spectroscopic factors for a particular ℓ-transfer as a function of Q-value (or the separation energy for the picked-up neutron), and of the relative values for different (ℓ=2 vs. ℓ=0) ℓ-transfers. The latter point reduces, in the limit, to the question of the certainty with which a weak component of one mode of ℓ-transfer can be identified in a transition dominated by the other. This,

of course, is important beyond just the spectroscopic factor, since the presence of a particular ℓ often has direct implications for the spin of the residual state.

The accuracy with which the Q-dependent effects on overall cross-section magnitudes are reproduced by DWBA calculations is difficult to pin down, but serious difficulties have been noted.[79,94] We mentioned in a previous section that details of the angular distributions as a function of Q-value are not well handled in all cases. We have merely tried rather different sets of optical-model parameters and examined the consistency of the results. This was also the tack used to examine the accuracy (really only the consistency) of the relative magnitudes of the peak cross-sections for different ℓ transfers. The results of these studies, covering not only the three types of DWBA calculations already discussed here in some detail, but also a good many others, indicate that most reasonable DWBA formulations for the (p,d) reaction yield consistent results within the domain of the residual nuclear states studied here. The extent to which these results are "correct" can be further explored by comparing extracted spectroscopic factors with those obtained from other reactions, as will be done in a following section.

The spectroscopic factors extracted from a fit to (generally) mixed-ℓ angular distributions contain Q-dependent and ℓ-dependent uncertainties arising from errors and lack of completeness in the data set, and from failures of the

Table 14. Experimental values of C^2S_ℓ for the transitions from ^{39}K to ^{38}K. The absolute values for the ground state are presented in parentheses. All other values are normalized such that $C^2S=1.75$ for the ground state.

E_x(keV)[a]	J^π,T	ℓ_n	DFRNL[a]	FRNL[a]	ADIABATIC[a]	(d,t)[b]	(^{3}He,α)[c]	(^{3}He,α)[d]	(d,^{3}He)	
000	3^+,0	2	1.75 (3.52)	1.75 (2.51)	1.75 (3.09)	1.75 (1.83)	1.75 (1.83)	1.75 (1.9)	e	f
130	0^+,1	2	0.31	0.31	0.31	0.25	0.32[g]	0.45	0.25	0.26
459	1^+,0	0	0.13	0.16	0.12	0.10	0.19	0.18		
		2	0.32	0.29	0.33	0.38	0.22	0.27		
1699	1^+,0	0	0.02	0.02	0.04	0.00	0.05	<0.07		
		2	0.57	0.53	0.52	0.72	0.56	0.68		
2404	2^+,1	0	0.03	0.00	0.05	0.05	0.27	<0.14		
		2	1.26	1.16	1.16	0.98	1.10	1.2	1.25	1.25
2648	,0	1				0.09	0.02	0.13		
		3	0.05	0.07	0.06		0.08			
3432	2^+,0	0	0.43	0.48	0.35	0.32	0.51	0.51		
		2	0.43	0.14	0.51	0.26	0.07	0.22		
3980	$(1,2)^+$,1	0	0.14	0.16	0.13	0.06	0.23	0.23	0.13	0.08
		2	0.42	0.25	0.43	0.48	0.31	0.34		
4673	$(1,2)^+$,1	0	0.19	0.20	0.15		0.21	0.29	0.31	0.24
		2	0.25	0.07	0.29	0.49[h]	0.15	0.12		
5249	$(1,2)^+$,1	0	0.16	0.16	0.13		0.18	0.23	0.16	0.12
		2	0.17	0.06	0.22		0.00	0.23		
5449	$(1,2)^+$,0	0	0.00	0.00	0.01		0.02			
		2	0.15	0.11	0.13		0.09			
5809	$(1,2)^+$	0	0.17	0.16	0.13					
		2	0.16	0.09	0.24					
5856	$(1,2)^+$	0	0.11	0.11	0.09				0.39	0.32
		2	0.12	0.05	0.16					
5891	$(1,2)^+$	0	0.06	0.06	0.05					
		2	0.04	0.01	0.07					

[a] Present work; all ℓ=2 spectroscopic factors for $d_{3/2}$ transfer.
[b] Reference 85.
[c] Reference 86; radial cut-off=2.8 fm.
[d] Reference 64; $E_{^3He}$=10 MeV; $C^2S_{2,3/2}$ below 2.5 MeV, $C^2S_{2,5/2}$ above 2.5 MeV.
[e] Reference 94.
[f] Reference 79.
[g] $C^2S_{0,1/2}$=0.03 also reported.
[h] ℓ=3.

DWBA curves to exactly reproduce the shapes of pure -ℓ distributions, as well as from the more fundamental uncertainties in cross-section trends mentioned above. By measuring the experimental distributions in to 3^{o} we have insured that the ℓ=0 spectroscopic factors are free from the extra uncertainties chronic in many previous studies, in which the data extends in to cover only the second maximum of the ℓ=0 shape. The intrinsic cross-section of the DWBA-calculated ℓ=0 transition at 3^{o} is $\sim$20 times the magnitude of the ℓ=2 prediction at its maximum. Hence, our extracted values for $C^2S(\ell=0)$ are extremely secure in an experimental sense. That is, there is no way to reproduce the shape of an experimental distribution which has a significant peaking at 0^{o} without putting in essentially the total amount of ℓ=0 strength obtained in our fits. The exact amount of ℓ=0 admixture in a predominantly ℓ=2 distribution can be given to an accuracy sufficient for any meaningful comparison with theoretical predictions. The more interesting question, involving weak to non-existent ℓ=0 components, concerns the limit to which their presence can definitely be assigned. The better the quality of the data and the better the theoretical fit to pure ℓ=2 shapes, the more stringent a criterion may be employed. We think that in the present work the presence of an ℓ=0 component is unambiguously established if $C^2S(\ell=0)\geq 0.005$.

The problem of extracting accurate ℓ=2 spectroscopic factors from shapes displaying significant ℓ=0 character is

much more difficult than the converse problem. Since the intrinsic magnitudes of the $\ell=2$ DWBA cross-sections are so much smaller than those of the $\ell=0$ predictions, and are also relatively unstructured, the amount (and the uncertainty thereof) of observed $\ell=2$ strength in an apparently $\ell=0$ experimental shape can be quite significant in terms of nuclear structure predictions. Unless one has perfect $\ell=0$ DWBA predictions and essentially perfect data, this problem seems impossible to overcome. An objective, integrating-fit criterion such as we have used is probably not the best approach to extracting $\ell=2$ components unless the theoretical $\ell=0$ fits are quite good. It is quite possible that the $\ell=2$ strength assigned by the fit serves predominantly to compenstate for the principle defect in the $\ell=0$ predicted shapes. We think that the fits of the DFRNL predictions to the data are good enough to justify an automatic, non-subjective analysis procedure. Some of the lack of consistency which crops up in the comparison between spectroscopic factors extracted with the three different calculations surely arises from deficiencies in the FRNL and ADIABATIC $\ell=0$ shapes.

IV.5. Discussion of Results

IV.5.A. Comparison with Previous Experimental Results

All levels in ^{38}Ar ($T=T_z=1$) should have analogues in the ^{38}K spectrum which have essentially the same properties.

Experiments[79,94] with the $^{39}K(d,^{3}He)^{38}Ar$ reaction show that the 0^+ ground state and the 2^+ first excited state at 2.167 MeV are strongly populated with $\ell=2$ transfer and that 2^+, 2^+, 2^+, and $(1,2)^+$ levels at 3.937, 4.565, 5.157, and 5.552 MeV, respectively,[95] are strongly populated via $\ell=0$ transfer. It was explained in Ref. 94, before unique spins for the higher states were known, that the spectroscopic factors for states below 6 MeV excitation observed in the $^{39}K(d,^{3}He)^{38}Ar$ reaction could be understood in terms of a $(d_{3/2}^{-1})_{J=3/2}$ model for ^{39}K, $(d_{3/2}^{-2})_{J=0}$ and 2 wave functions for the ground and first excited states ($d_{3/2}$ pickup) and $(d_{3/2}^{-1}s_{1/2}^{-1})_{J=1,2}$ wave-functions for the higher lying $\ell=0$ strength. Since only one 1^+ and one 2^+ state can be formed from the $s_{1/2}$-$d_{3/2}$ coupling and four $\ell=0$ states are observed, it is obvious that fragmentation of the $\ell=0$ strength into states arising from other configurations occurs. It was argued in Ref. 94 that the fragmentation most probably involved 2^+ states (since confirmed), and that the extra two 2^+ states had their origins in f-p shell configurations rather than in $d_{5/2}$ hole excitations. The state at 5.55 MeV was suggested to have $J^{\pi}=1^+$.

All of these strongly excited levels in ^{38}Ar should be observed, with similar relative strength, in the $^{39}K(p,d)^{38}K$ spectra. The total number of ^{38}Ar states presently known to exist below 6 MeV excitation is 21. Our present high resolution data may allow the observation of others. The analogues of the first five strongly excited ^{38}Ar levels are observed at 130, 2404, 3980, 4673, and 5249 keV. Relative to the lowest 0^+,T=1 state, the energy shifts of these five

excited states in ^{38}K, relative to ^{38}Ar, are +107, -87, -22, and -42 keV, respectively.

The analogue of the 5.552 ("5.85") MeV level in ^{38}Ar observed in (d,^{3}He) is not clearly identifiable in ^{38}K. We observe three ℓ=0 transitions in the 5800-5900 keV region in the present experiment which would not have been resolved in the (d,^{3}He) study. However, only one (at 5.552 MeV) positive-parity level is known to exist[95] in the appropriate energy region of ^{38}Ar, implying that the ℓ=0 transition observed in (d,^{3}He) proceeds to a single state. All this implies that two of the three ℓ=0 states we observe in ^{38}K near 5.85 MeV excitation have T=0. However, the ℓ=0 spectroscopic strength observed in (d,^{3}He) is significantly greater than that of any one of the 5.85 MeV states in ^{38}K.

The consistency between the spectroscopic factors extracted from the (d,^{3}He) data and the (p,d) data can be inspected in Table 14. The apparent analogues of the first five strongly excited levels in ^{38}Ar have $^{39}K(p,d)^{38}K$ spectroscopic factors consistent with the (d,^{3}He) values, the largest deviation occuring for the 4.673 MeV state. Thus, it seems likely that the failure to find a single state in the 5.85 MeV region of ^{38}K which has spectroscopic strength comparable to the $(1)^{+}$,T=1 state at the corresponding energy in ^{38}Ar, together with the other features of the situation just discussed, is evidence of almost complete mixing of the 1^{+},T=1

state which must occur in this region in ^{38}K with one, and probably two, close lying T=0 neighbors. Indeed, the summed spectroscopic strength of the three ^{38}K levels at 5.85 nicely equals the strength of the (presumed) single state in ^{38}Ar.

It is not possible to establish further isospin assignments in ^{38}K via correspondence between the ^{38}K and ^{38}Ar level schemes because the level densities are high relative to the average Coulomb shifts and because proton pick-up data comparable to the present neutron pick-up work does not exist.

The agreement between the present results and those of previous neutron pick-up studies of ^{38}K seems quite good, considering the limitations of the older data. It is perhaps interesting that, on the average, all of the neutron pick-up results exhibit the same deviations from the proton pick-up results, namely a larger $C^2S(\ell=2)$ for the first 0^+,T=1 state and a smaller $C^2S(\ell=0)$ for the 4.67 MeV, 2^+ state.

IV.5.B. Comparison of Results with Structure Theory

Pick-up spectroscopic factors predicted for $^{39}K \rightarrow ^{38}K$ transitions are compared with the present experimental results in Table 15. The listed theoretical numbers are averages of the predictions derived from the two most successful Hamiltonians presented in Ref. 3, Kuo-type Hamiltonians 12.5p+^{17}O and 11.0h+ASPE. The agreement appears quite

Table 15. Experimental and theoretical values of C^2S for single neutron pick-up from ^{39}K.

Ex (keV)[a]	J^π,T	ℓ	DFRNL[a]	THEORY[b]
000	3^+,0	2	,1.75	,1.72
130	0^+,1	2	,0.31	,0.23
459	1^+,0	0,2	0.13,0.32	0.13,0.40
1699	1^+,0	0,2	0.02,0.57	0.04,0.46
2404	2^+,1	0,2	0.03,1.26	0.01,1.20
3432	2^+,0	0,2	0.43,0.43	0.43,0.15
3980	$(1,2)^+$,1	0,2	0.14,0.42	
4673	$(1,2)^+$,1	0,2	0.19,0.25	0.58,0.05
5249	$(1,2)^+$,1	0,2	0.16,0.17	
5809	$(1,2)^+$	0,2	0.17,0.16	
5856	$(1,2)^+$	0,2	0.11,0.12	0.37,0.00
5891	$(1,2)^+$	0,2	0.06,0.04	

[a]Present Work.
[b]Reference 3.

impressive, and seems to confirm the essential validity of this particular approach to calculating low-lying positive parity states at the top of the s-d shell. While the comparison definitely confirms the success of the Kuo matrix elements relative to the other interactions studied, the differences between the individual predictions of these two interactions were too small to be resolved. Indeed, it would seem to be almost beyond the scope of single nucleon pick-up experiments to meaningfully discriminate between the two sets of wave-functions.

The density of states observed in ^{38}K is far in excess of what is predicted by the $d_{5/2}$-$s_{1/2}$-$d_{3/2}$ shell-model calculations just discussed, which so successfully predict the observed apportionment of ℓ=0 and ℓ=2 (mostly but not all, $d_{3/2}$) strength among the low-lying levels. The drastic fragmentation of the ℓ=0 spectroscopic strengths to "extra" T=1 levels provides another view of the existence and significance of states which should arise from f-p shell configurations. All s-d shell calculations firmly exclude any reasonable supposition that the extra T=1 states below 6 MeV excitation, which cannot be contracted from $d_{3/2}$-$s_{1/2}$ couplings, arise from $d_{5/2}$ excitations. The (d,^{3}He) data support this view, indicating that the next ℓ=2 level above the 2^+ first excited state falls at 7 MeV excitation.

IV.6. Conclusions

We have found that the angular distributions of the (p,d) reaction on ^{39}K, using a proton energy of 35 MeV and covering 6 MeV of excitation in the residual nucleus, can be successfully analyzed with DWBA calculations which employ the most broadly based proton and deuteron optical-model potentials available. The finite-range, non-local DWBA calculations which use these parameters fit both $\ell=0$ and $\ell=2$ distributions quite well in the 3^{o}-25^{o} range. At larger angles, the predicted cross-sections do not drop off as rapidly as do the data. Use of a deuteron potential constructed by folding neutron and proton potentials, or use of a damped V_{pn} interaction serve to improve agreement at larger angles. The density-dependent damping procedure yields the best fits to the present data. Any of these DWBA prescriptions yields stable and theoretically sensible spectroscopic factors if only the 3^{o}-20^{o} data are used.

Many new levels have been observed in the present experiment and assigned excitation energies accurate to 1-3 keV. The detailed angular distribution measurements permitted the assignment of a positive parity and spin limits to many of the observed levels, and tentative negative parity to many others. The spectroscopic factors extracted for the more strongly populated states are, in general, consistent with results of previous neutron and proton pick-up experiments. The

results for the low-lying positive parity levels provide conclusive verification for the relevant predictions of recent shell-model calculations.

The details of structure observed above 3 MeV excitation are evidence of extensive effects of f-p shell configuration states, but aside from energy level schemes, no predictions from extended (s-d-f-p) shell-model calculations are yet available to compare to our results. We observe what appears to be very strong mixing between T=0 and T=1,$J=1^+$ states at 5.85 MeV excitation.

LIST OF REFERENCES

REFERENCES

1. E.C. Halbert, J.B. McGrory, B.H. Wildenthal, and S.P. Pandya, Advances in Nuclear Physics, Vol. IV, Ed. by M. Baranger and E. Vogt, (Plenum Press, New York, 1971).

2. B.H. Wildenthal, J.B. McGrory, E.C. Halbert, and H.D. Graber, Phys. Rev. C4, 1708(1971).

3. B.H. Wildenthal, E.C. Halbert, J.B. McGrory, and T.T.S. Kuo, Phys. Rev. C4, 1266(1971).

4. B.M. Preedom and B.H. Wildenthal, Phys. Rev. C6, 1633(1972).

5. T.T.S. Kuo and G.E. Brown, Nucl. Phys. 85, 40(1966).

6. D.L. Show, J.A. Nolen, E. Kashy, and B.H. Wildenthal, Bull. Am. Phys. Soc. 17, 533(1972).

7. J.A. Rice, B.H. Wildenthal, and B.M. Preedom, Bull. Am. Phys. Soc. 17, 485(1972).

8. B.H. Wildenthal and J.A. Rice, Bull. Am. Phys. Soc. 17, 534(1972).

9. J.W. Olness, W.R. Harris, P. Paul, and E.R. Warburton, Phys. Rev. C1, 958(1970).

10. J.D. Garrett, H.T. Fortune, and R. Middleton, Phys. Rev. C4, 1138(1971).

11. J.D. Garrett, R. Middleton, D.J. Pullen, S.A. Andersen, O. Nathan, and Ole Hansen, Nucl. Phys. A164, 449(1971).

12. J.N. Hallock, H.A. Enge, A. Sperduto, R. Middleton, J.D. Garrett, and H.T. Fortune, Phys. Rev. C6, 2148(1972).

13. S. Hinds, H. Marchant, and R. Middleton, Nucl. Phys. 51, 427(1964).

14. J.D. Garrett, R. Middleton, and H.T. Fortune, Phys. Rev. C4, 165(1971).

15. H.D. Graber and G.I. Harris, Phys. Rev. 188, 1685(1969).

16. A.K. Hyder and G.I. Harris, Phys. Rev. C4, 2046(1971).

17. J.R. Erskine, D.J. Crozier, J.P. Schiffer, and W.P. Alford, Phys. Rev. C3, 1976(1971).

18. P.M. DeLuca, J.C. Lawson, E.D. Berners, and P.R. Chagnon, Nucl. Phys. A173, 307(1971).

19. R.N. Horoshko and M.H. Shapira, Nucl. Phys. A180, 37(1971).

20. H. Brunnader, J.C. Hardy, and J. Cerny, Nucl. Phys. A137, 487(1969).

21. K.A. Snover, J.M. McDonald, D.B. Fossan, and E.K. Warburton, Phys. Rev. C4, 398(1971).

22. B. Vignon, J.P. Longequeue, and I.S. Towner, Nucl. Phys. A189, 513(1972).

23. H. Nann, L. Armbruster, and B.H. Wildenthal, Nucl. Phys. A198, 11(1972).

24. W. Kutschera, D. Pelte, and G. Schrieder, Nucl. Phys. A111, 529(1968).

25. B.H. Wildenthal and E. Newman, Phys. Rev. 175, 1431 (1968).

26. J.G. van der Baan and B.R. Sikora, Nucl. Phys. A173, 456(1971).

27. P.J. Mulhern, G.D. Jones, I.G. Main, B.T. McCrone, R.D. Symes, M.F. Thomas, and P.J. Twin, Nucl. Phys. A162, 259(1971).

28. H.G. Blosser and A.I. Galonsky, IEEE Trans. on Nuclear Science, NS-B, No. 4, 466(1966).

29. J.E. Spencer and H.A. Enge, Nucl. Instr. and Methods 49, 181(1967).

30. B.L. Cohen, Rev. Sci. Instr. 30, 415(1959).

31. H.G. Blosser, G.M. Crawley, R. deForest, E. Kashy, and B.H. Wildenthal, Nucl. Instr. and Methods 91, 61(1971).

32. W.A. Lanford, unpublished.

33. R. Au, G. Stark, R. deForest, and R. Dumit, unpublished.

34. A.H. Wapstra and N.B. Gove, Nuclear Data Tables, Vol. 9, Numbers 4-5, July 1971.

35. R.C. Haight, Ph.D. Thesis, Princeton University, 1969.

36. S.G. Nilsson, Kgl. Danske Videnskab Selskab, Mat. Fys. Medd. 29, No. 16(1955).

37. F.D. Becchetti and G.W. Greenlees, Phys. Rev. 182, 1190(1969).

38. R.J. Philpott, W.T. Pinkston, and G.R. Satchler, Nucl. Phys. A119, 241(1968).

39. C.A. Whitten, N. Stein, G.E. Holland, and D.A. Bromley, Phys. Rev. 188, 1941(1969).

40. J.L. Snelgrove and E. Kashy, Phys. Rev. 187, 1246(1969).

41. R. Sherr, B.F. Bayman, E. Rost, M.E. Rickey, and C.G. Hoot, Phys. Rev. 139, B1272(1965).

42. P.J. Plauger and E. Kashy, Nucl. Phys. A152, 609(1970).

43. R.C. Johnson and P.J.R. Soper, Phys. Rev. C1, 976(1970).

44. J.D. Harvey and R.C. Johnson, Phys. Rev. C3, 636(1971).

45. G.R. Satchler, Phys. Rev. C4, 1485(1971).

46. B.M. Preedom, Phys. Rev. C5, 587(1972).

47. G.M. McAllen, W.T. Pinkston, and G.R. Satchler, Particles and Nuclei 1, 412(1971).

48. B.M. Preedom J.L. Snelgrove, and E. Kashy, Phys. Rev. C1, 1132(1970).

49. P.D. Kunz, unpublished.

50. M.P. Fricke, E.E. Gross, B.J. Morton, and A. Zucker, Phys. Rev. 156, 1207(1967).

51. F. Hinterberger, G. Mairle, U. Schmidt-Rohr, G.J. Wagner, and P. Turek, Nucl. Phys. A111, 265(1968).

52. E. Newman, L.C. Becker, B.M. Preedom, and J.C. Hiebert, Nucl. Phys. A100, 225(1967).

53. C.M. Perey and F.G. Perey, Phys. Rev. 152, 923(1966).

54. P. Schwandt and W. Haeberli, Nucl. Phys. A123, 401(1969).

55. M.C. Mermaz, C.A. Whitten, J.W. Champlin, A.J. Howard, and D.A. Bromley, Phys. Rev. C4, 1778(1971).

56. P.W.M. Glaudemans, G. Wiechers, and P.J. Brussaard, Nucl. Phys. 56, 548(1964).

57. I. Lovas and J. Révai, Nucl. Phys. 59, 364(1964).

58. P.W.M. Glaudemans, P.J. Brussaard, and B.H. Wildenthal, Nucl. Phys. A102, 593(1967).

59. A.E.L. Dieperink and P.J. Brussaard, Nucl. Phys. A128, 34(1969).

60. F.C. Ernè, Nucl. Phys. 84, 91(1966).

61. G.A.P. Engelbertink and P.W.M. Glaudemans, Nucl. Phys. A123, 225(1969).

62. N.G. Puttaswamy and J.L. Yntema, Bull. Am. Phys. Soc. 11, 12, 1123(1967): results reported in Ref. 64.

63. Lars Broman, C.M. Fou, and Baruch Rosner, Nucl. Phys. A112, 195(1968).

64. G. Ronsin, M. Vergnes, G. Rotbard, J. Kalifa, and I. Linck, Nucl. Phys. A187, 96(1972).

65. J. Kroon, B. Hird, and G.C. Ball, Nucl. Phys. A204, 609(1973).

66. E.K. Warburton, J.W. Olness, and A.R. Poletti, Phys. Rev. 160, 938(1967).

67. J.A. Nolen, E. Kashy, I.D. Proctor, and G. Hamilton, to be published.

68. H.J. Maier, J.G. Pronko, and C. Rolfs, Nucl. Phys. A146, 99(1970).

69. A.M. Green, Phys. Letters 24B, 384(1967).

70. W. Rudolph and H.U. Gersch, Nucl. Phys. 71, 221(1965).

71. J. Honzátko, J. Kajfosz, and Z. Kosina, Nucl. Phys. A174, 668(1971).

72. R.N. Alves, J.M. Kuchly, J. Julien, C. Samour, and J. Morgenstern, Nucl. Phys. A135, 241(1969).

73. A.M. Hoogenboom, E. Kashy, and W.W. Buechner, Phys. Rev. 128, 305(1962).

74. P. Decowski, Nucl. Phys. A169, 513(1971).

75. L. Meyer, Nucl. Phys. 52, 213(1964).

76. G. van Middelkoop and P. Spilling, Nucl. Phys. 77, 267(1966).

77. J. Kopecky and E. Warming, Nucl. Phys. A127, 385(1969).

78. J.C. Hardy, H. Brunnader, and J. Cerny, Phys. Rev. C1, 561(1970).

79. W.S. Gray, P.J. Ellis, T. Wei, R.M. Polichar, and J. Jänecke, Nucl. Phys. A140, 494(1970).

80. N.G. Puttaswamy and J.L. Yntema, Phys. Rev. 177, 1624(1969).

81. R.D. Lawson, reported in Ref. 85.

82. I.J. Taylor, Nucl. Phys. 41, 227(1963).

83. J. Jänecke, Nucl. Phys. 48, 129(1963).

84. L.M. Blau, W.P. Alford, D. Cline, and H.E. Gove, Nucl. Phys. 76, 45(1965).

85. H.T. Fortune, N.G. Puttaswamy, and J.L. Yntema, Phys. Rev. 185, 1546(1969).

86. J.A. Fenton, T.H. Kruse, N. Williams, M.E. Williams, R.N. Boyd, and W. Savin, Nucl. Phys. A187, 123(1972).

87. W.K. Collins, C.S.C., D.S. Longo, and L.A. Alexander, University of Notre Dame Nuclear Structure Laboratory, Annual Report, 1971.

88. S. Maripuu, Nucl. Phys. A151, 465(1970).

89. J.J. Kolata, R. Auble, and A. Galonsky, Phys. Rev. 162, 957(1967).

90. A.N. James, P.R. Alderson, D.C. Bailey, P.E. Carr, J.L. Durell, M.W. Greene, and J.F. Sharpey-Schafer, Nucl. Phys. A172, 401(1971).

91. G.A.P. Engelbertink, private communication.

92. A. Gallmann, E. Aslanides, F. Jundt, and E. Jacobs, Phys. Rev. 186, 1160(1969).

93. H. Hasper, Ph.B. Smith, and P.J.M. Smulders, Phys. Rev. C5, 1261(1972).

94. B.H. Wildenthal and E. Newman, Nucl. Phys. A118, 347(1968).

95. P.M. Endt and C. van der Leun, to be published.

96. G.F. Trentelman, unpublished.

97. D.D. Duncan, K.H. Buerger, R.L. Place, and B.D. Kern, Phys. Rev. 185, 1515(1969).

98. A.A. Cowley, G. Heymann, and R.L. Keizer, Nucl. Phys. 86, 363(1966).

APPENDIX A

MONSTER2

APPENDIX A

MONSTER2

MONSTER2 is the computer code used to analyze all of the nuclear emulsion plate and position-sensitive proportional counter data taken for this thesis using the MSU split-pole magnetic spectrograph. The code accepts input in the form of experimental parameters (beam energy, scattering angle, spectrograph magnetic field strength (in terms of the field-sampling NMR frequency) and focal-plane-position settings), reactions appropriate to the experiment and spectral peak specifications (excitation energy, or centroid and total counts). Relativisitic reaction kinematics are calculated with a modified version of the function KINE.[96] MONSTER2 is multi-functional with options to perform the following tasks: (1) transform cross-sections from laboratory to center-of-mass (CM) coordinates, (2) perform spectrograph calibration and evaluate excitation energies, (3) predict positions of particle groups in the spectrograph focal plane, (4) identify contaminant peaks and (5) perform multi-angle excitation energy averaging and cross-section compilation.

1. CROSS-SECTION TRANSFORMATION: When particle group yields are input, they are multiplied by a user-supplied normalization factor to yield an absolute cross-section in the laboratory. They are converted to a CM cross-section by multiplying by σ_{CM}/σ_{LAB} as calculated in KINE

for the particular reaction and Q-value under consideration. The statistical error in the CM cross-section is automatically calculated.

2. EXCITATION ENERGIES: Nuclear reactions are typically designated as A(a,b)B, where A is the target nucleus, a the projectile, b the outgoing particle, and B is the residual nucleus. B may be left in any of its states for which the transition is energetically and quantum mechanically allowed. Accurate observation of the momentum of particle b, (p), allows a precise excitation energy assignment to the appropriate level in B via reaction kinematics.

In an Enge-type split-pole spectrograph, the radius of curvature (ρ) of the outgoing particle is roughly proportional to the position in the focal plane at which it is detected. Since $p \alpha \rho$, a ρ vs. position calibration allows the determination of the particle momentum and, hence the excitation energy of the corresponding level in the residual nucleus.

The MSU spectrograph focal plane is assumed to be described by the relation[67]

$$B\rho = B\rho_{KINE} + \Delta B\rho = B(\rho_o + \alpha D + \beta D^2 + \alpha\delta) \qquad A.1$$

with the following definitions:

B - spectrograph magnetic field (kilo-gauss), determined from NMR frequency.

$B\rho$ - "real" particle rigidity ($p=qB\rho$, where q is the charge of the outgoing particle).

$B\rho_{KINE}$ - particle rigidity calculated from relativistic kinematics based on the reaction, Q-value and nominal beam energy and scattering angle.

D - absolute focal plane peak position relative to a designated reference position, D_o, usually 9-13 inches from the high energy end.

ρ_o - radius of curvature corresponding to D_o.

α, β - linear and quadratic coefficients of the expansion about D_o ($\sim$-0.4 and $\lesssim 10^{-4}$/inch, respectively).

δ - a first-order estimation of the gap between abutting plates when a single spectrum is recorded on two consecutive plates in the focal plane; δ is non-zero only for particle groups falling on the second (low energy) plate.

$\Delta B\rho$ - a correction to $B\rho_{KINE}$ necessitated by small, but real, variations in the nominal experimental parameters. To first order,

$$\Delta B\rho = \frac{\Delta B\rho}{\Delta E_{beam}} \Delta E_{beam} + \frac{\Delta B\rho}{\Delta \theta_L} \Delta \theta_L \qquad \text{A.2}$$

where $\frac{\Delta B\rho}{\Delta E_{beam}}$ is evaluated for a 50 keV change in the beam

energy and $\frac{\Delta B\rho}{\Delta\theta_L} = \frac{\Delta B\rho}{\Delta T}\frac{\Delta T}{\Delta\theta_L}$ with $\frac{\Delta T}{\Delta\theta_L}$ calculated in KINE (T=particle kinetic energy) and $\frac{\Delta B\rho}{\Delta T} = E_{TOT}/B\rho$ (E_{TOT}=T+particle rest mass).

2A. When sufficient particle groups from known energy levels (reference peaks-RP) are present, one may perform a complete energy calibration on the given spectrum. Once these RP and their associated reactions and excitation energies are input, MONSTER2 calculates $B\rho_{KINE}$ and the coefficients of ρ_o, α, β, $\alpha\delta$, ΔE_{beam}, and $\Delta\theta_L$ (see equations A.1 and A.2) from the nominal input beam energy and scattering angle. ρ_o, α, β, ΔE_{beam}, $\Delta\theta_L$, and $\alpha\delta$ (when δ is not constrained to be zero) are then calculated via a least-squares fit to the RP energies. Any of the variables may be held constant and error messages are issued if the data is insufficient, or incorrect (ΔE_{beam}>100 keV or $\Delta\theta_L$>2^o). If the fit is reasonable, i.e., no error flags, the appropriate corrections to the beam energy, scattering angle and plate gap are made and the entire spectrum is analyzed, resulting in excitation energies for all peaks and reactions. If particle group yields are also input, lab-to-CM cross-section conversion takes place automatically.

2B. If the number and/or type of known reference levels is not sufficient to perform a complete calibration for a given spectrum, the user may opt to use the approximate parameters stored in MONSTER2.[67] In this case, δ, ΔE_{beam},

and $\Delta\theta_L$ are assumed to be zero, i.e., all kinematics are calculated using input beam energy and scattering angle values, and a plate gap is specified by the user. α and β are calculated as a function of focal plane orientation (input as the parameters DS and DL), D_o is assumed to be 10 inches, and ρ_o is calculated on the basis of the first reference peak position.

When operating in this mode, insertion of one reference level forces all other peaks to be analyzed relative to it using the available calibration parameters. If more than one RP is specified from the same or different reactions, MONSTER2 also performs a linear particle momentum match to obtain a best fit to all reference energies. This results in an effective adjustment of α. Table A1 shows the extent to which this fitting procedure can compensate for errors in the nominal experimental and calibration parameters. The trial errors in Table A1, except $\Delta\beta$, were chosen as approximate maximum uncertainties usually associated with the respective parameters. At present, β appears to be the most important single parameter for spectra covering more than $\sim$10 inches of focal plane distance. Unfortunately, it is also the most poorly known, the values for β currently stored in MONSTER2 are based on theoretical predictions and prove to be very different from those calculated in several individual calibration runs on actual spectra. The change in β considered

Table A1. Extrapolations from the MONSTER2 momentum matching fits to known energy levels. Nominal energies and calibration parameters were obtained from a complete calibration run on the test spectrum. All other energies (MeV) are obtained from a fit to the first three (0.000, 0.130, 0.459 MeV) levels after the indicated shift the given parameter had been assumed.

Nominal	ΔE_{beam}=+35 keV	$\Delta\Theta_L$=+0.3°	$\Delta\alpha$=-1%	$\Delta\beta$=3x10^{-5}	Δf_s=+1%
0.000	0.000	0.000	0.000	0.000	0.000
0.130	0.130	0.130	0.130	0.130	0.130
0.459	0.459	0.459	0.459	0.459	0.459
1.699	1.698	1.698	1.698	1.698	1.699
2.403	2.402	2.402	2.402	2.402	2.402
3.431	3.430	3.430	3.430	3.429	3.430
3.977	3.978	3.977	3.977	3.976	3.978
5.249	5.248	5.248	5.248	5.245	5.248
5.890	5.891	5.890	5.891	5.887	5.891
7.115	7.114	7.113	7.113	7.107	7.113
8.236	8.235	8.233	8.234	8.226	8.234
9.118	9.117	9.116	9.116	9.106	9.116

in Table A1 serves to indicate the effect of uncertainties in this parameter. The fitting procedure compensates for the other uncertainties to <0.5 keV/MeV to 9 MeV above the fitting region and can handle β uncertainties reasonably well over shorter extrapolation ranges. Accuracies can be significantly improved using the option to manually adjust α and β or by the use of contaminant peaks (see 4.) as additional reference levels in "unknown" regions of the spectrum.

3. PARTICLE GROUP POSITIONS: A knowledge of particle group placement in the spectrograph focal plane is useful not only for experimental set-up, but also in preliminary data analysis. Peak positions for specified reactions may be predicted with MONSTER2 from the experimental parameters and appropriate excitation energies. The positions are predicted, and listed in order, using the internal calibration parameters and the inverse of the excitation analysis process. Although uncertainties in beam energy and precise scattering angle impose the main limitation on the absolute position accuracy, relative spacings of known levels from the same and different reactions have been reproduced to ≤0.2 mm in test case comparisons with actual plate data.

4. CONTAMINANT IDENTIFICATION: Reaction products from target impurities often fall on the focal plane in the same region as the specific particles under investigation. The

specification of any "reasonable" reaction requires that MONSTER2 analyze every peak as though it were produced by that reaction in the pertinent experimental configuration. Comparison of the output excitation energies with known impurity levels may allow one to identify contaminants or particle groups in the spectrum which are different from those being studied. From example, the $^{16}O(p,d)^{15}O_{0.000}$, the $^{12}C(p,d)^{11}C_{0.000}$, and the $^{39}K(p,t)^{37}K$ peaks seen in the present studies were all identified in this manner, usually within ± 3 keV when the fitting procedure was used with known levels from target nuclei.

5. MULTI-ANGLE AVERAGING: Excitation energies are generally assigned on the basis of 2 or more spectra. MONSTER2 can search on up to 10 spectra input on the same job and perform an average of appropriate excitation energies, weighted by the raw yield for the appropriate peaks. One can also punch corresponding differential cross-sections, yielding angular distributions for specific energy levels in given residual nuclei.

APPENDIX B

ELASTIC SCATTERING DATA

APPENDIX B

ELASTIC SCATTERING DATA

All of the (p,d) data presented herein has been normalized by comparison with proton elastic scattering data. The (p,d) and (p,p_o) spectra for each target were recorded with a single-wire proportional counter under identical experimental conditions, except for an appropriate adjustment of the spectrograph magnetic field. Consequently, with proper relative data normalizations, a knowledge of the absolute cross-section to observed proton ratio for the (p,p_o) data allows the observed deuteron cross-sections to be expressed in an absolute manner.

Figure B1 shows the spectra recorded from proton scattering on the ^{23}Na-^{35}Cl, ^{23}Na-^{37}Cl, and ^{39}K targets at 40^o. Angular distributions were recorded from 25^o to 50^o at 5^o intervals. The distributions are shown in Figs. B2, B3, and B4 normalized to optical-model calculations using the Becchetti-Greenlees[37] parameters for the appropriate masses. The Na and Cl experimental cross-sections for the two sodium-chloride targets are presented in the observed relative configuration at each angle.

Figure B1. Proton elastic scattering spectra recorded at 40° with a single-wire proportional counter.

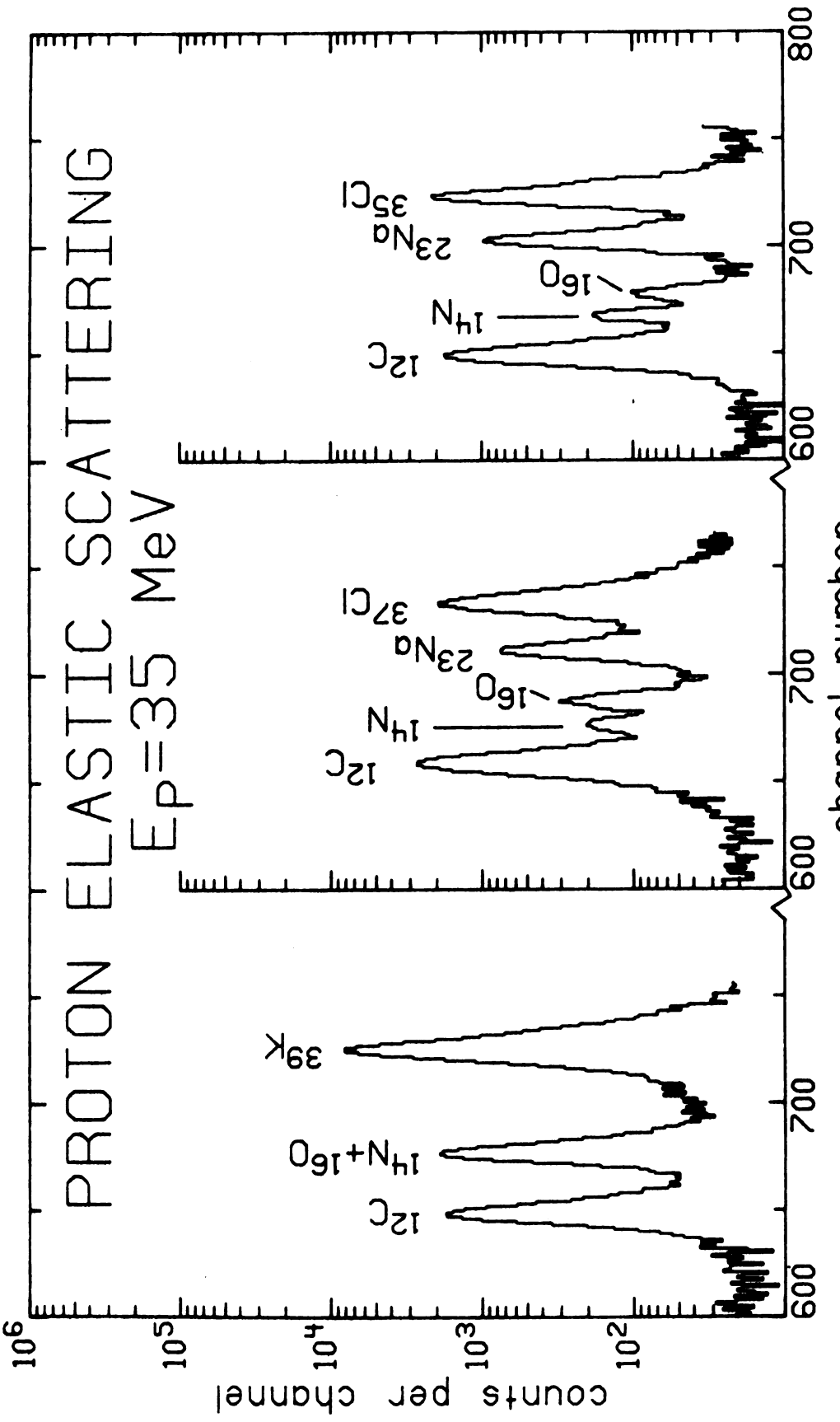
PROTON ELASTIC SCATTERING
Ep=35 MeV
counts per channel
channel number
39K
14N+16O
12C
37Cl
23Na
16O
14N
12C
35Cl
23Na
16O
14N
12C

Figure B1

Figure B2. Measured proton elastic scattering differential cross-sections for the ^{23}Na-^{35}Cl target.

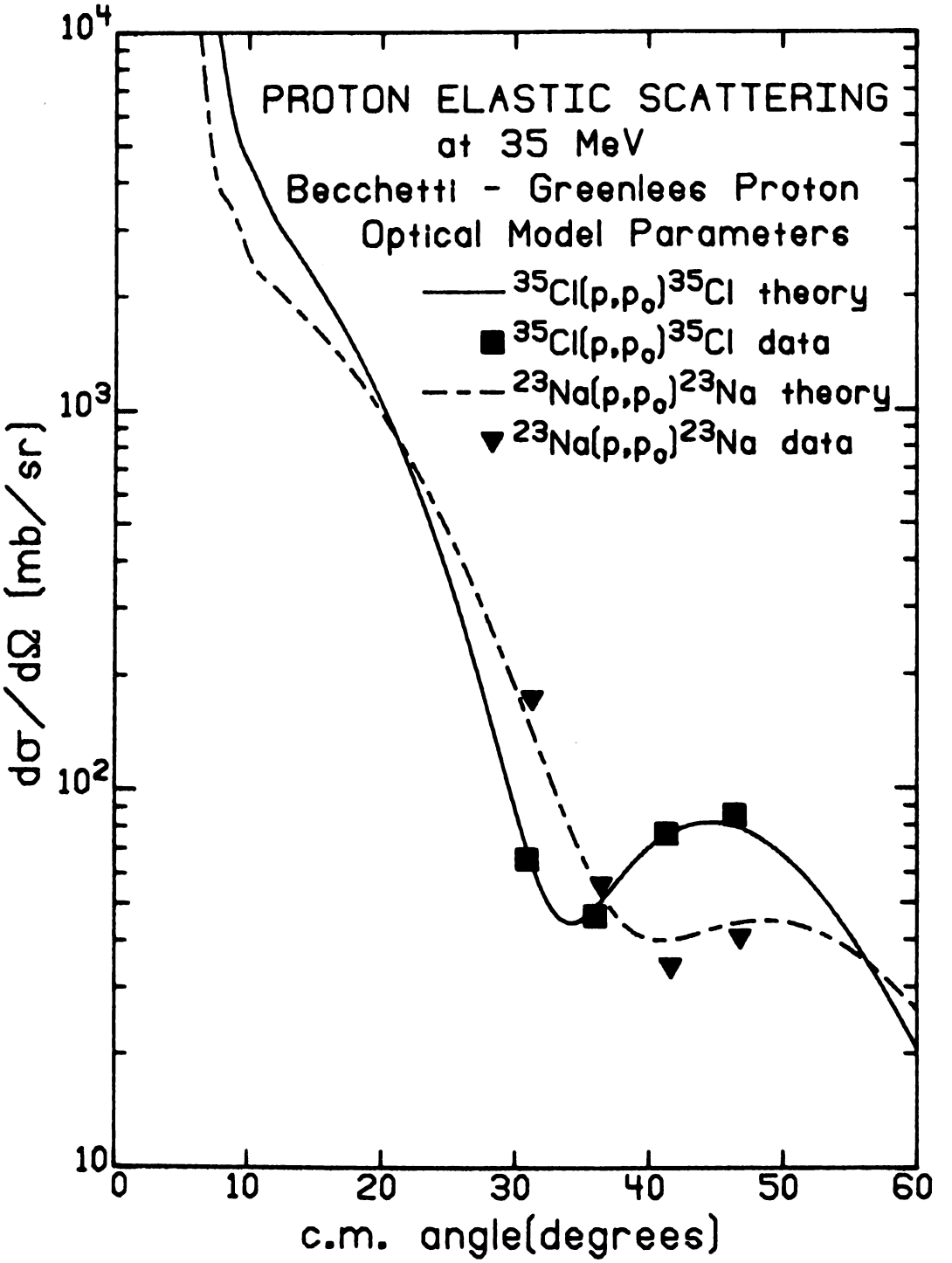
PROTON ELASTIC SCATTERING
at 35 MeV
Becchetti - Greenlees Proton
Optical Model Parameters
35Cl(p,p0)35Cl theory
35Cl(p,p0)35Cl data
23Na(p,p0)23Na theory
23Na(p,p0)23Na data
dσ/dΩ (mb/sr)
10^4
10^3
10^2
10
0
10
20
30
40
50
60
c.m. angle(degrees)

Figure B2

Figure B3. Observed proton elastic scattering cross-sections for the ^{23}Na-^{37}Cl target.

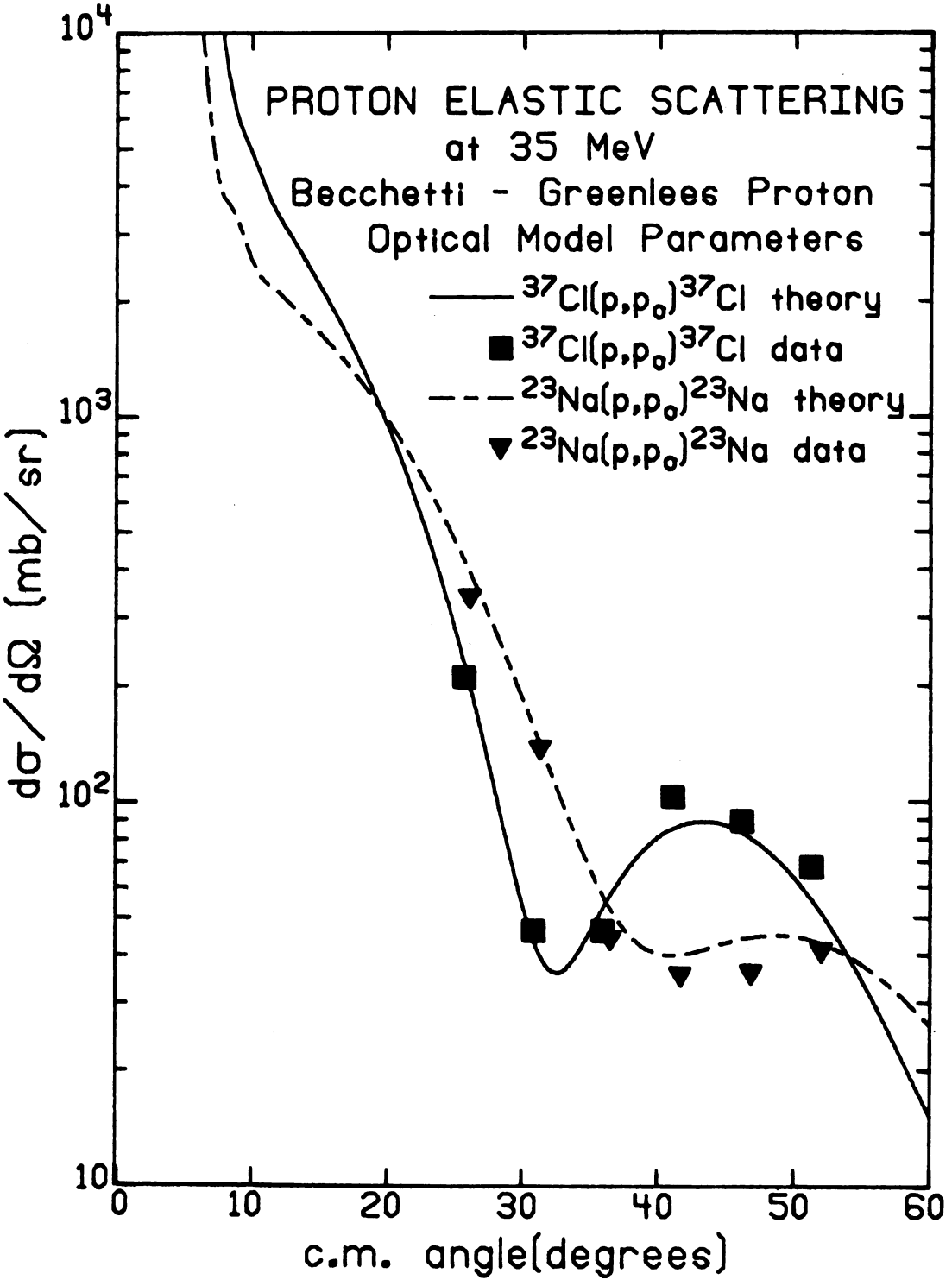
PROTON ELASTIC SCATTERING
at 35 MeV
Becchetti - Greenlees Proton
Optical Model Parameters
$^{37}Cl(p,p_0)^{37}Cl$ theory
$^{37}Cl(p,p_0)^{37}Cl$ data
$^{23}Na(p,p_0)^{23}Na$ theory
$^{23}Na(p,p_0)^{23}Na$ data
$d\sigma/d\Omega$ (mb/sr)
10^4
10^3
10^2
10
0
10
20
30
40
50
60
c.m. angle(degrees)

Figure B3

Figure B4. Measured proton elastic scattering cross-sections for the ^{39}K target.

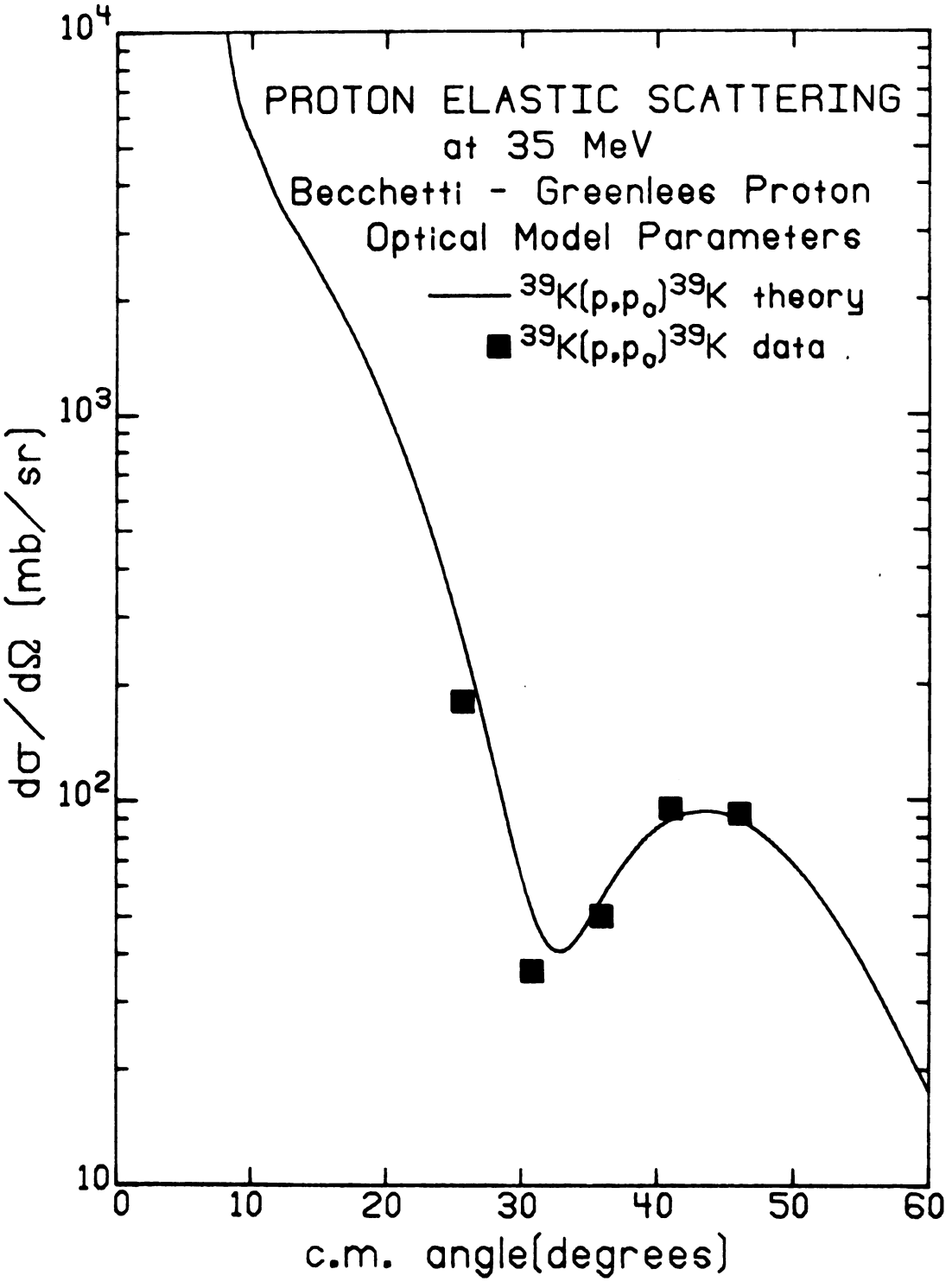
PROTON ELASTIC SCATTERING
at 35 MeV
Becchetti - Greenlees Proton
Optical Model Parameters
$^{39}K(p,p_o)^{39}K$ theory
$^{39}K(p,p_o)^{39}K$ data
$d\sigma/d\Omega$ (mb/sr)
10^4
10^3
10^2
10
0
10
20
30
40
50
60
c.m. angle(degrees)

Figure B4

MICHIGAN STATE UNIVERSITY LIBRARIES
3 1293 03196 6025